THE UNIVERSITY OF QUEENSLAND

AUSTRALIA

TESTING THE TIDAL STRIPPING ORIGIN OF ULTRA-COMPACT DWARF GALAXIES

Joel Pfeffer

Bachelor of Science (Honours)

A THESIS SUBMITTED FOR THE DEGREE OF DOCTOR OF PHILOSOPHY AT
THE UNIVERSITY OF QUEENSLAND IN 2015

School of Mathematics and Physics

Abstract

Ultra-compact dwarf galaxies (UCDs) are intermediate objects between globular clusters and dwarf galaxies, with many similarities to the nuclear clusters of dwarf galaxies. Tidal stripping of nucleated galaxies is a likely origin for UCDs since tidal stripping must occur in any hierarchical galaxy formation scenario. During the tidal stripping process the main body of the galaxy is removed while the nucleus remains since the nuclear clusters are too compact to be destroyed. In this thesis I present new theoretical work addressing the possibility of UCDs having a tidal stripping origin.

Through the use of N-body simulations I show that tidal stripping of nucleated galaxies in galaxy clusters under the assumption of dark matter free galaxies can account for the observed sizes and masses of UCDs. I find that incomplete stripping of the UCD progenitor galaxy, resulting in a UCD with an extended stellar envelope, may account for the observed size difference between nuclear clusters and UCDs.

In a second study, I use a semi-analytic model of galaxy formation to predict the number of UCDs expected to form via tidal stripping. I find that tidal stripping cannot account for all UCDs observed in the Fornax cluster but is most important for high mass UCDs, accounting for about 50 per cent of objects with masses larger than $10^7 \, \mathrm{M_\odot}$. Additionally, I compare the predictions for radial distributions, metallicities and implied central black hole masses from the semi-analytic models with observed UCDs in the Fornax and Virgo clusters, finding good agreement between the predictions and observations. This work suggest most UCDs are simply high-mass globular clusters, with the most massive and extended UCDs being formed by tidal stripping.

Finally, I present a new method to incorporate tidal stripping of satellite galaxies into semi-analytic models of galaxy formation. Comparing with observed dwarf galaxies in the Fornax cluster, I find this method gives better agreement with the predicted numbers and radial distributions of galaxies when compared with models not taking into account tidal stripping.

Declaration by author

This thesis is composed of my original work, and contains no material previously published or written by another person except where due reference has been made in the text. I have clearly stated the contribution by others to jointly-authored works that I have included in my thesis.

I have clearly stated the contribution of others to my thesis as a whole, including statistical assistance, survey design, data analysis, significant technical procedures, professional editorial advice, and any other original research work used or reported in my thesis. The content of my thesis is the result of work I have carried out since the commencement of my research higher degree candidature and does not include a substantial part of work that has been submitted to qualify for the award of any other degree or diploma in any university or other tertiary institution. I have clearly stated which parts of my thesis, if any, have been submitted to qualify for another award.

I acknowledge that an electronic copy of my thesis must be lodged with the University Library and, subject to the policy and procedures of The University of Queensland, the thesis be made available for research and study in accordance with the Copyright Act 1968 unless a period of embargo has been approved by the Dean of the Graduate School.

I acknowledge that copyright of all material contained in my thesis resides with the copyright holder(s) of that material. Where appropriate I have obtained copyright permission from the copyright holder to reproduce material in this thesis.

Publications during candidature

Peer-reviewed papers:

Pfeffer J., Baumgardt H., 2013, MNRAS, 433, 1997: *Ultra-compact dwarf galaxy formation by tidal stripping*

Pfeffer J., Griffen B. F., Baumgardt H., Hilker M., 2014, MNRAS, 444, 3670: *Contribution of stripped nuclear clusters to globular cluster and ultracompact dwarf galaxy populations of nucleated dwarf galaxies*

Publications included in this thesis

Pfeffer J., Baumgardt H., 2013, MNRAS, 433, 1997 – incorporated as Chapter 2.

Contributor	Statement of contribution
Joel Pfeffer (candidate)	Design of project (50%)
	Analysis (85%)
	Wrote the paper (100%)
Holger Baumgardt	Design of project (50%)
	Analysis (15%)

Pfeffer J., Griffen B. F., Baumgardt H., Hilker M., 2014, MNRAS, 444, 3670 – incorporated as Chapter 4.

Contributor	Statement of contribution
Joel Pfeffer (candidate)	Design of project (70%) Analysis (85%) Wrote the paper (95%)
Brendan Griffen	Design of project (15%) Analysis (5%)
Holger Baumgardt	Design of project (10%) Analysis (5%) Wrote the paper (2.5%)
Michael Hilker	Design of project (5%) Analysis (5%) Wrote the paper (2.5%)

Contributions by others to the thesis

Chapter 3:

The analysis and text is my own work, but some interpretation of the results was contributed by Holger Baumgardt.

Chapter 5:

The analysis and most of the text is my own work, but the compilation of observational data and the relevant text and some designing of the project was contributed by Michael Hilker.

Statement of parts of the thesis submitted to qualify for the award of another degree

None.

Acknowledgements

There are a number of people I wish to thank who have contributed in some way towards this thesis.

- First and foremost my wife Hannah and daughter Isabelle for their love, support, understanding and patience.

- My supervisors Holger Baumgardt, Michael Drinkwater and Michael Hilker, for their guidance, encouragement, mentorship and just generally steering me in the right direction.

- My parents for their encouragement and giving me the opportunity to pursue a career in science.

- My friends and colleagues at UQ and ESO for their friendship and stimulating discussions.

Keywords

dwarf galaxies, globular clusters, galaxy formation, galaxy interactions, numerical simulations

Australian and New Zealand Standard Research Classifications (ANZSRC)

020104 Galactic Astronomy: 50%

020103 Cosmology and Extragalactic Astronomy: 50%

Fields of Research (FoR) Classification

0201 Astronomical and Space Sciences: 100%

Contents

List of Figures

List of Tables

List of Abbreviations

ACS	Advanced Camera for Surveys
ACSVCS	Advanced Camera for Surveys Virgo Cluster Survey
dE	Dwarf elliptical galaxy
dE,N	Nucleated dwarf elliptical galaxy
GC	Globular cluster
GPU	Graphics processing unit
IMF	Initial mass function
ΛCDM	Lambda Cold Dark Matter
$L_\odot$	Unit of luminosity (1 solar luminosity $\simeq 3.85 \times 10^{26}$ W)
magnitude, mag	Unit of brightness
$M_\odot$	Unit of mass (1 solar mass $\simeq 1.99 \times 10^{30}$ kg)
M/L	Mass-to-light ratio
NGP	Nearest grid point
NGVS	Next Generation Virgo cluster Survey
parsec, pc	Unit of distance (1 parsec $\simeq 3.09 \times 10^{16}$ m)

SAM   Semi-analytic model

SDSS   Sloan Digital Sky Survey

SMBH   Supermassive black hole

UCD   Ultra-compact dwarf galaxy

WMAP   Wilkinson Microwave Anisotropy Probe

1

Introduction

Just over 15 years ago stellar systems were cleanly divided into star clusters and galaxies; star clusters, including globular and open clusters, being compact, spherical systems of up to a few million stars with effective radii on the scale of parsecs and galaxies being extended, dark matter dominated systems of seemingly endless morphologies with effective radii on the scale of kilo-parsecs (this divide is known as the Gilmore Gap; Gilmore et al. 2007); star clusters formed out of the very densest clumps of gas within giant molecular clouds in one burst of star formation while galaxies formed from multiple bursts of star formation through continuous accretion of gas (Ashman & Zepf 1998; Harris 2001). Since that time the divide between star clusters and galaxies have become increasingly blurred with the discovery of ultra-compact dwarf galaxies (Hilker et al. 1999a; Drinkwater et al. 2000), ultra-faint dwarf galaxies (Willman et al. 2005; Zucker et al. 2006), extended clusters (Brodie & Larsen 2002; Huxor et al. 2005) and globular clusters with evidence of supernovae enrichment (Lee et al.

1999; Hilker & Richtler 2000).

1.1 Ultra-compact dwarf galaxies

The first ultra-compact dwarf galaxies (UCDs) were discovered in large-scale spectroscopic surveys of the Fornax galaxy cluster (Hilker et al. 1999a; Drinkwater et al. 2000). They had surface brightnesses similar to globular clusters (GCs, $\mu_{V,0} \sim$ 19-23 mag arcsec^{-2}), luminosities similar to dwarf elliptical (dE) nuclei ($-14 \lesssim M_V/\text{mag} \lesssim -12$) and sizes intermediate between GCs and dwarf galaxies ($10 \lesssim R_{\text{eff}}/\text{pc} \lesssim 50$). Follow-up high resolution spectroscopy found they had similar internal velocity dispersions to dE nuclei ($\sigma_0 \sim 30$ km s^{-1}, Drinkwater et al. 2003).

Through dedicated surveys many new UCDs have been found (Mieske, Hilker, & Infante 2004a; Firth et al. 2007; Firth, Drinkwater, & Karick 2008; Gregg et al. 2009), to the point where the confirmed objects now number in the hundreds in the Fornax cluster alone (Mieske et al. 2012). UCDs have since been discovered in all environments, including other galaxy clusters (Abell 1689: Mieske et al. 2004b; Virgo: Haşegan et al. 2005; Jones et al. 2006; Centaurus: Mieske et al. 2007; Coma: Price et al. 2009; Chiboucas et al. 2010; Hydra I: Misgeld et al. 2011; Perseus: Penny et al. 2012), galaxy groups (Dorado and NGC 1400: Evstigneeva et al. 2007a; NGC 5128: Rejkuba et al. 2007; HCG 22 and HCG 90: Da Rocha et al. 2011; NGC 3923: Norris & Kannappan 2011) and around isolated galaxies (NGC 7252: Maraston et al. 2004; Sombrero: Hau et al. 2009; NGC4546: Norris & Kannappan 2011).

1.1.1 Location on the Fundamental Plane

The exact definition of an UCD varies in the literature but they are typically defined as either having masses $> 2 \times 10^6 \, \text{M}_\odot$ and sizes $R_{\text{eff}} \sim$ 7–100 pc (e.g. Mieske et al. 2008) or luminosities $M_V \lesssim -8$ mag (corresponding to masses $\gtrsim 2 \times 10^5 \, \text{M}_\odot$ for a mass-to-light ratio in the V-band $M/L_V = 1.5 \, (\text{M/L})_\odot$) and sizes $R_{\text{eff}} \sim$ 10–100 pc (e.g. Brodie et al. 2011), with the former definition based on the elevated mass-to-light ratios of UCDs and the later an observational definition to include the recently discovered low luminosity UCDs ($M_V \sim -9$

mag, $R_{\mathrm{eff}} \sim 40$ pc).

Figure 1.1 shows the sizes and masses of UCDs relative to other spheroidal stellar systems. Despite their large range in mass, GCs have sizes of a few pc with no correlation in mass. In contrast, UCDs have sizes from a few pc up to hundreds of pc (depending on the definition of an UCD). UCDs have similar masses to nuclear clusters, but have effective radii a factor of two larger on average (Evstigneeva et al. 2008). UCDs were thought to be defined by a size-luminosity (or size-mass) relation ($R_{\mathrm{eff}} \propto L_V{}^{0.88}$, Evstigneeva et al. 2008), although as more UCDs are discovered this is being called into question (Brodie et al. 2011; Forbes et al. 2013). One possibility is that the size-mass relation for high-mass UCDs is related to the so-called 'zone of avoidance' (a minimum effective radius for a given stellar mass: $R_{\mathrm{eff}}(M) \geq c_1 M_*{}^{4/5}$ where $c_1 = 2.24 \times 10^{-6}$ pc $M_\odot^{-4/5}$, Misgeld & Hilker 2011) through the existence of a maximum mass surface density (Hopkins et al. 2010a; Norris et al. 2014). Alternatively, all star clusters may have formed with a mass–size relation and low-mass systems have undergone expansion (Gieles et al. 2010) or it may be due to a physical mechanism which causes an increasing lower size limit with increasing mass (e.g. Murray 2009).

Figure 1.2 shows the internal velocity dispersions of UCDs relative to other spheroidal systems. Most UCDs have velocity dispersions similar to GCs, dwarf galaxies and, in particular, the nuclei of dwarf galaxies ($\sigma \sim 30$ km s^{-1}, Drinkwater et al. 2003). Many UCDs also follow a similar trend in σ–M space to GCs. However a number of objects have velocity dispersions similar to cEs and giant ellipticals ($\sigma \sim 60$-100 km s^{-1}) and GCs and dSphs ($\sigma \sim 10$ km s^{-1}). This overlap between many different stellar systems highlights the difficulty in determining the nature of any given UCD based on its location in the Fundamental Plane.

1.1.2   Metallicities and ages

Many studies have investigated the ages and metallicities of UCDs (Haşegan et al. 2005; Mieske et al. 2006; Evstigneeva et al. 2007b; Firth, Evstigneeva, & Drinkwater 2009; Paudel, Lisker, & Janz 2010; Chilingarian et al. 2011; Norris & Kannappan 2011; Francis et al. 2012). Figure 1.3 shows the metallicities of UCDs relative to other stellar systems. Most UCDs
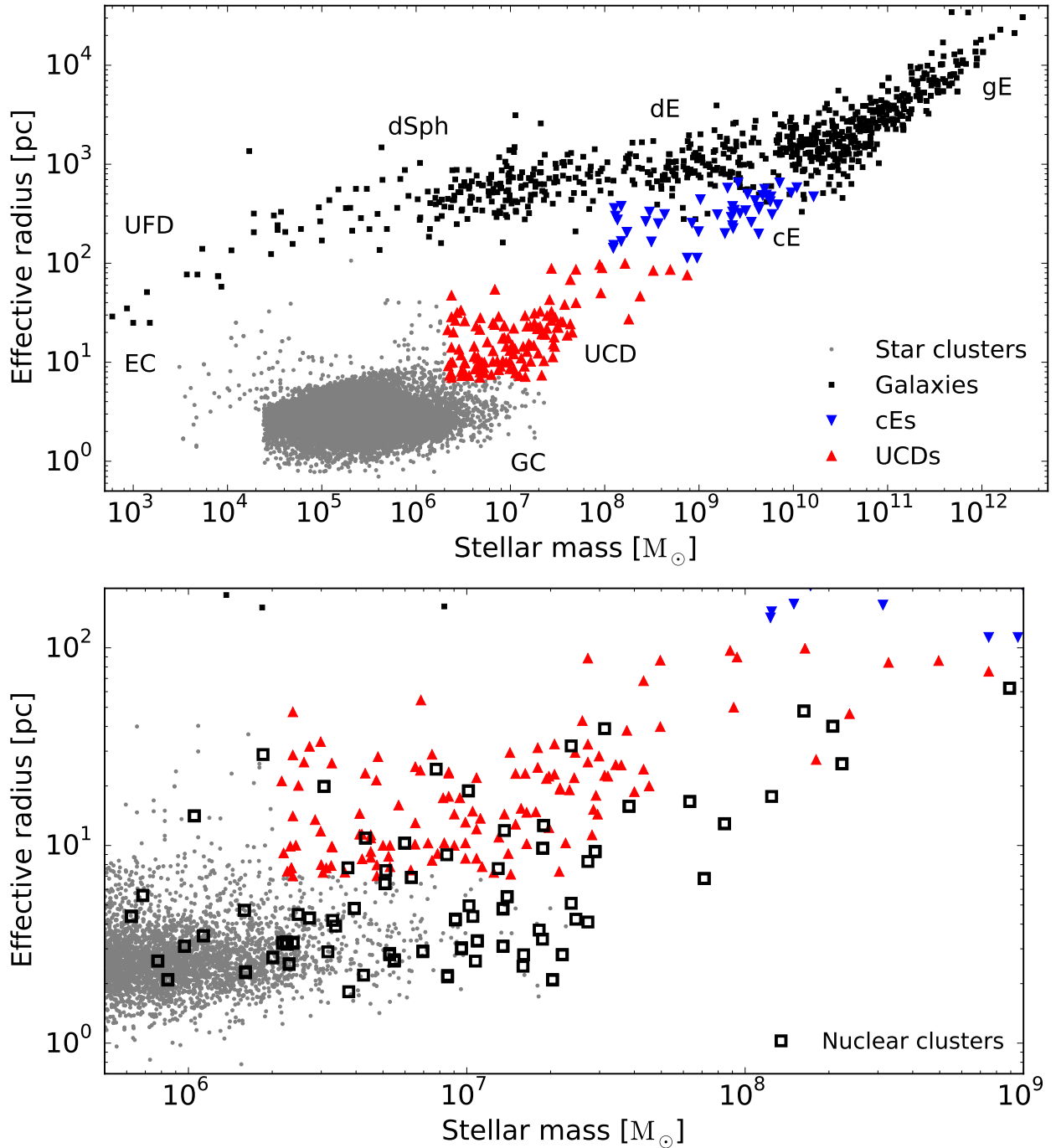
FIGURE 1.1: The upper panel shows the sizes and masses of dispersion supported stellar systems, including GCs, UCDs (defined as having masses $> 2 \times 10^6 \, M_\odot$ and sizes $7 < R_{\mathrm{eff}}/\mathrm{pc} \lesssim 100$), extended clusters (ECs), dwarf spheroidals (dSphs), ultra-faint dSphs (UFDs), dwarf ellipticals (dEs), compact ellipticals (cEs) and giant ellipticals (gEs). UCDs are shown as red triangles, cEs as blue triangles, star clusters (GCs/ECs) as grey dots and galaxies (gEs/dEs/dSphs/UFDs) as black squares. The lower panel shows the sizes and masses of nuclear clusters relative to GCs and UCDs. The objects are from the compilations of Misgeld & Hilker (2011) and Norris et al. (2014).
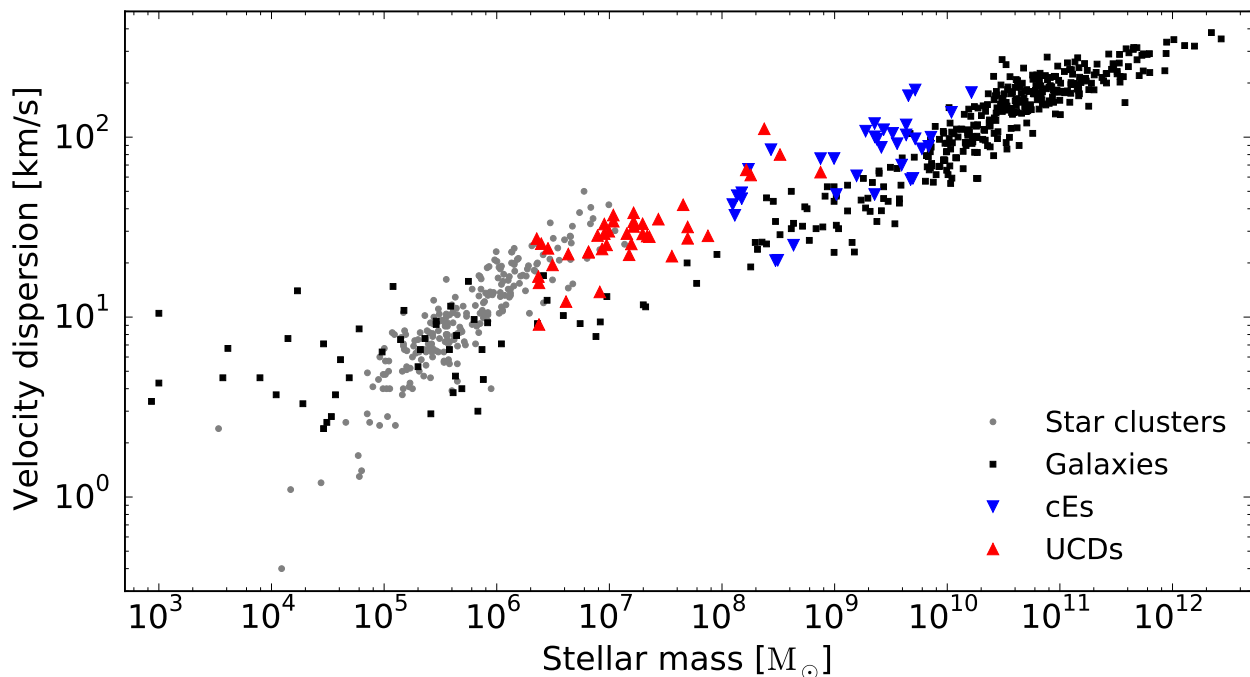
FIGURE 1.2: Stellar mass versus velocity dispersion for objects compiled by Norris et al. (2014). The symbols are the same as in Figure 1.1: UCDs are shown as red triangles, cEs as blue triangles, star clusters (GCs/ECs) as grey dots and galaxies (gEs/dEs/dSphs/UFDs) as black squares.

have metallicities ([Fe/H] > -1 dex) that place them well above the metallicity–luminosity relation for early-type galaxies, having similar metallicities to dE galaxies. However there are objects with low metallicities ([Fe/H] < -1.5 dex) similar to most GCs and also intermediate objects between GCs/UCDs and UCDs/cEs. The metallicities of some of the most massive UCDs ([Fe/H] ~ 0 dex) indicate they may be associated with giant galaxies rather than dwarfs.

Given their distances and unresolved stellar populations, accurate ages for UCDs are difficult to obtain. Simple stellar population modelling finds typical ages of 8-15 Gyr, with an average of 10-11 Gyr (Evstigneeva et al. 2007b; Francis et al. 2012), although very young objects exist (NGC 4546 UCD: age ~3 Gyr, Norris & Kannappan 2011; W3: age <0.5 Gyr, Schweizer & Seitzer 1998; Maraston et al. 2001).
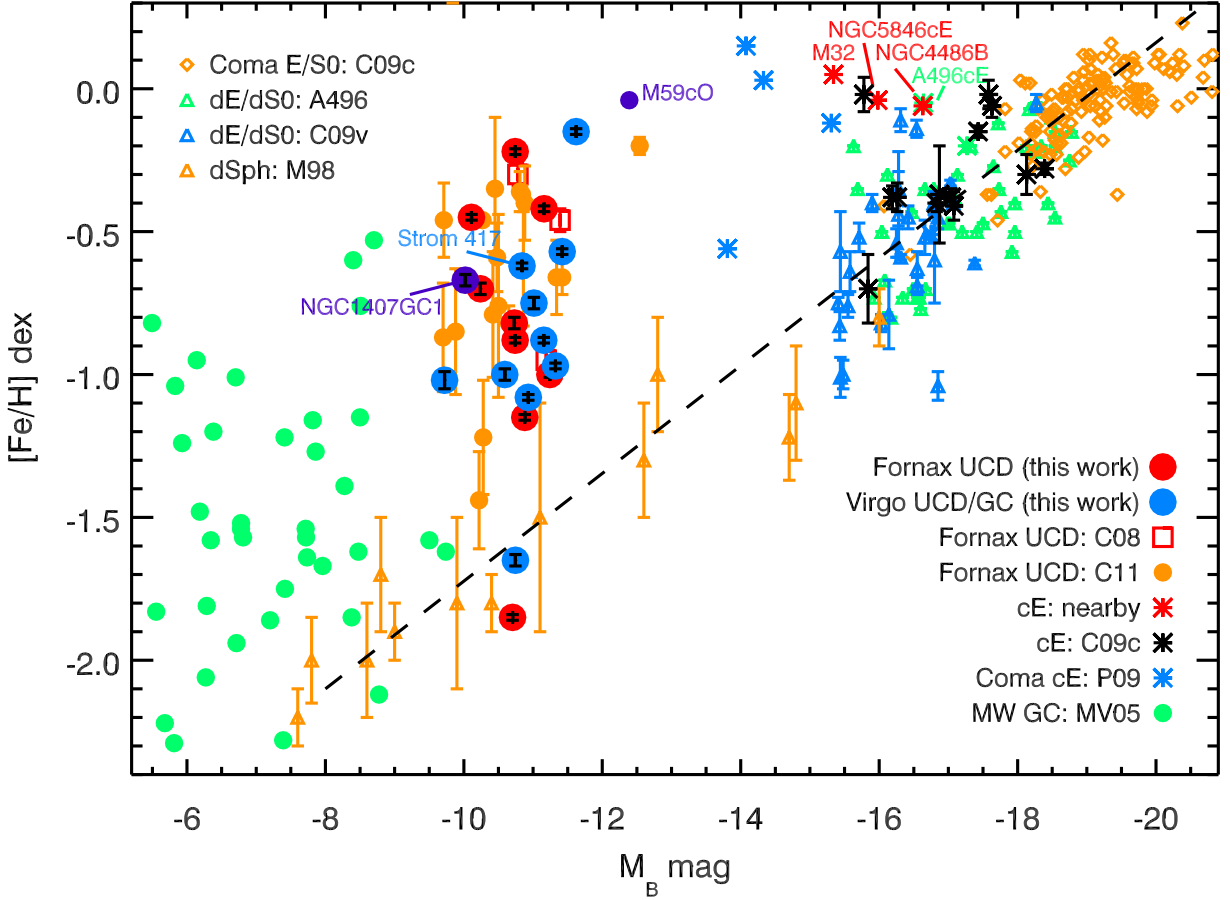
FIGURE 1.3: Metallicities and luminosities of UCDs compared to other stellar systems. Giant early-type galaxies are shown as diamonds, dwarf early-type galaxies are shown as triangles, cEs are shown as asterisks and GCs and UCDs are shown as circles and red squares. Early-type galaxies follow the well known metallicity–luminosity relation (dashed-line, e.g. Chilingarian et al. 2011). The figure is reproduced from Francis et al. (2012).

1.1.3 Dynamical mass-to-light ratios

One of the most interesting properties of UCDs are their mass-to-light ratios (M/L): UCDs have, on average, dynamical M/L about twice that expected from stellar population models given their metallicities and ages (Haşegan et al. 2005; Mieske et al. 2008, 2013). Since this discovery, the topic has received significant attention in the literature (Haşegan et al. 2005; Dabringhausen, Kroupa, & Baumgardt 2009; Dabringhausen, Fellhauer, & Kroupa 2010; Dabringhausen et al. 2012; Baumgardt & Mieske 2008; Mieske & Kroupa 2008; Mieske et al. 2008, 2013; Murray 2009; Taylor et al. 2010; Frank et al. 2011; Phillipps et al. 2013; Strader
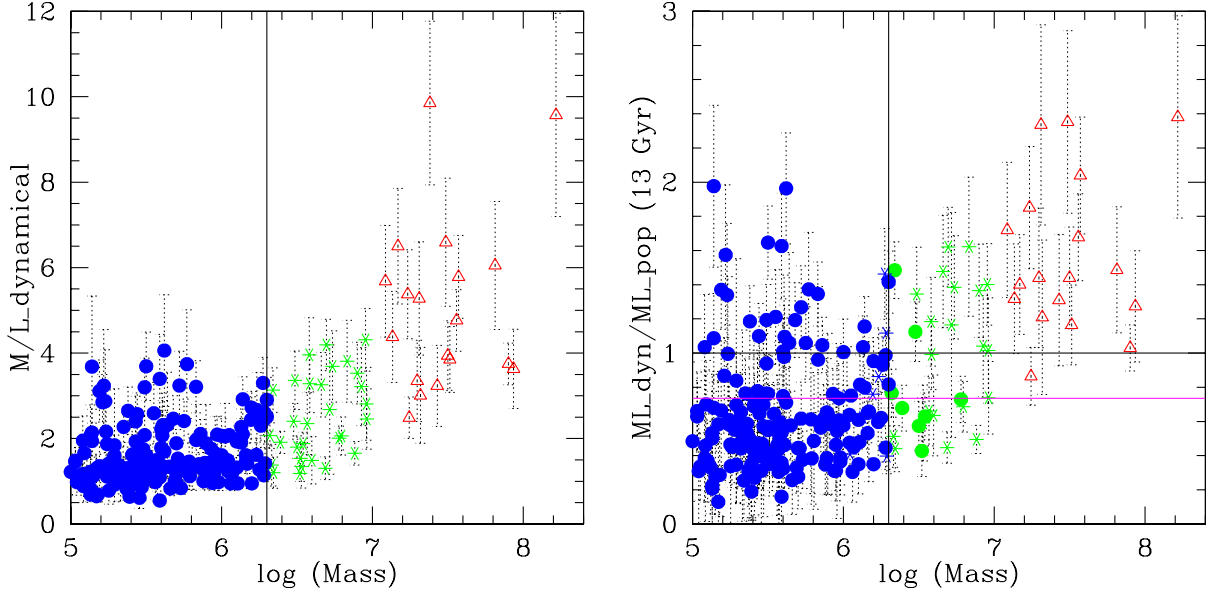
FIGURE 1.4: Dynamical M/L of GCs and UCDs compared with dynamical mass (left) and the ratio of dynamical-to-stellar M/L compared with mass (right). The sample is divided into 'GCs' ($M < 2 \times 10^6 \, \mathrm{M_\odot}$, blue circles), 'low-mass UCDs' ($2 \times 10^6 < M/\mathrm{M_\odot} < 10^7$, green triangles) and 'high-mass UCDs' ($M > 10^7 \, \mathrm{M_\odot}$, red triangles). In the right panel, the black horizontal line indicates an assumed age of 13 Gyr for the stellar population, while the magenta line indicates an assumed age of 9 Gyr. The figure is reproduced from Mieske et al. (2013).

et al. 2013; Forbes et al. 2014; Seth et al. 2014).

In Figure 1.4 the dynamical mass-to-light ratios $(M/L)_{\mathrm{dyn}}$ and ratio of $(M/L)_{\mathrm{dyn}}$ to the M/L predicted from stellar population modelling $(M/L)_{\mathrm{pop}}$ are shown for the sample of GCs and UCDs from Mieske et al. (2013). The sample is divided into 'GCs' ($M < 2 \times 10^6 \, \mathrm{M_\odot}$), 'low-mass UCDs' ($2 \times 10^6 < M/\mathrm{M_\odot} < 10^7$) and 'high-mass UCDs' ($M > 10^7 \, \mathrm{M_\odot}$). The left panel of Figure 1.4 shows the well-known increase of $(M/L)_{\mathrm{dyn}}$ with increasing mass, from $\sim 1 \, (\mathrm{M/L})_\odot$ for GCs to $\sim 5 \, (\mathrm{M/L})_\odot$ for high-mass UCDs. The break between a constant $(M/L)_{\mathrm{dyn}}$ and a $(M/L)_{\mathrm{dyn}}$ increasing with mass occurs at a mass of approximately $2 \times 10^6 \, \mathrm{M_\odot}$.

The right panel of Figure 1.4 shows the ratio $\Psi = (M/L)_{\mathrm{dyn}}/(M/L)_{\mathrm{pop}}$ for the same sample. Most GCs have $\Psi < 1$ due to the preferential loss of low-mass stars through internal dynamical processes (Baumgardt & Makino 2003; Kruijssen & Mieske 2009), while most high-mass UCDs have $\Psi > 1$. For the low-mass UCDs there is a hint of a bimodal distribution in Ψ with one population having Ψ similar to GCs and the other having an elevated Ψ like the high-mass UCDs (Mieske et al. 2013). This finding hints at at least two

different formation processes for UCDs.

A number of possible explanations for the elevated M/L ratios of UCDs have been suggested depending on the assumed formation mechanisms of UCDs (which anticipates the discussion of UCD formation mechanisms in Section 1.2). UCDs may simply be giant GCs formed in the most extreme starbursts during galaxy formation, the remnant nuclei of galaxies disrupted by tidal processes or 'hyper-compact stellar systems' bound to recoiling SMBHs that were ejected from the centres of massive galaxies. Due to the extreme environments in which UCDs may form the stellar initial mass function (IMF) may change, resulting in an overabundance of massive stellar remnants (Murray 2009; Dabringhausen et al. 2009, 2010) or low-mass stars (Mieske & Kroupa 2008). This explanation is applicable to all UCD formation mechanisms. The viability of this explanation in relation to massive stellar remnants is unclear, with evidence both for (Dabringhausen et al. 2012) and against (Phillipps et al. 2013) a top-heavy IMF. For UCDs that form by the tidal stripping of nucleated galaxies other explanations include remnant dark matter haloes or central black holes from the host galaxies and unbound stars from the tidal stripping process which have not had sufficient time to escape from the UCDs (which are further discussed in Section 1.2.1).

1.2 Theories of ultra-compact dwarf galaxy formation

1.2.1 Nuclei of disrupted galaxies

Given their similar masses and velocity dispersions to nuclear clusters, one of the first suggestions for the origin of UCDs is that they are the nuclei of disrupted dwarf galaxies (referred to as the tidal stripping or 'threshing' scenario; Hilker et al. 1999a; Drinkwater et al. 2000; Bekki, Couch & Drinkwater 2001; Phillipps et al. 2001). UCDs have similar masses (Figure 1.1), internal velocity dispersions (Drinkwater et al. 2003), colour–magnitude trends (Côté et al. 2006; Evstigneeva et al. 2008; Brodie et al. 2011) and metallicities and ages (Paudel et al. 2010; Brodie et al. 2011; Chilingarian et al. 2011; Francis et al. 2012) to nuclear clusters. UCDs lie above the metallicity–luminosity trend for early-type galaxies (Figure 1.3), as would be expected if UCDs are tidally stripped dwarf galaxies since the luminosity would

decrease while the metallicity remains high. Some UCDs are surrounded by stellar haloes which might be the remnants of the stripped dwarf galaxies (Drinkwater et al. 2003; Haşegan et al. 2005; Chilingarian & Mamon 2008; Evstigneeva et al. 2008; Chiboucas et al. 2011). Irregular objects with asymmetric extensions have been found which may be dwarf galaxy nuclei undergoing tidal stripping (Richtler et al. 2005; Brodie et al. 2011; Annibali et al. 2012). Simulations have shown that nucleated dwarf galaxies orbiting in a galaxy cluster on highly eccentric orbits become tidally stripped and form objects with sizes and luminosities similar to UCDs (Bekki et al. 2001, 2003).

In the Milky Way, GCs such as ω Cen (Lee et al. 1999; Hilker & Richtler 2000) are thought to form via such a process and may be considered to be 'low-mass' UCDs, while the ongoing formation of such a low-mass UCD may be observed in the M54–Sagittarius dwarf galaxy system (Ibata et al. 1997). All these GCs have either stellar populations with multiple ages or stellar populations with a spread in heavy element abundances indicating enrichment by supernovae. Since most GCs have no intrinsic spread in heavy elements, this suggest these GCs must have formed at the centre of dwarf galaxies (e.g. Da Costa, Held, & Saviane 2014).

A tidal stripping origin for UCDs also offers a number of solutions for the elevated mass-to-light ratios of UCDs. UCDs formed by tidal stripping may retain a remnant dark matter halo, assuming the central dark matter concentration was enhanced during the formation of the progenitor nucleus via the infall of gas (Baumgardt & Mieske 2008; Goerdt et al. 2008). However for UCDs with a measurable velocity dispersion profile no evidence of an extended dark matter halo has been found (Frank et al. 2011; Seth et al. 2014). Alternatively, UCDs formed by tidal stripping may contain supermassive black holes (SMBHs) from their progenitor galaxies (Mieske et al. 2013; Seth et al. 2014). Recently, Seth et al. (2014) discovered the first UCD (M60-UCD1) to host a SMBH, providing direct support for SMBHs as a possible explanation for the elevated dynamical mass-to-light ratios of UCDs (although interestingly the dynamical mass of M60-UCD1 is consistent with the stellar mass predicted from population synthesis models, Strader et al. 2013) and also direct evidence of the formation of a UCD by tidal stripping. The most recent suggestion is that the elevated dynamical mass-to-light ratios of UCDs are due to unbound material left over from tidal

stripping (Forbes et al. 2014).

However, a number of potential problems with the tidal stripping scenario still remain. UCDs have sizes a factor of two larger than nuclear clusters at the same luminosity (Evstigneeva et al. 2008), which suggests that if nuclei are UCD progenitors the nuclei must undergo expansion during tidal stripping. A population of extended, low-mass UCDs has been found in the Virgo cluster (Brodie et al. 2011) and it is unclear if such objects can form by tidal stripping. Although early studies found the predicted number of UCDs formed by tidal stripping matched observations (Bekki et al. 2003; Goerdt et al. 2008), comparisons with more complete numbers of UCDs found tidal stripping cannot account for all the observed UCDs (Thomas, Drinkwater & Evstigneeva 2008).

1.2.2 Giant globular clusters

Perhaps the simplest explanation for the formation of UCDs is that they are the high-mass end of the GC mass function observed around galaxies with rich GC systems (Mieske, Hilker & Infante 2002; Mieske, Hilker & Misgeld 2012). There is a smooth transition in sizes, luminosities and numbers between GCs and UCDs (e.g. Mieske et al. 2004a; Gregg et al. 2009, see also Figure 1.1) and UCDs are consistent with being the bright tail of the GC population (Mieske et al. 2012).

UCDs have similar sizes and masses to young massive clusters (YMCs; Bastian et al. 2006; Kissler-Patig, Jordán, & Bastian 2006) which might be very young analogues of GCs. Recent simulations show gas rich galaxy mergers may form YMC- and UCD-like objects via a merger of gas clouds or a violent expansion after flying through the galactic centre (Renaud, Bournaud, & Duc 2015). In strong starbursts, star clusters do not form in isolation, but in complexes containing dozens and up to several hundred star clusters (e.g. Whitmore et al. 1999). These systems of star clusters might merge to become YMCs and UCDs (Kroupa 1998; Fellhauer & Kroupa 2002, 2005) which might explain the large range of sizes for GCs and UCDs (Brüns et al. 2011; Brüns & Kroupa 2012). Alternatively, all star clusters may have formed with an initial size–mass relation with the lowest mass objects evolving off this relation and towards a constant size due to dynamical and stellar evolution (Gieles et al.

2010).

1.2.3 Hyper-compact stellar systems

Related to UCDs hosting central SMBHs from disrupted galaxies is the possibility of 'hyper-compact stellar systems' bound to recoiling SMBHs that were ejected from the centres of massive galaxies (Merritt, Schnittman, & Komossa 2009). However in this case the mass of stars accompanying the black holes is expected to be $\sim 10^{-2}$ times the black hole mass. This is in conflict with the observed M/L ratios of UCDs, which would have to be far higher than observed if UCDs host such massive black holes.

1.2.4 Multiple formation channels

As more UCDs are found, it is becoming apparent there is no single formation mechanism for UCDs but that they are a *superposition* of giant GCs and stripped dwarf galaxies (Haşegan et al. 2005; Mieske et al. 2006; Chilingarian et al. 2011; Da Rocha et al. 2011; Norris & Kannappan 2011; Norris et al. 2014). Although the formation mechanism of a few peculiar objects can be determined (e.g. Norris & Kannappan 2011; Seth et al. 2014), disentangling the individual formation mechanism of most UCDs is almost impossible due to the similar predictions of internal UCD properties from each formation scenario. Determining the origin of UCDs therefore requires detailed predictions of how much each mechanism contributed to UCD populations.

1.3 Key science questions

Although there have been many studies of UCDs in recent years, a number of questions about their formation still remain. This thesis concentrates on the formation of UCDs by tidal stripping of dwarf galaxies. This scenario for UCD formation has the largest uncertainty remaining for its predictions, particularly with respect to the findings of recent observational studies.

(i) Can tidal stripping account for the sizes and masses of all observed UCDs?

UCDs have sizes a factor of two larger than nuclear clusters at the same luminosity (Evstigneeva et al. 2008), which suggests that if nuclei are UCD progenitors the nuclei must undergo expansion during tidal stripping. Additionally, a population of extended, low-mass UCDs ($R_{\mathrm{eff}} \sim 40$ pc, $M_V \sim -9$ mag) have been found in the Virgo cluster (Brodie et al. 2011). These objects have sizes about ten times that of nuclear clusters of similar luminosities. However, most UCDs and similar mass nuclear clusters have relaxation times greater than a Hubble time (Misgeld & Hilker 2011) meaning significant expansion by internal dynamical processes is unlikely. Since nuclear clusters dominate the mass at the centre of galaxies, the removal of the host galaxy is unlikely to significantly affect them unless the stars in nuclear clusters are on orbits which take them to many times the effective radius of the nuclear cluster. Whether tidal stripping can account for UCDs of all sizes and masses is thus unclear.

(ii) What is the number of UCDs predicted by tidal stripping?

There have been a number of studies investigating whether tidal stripping can account for the number of UCDs observed. Bekki et al. (2003) and Thomas et al. (2008) modelled dwarf galaxies as test particles in a static potential and used a 'threshing radius' to decide if a UCD has formed or not. Goerdt et al. (2008) used the orbital distributions of particles in a cosmological simulation combined with simulations of disc galaxies and dark matter haloes being disrupted in a static galaxy cluster to predict the number of UCDs formed. Both Bekki et al. and Goerdt et al. found their predictions matched observations, however, these studies were based on a very small sample of UCDs known at the time. Thomas et al., using a larger UCD sample, extended the analysis to lower luminosity UCDs and dwarf galaxies and found a static threshing model underpredicts the number of UCDs at radii greater than 30 kpc in the Fornax cluster.

Although they are simple to implement, static models of UCD formation in galaxy clusters have a number of disadvantages. As noted by Thomas et al. (2008), static models do not take into account UCD formation that may have occurred within smaller subclusters that later fell into the main cluster. Galaxy clusters are expected to form

by many mergers which in the process may change the orbital distribution of galaxies within the cluster. Therefore, predictions of UCD properties within the context of cosmologically motivated galaxy cluster formation are needed to provide a definite answer on the number of UCDs expected to form via tidal stripping.

(iii) How do ultra-compact dwarf galaxies form?

Addressing the two previous questions will enable us to answer the question of how UCDs form. If tidal stripping cannot account for the numbers and physical properties of observed UCDs then it is clearly not a dominant mechanism for UCD formation. In this case, the question is then what fraction of UCDs formed via each mechanism. Alternatively, if tidal stripping can account for all observed UCDs the question is what limits the sizes, masses and numbers of GCs.

1.4 Thesis outline

This thesis aims to test the formation scenarios of UCDs using theoretical methods. In Chapter 2 we address the first key science question and perform numerical simulations of nucleated dwarf galaxies being disrupted in a galaxy cluster to predict the sizes and masses of UCDs formed by tidal stripping and test whether they are consistent with the properties of observed UCDs. In Chapter 3 we address the recent claim that UCDs formed by tidal stripping have elevated dynamical mass-to-light ratios. In Chapter 4 we address the second key science question and present the first work to predict the properties of UCDs using a cosmologically motivated galaxy formation model. In Chapter 5 we compare the predictions of our model in Chapter 4 with the observed properties of UCDs in the local universe. In Chapter 6 we present a new method to include tidal stripping in semi-analytic models of galaxy formation. Finally, Chapter 7 summarises how this work addresses our key science questions, in particular the question of the origin of UCDs, and what future work remains.

2

Paper one: Ultra-compact dwarf galaxy formation by tidal stripping of nucleated dwarf galaxies

Pfeffer J., Baumgardt H., 2013, MNRAS, 433, 1997: *Ultra-compact dwarf galaxy formation by tidal stripping*

Ultra-compact dwarf galaxy formation by tidal stripping of nucleated dwarf galaxies

J. Pfeffer* and H. Baumgardt

School of Mathematics and Physics, The University of Queensland, Brisbane, QLD 4072, Australia

ABSTRACT

Ultra-compact dwarf galaxies (UCDs) and dwarf galaxy nuclei have many common properties, such as internal velocity dispersions and colour–magnitude trends, suggesting tidally stripped dwarf galaxies as a possible UCD origin. However, UCDs typically have sizes more than twice as large as nuclei at the same luminosity. We use a graphics processing unit (GPU)-enabled version of the particle-mesh code SUPERBOX to study the possibility of turning nucleated dwarf galaxies into UCDs by tidally stripping them in a Virgo-like galaxy cluster. We find that motion in spherical potentials, where close passages happen many times, leads to the formation of compact ($r_h \lesssim 20$ pc) star clusters/UCDs. In contrast, orbital motion where close passages happen only once or twice leads to the formation of extended objects which are large enough to account for the full range of observed UCD sizes. For such motion, we find that dwarf galaxies need close pericentre passages with distances less than 10 kpc to undergo strong enough stripping so that UCD formation is possible. As tidal stripping produces objects with similar properties to UCDs, and our estimates suggest dwarf galaxies have been destroyed in sufficient numbers to explain the observed number of UCDs in M87, we consider tidal stripping to be a likely origin of UCDs. However, comparison with cosmological simulations is needed to determine if the number and spatial distribution of UCDs formed by tidal stripping matches the observations of UCDs in galaxy clusters.

Key words: methods: numerical – galaxies: dwarf – galaxies: formation – galaxies: interactions – galaxies: star clusters: general.

1 INTRODUCTION

Ultra-compact dwarf galaxies (UCDs) are a class of stellar systems that was discovered in the Fornax galaxy cluster more than a decade ago (Hilker et al. 1999a; Drinkwater et al. 2000). Since then, UCDs have been discovered in other galaxy clusters (Mieske et al. 2004, 2007; Haşegan et al. 2005; Jones et al. 2006; Misgeld et al. 2011; Madrid 2011; Penny, Forbes & Conselice 2012), galaxy groups (Evstigneeva et al. 2007b; Da Rocha et al. 2011), as well as isolated spiral galaxies (Hau et al. 2009). UCDs are typically defined to have half-light radii $7 \lesssim r_h/\mathrm{pc} \lesssim 100$ and masses $M \gtrsim 2 \times 10^6 \ \mathrm{M_\odot}$ (Mieske et al. 2008), making them an intermediate object between globular clusters (GCs) and dwarf galaxies.

The formation mechanism of UCDs is currently unknown, although a number of scenarios have been proposed. The simplest explanation is that they are the high-mass end of the GC mass function observed around galaxies with rich GC systems (Mieske, Hilker & Infante 2002; Mieske, Hilker & Misgeld 2012). Since UCDs have larger sizes than typical GCs, they may form from the merger of many GCs (Kroupa 1998; Fellhauer & Kroupa 2002; Brüns et al. 2011; Brüns & Kroupa 2012). Alternatively, they could be dwarf galaxies stripped by tidal interactions such that only their central nuclei remain, referred to as the tidal stripping or 'threshing' scenario (Bassino, Muzzio & Rabolli 1994; Bekki, Couch & Drinkwater 2001; Bekki et al. 2003; Drinkwater et al. 2003). There is also evidence suggesting UCDs are formed by a combination of mechanisms rather than a single one (Mieske et al. 2006; Brodie et al. 2011; Chilingarian et al. 2011; Norris & Kannappan 2011).

Tidally stripped dwarf galaxies, in particular nucleated dwarf elliptical galaxies (dE,Ns), have been proposed as UCD progenitors for a number of reasons: UCDs and dwarf elliptical nuclei have similar internal velocity dispersions (Drinkwater et al. 2003) and colour–magnitude trends (Côté et al. 2006; Evstigneeva et al. 2008; Brodie et al. 2011). UCDs lie above the metallicity–luminosity trend for early-type galaxies and have a similar metallicity to dwarf galaxies (Chilingarian et al. 2011; Francis et al. 2012). Such a situation would be expected if UCDs are tidally stripped dwarf galaxies since the luminosity would decrease while the metallicity remains high. In addition, some UCDs are surrounded by stellar haloes which might be the remnants of the stripped dwarf galaxies (Drinkwater et al. 2003; Haşegan et al. 2005; Chilingarian & Mamon 2008;

---

*E-mail: j.pfeffer@uq.edu.au

Evstigneeva et al. 2008; Chiboucas et al. 2011). Finally, irregular objects with asymmetric extensions have been found which may be dwarf galaxy nuclei undergoing tidal stripping (Richtler et al. 2005; Brodie et al. 2011).

Simulations of UCD formation in the tidal stripping scenario were first performed by Bekki et al. (2001, 2003), who showed that nucleated dwarf galaxies orbiting in a galaxy cluster on highly eccentric orbits are almost completely tidally stripped, with only the nucleus surviving. In this case the size and luminosity of the stripped galaxy are such that it would be classified as a UCD. More recently, Goerdt et al. (2008) sought to understand UCD formation by tidal stripping within the context of the cold dark matter (CDM) model, and found the cosmological prediction matches the observed spatial distribution of UCDs.

Despite this, a number of potential problems with the tidal stripping scenario still remain unanswered. Brodie et al. (2011) have recently found a population of extended, low-mass UCDs ($r_h \sim$ 40 pc, $M_V \sim -9$) in the Virgo galaxy cluster which do not follow the size–magnitude relation observed for the most massive UCDs (Mieske et al. 2006; Evstigneeva et al. 2008). Such objects may form from merged star cluster complexes (Brüns et al. 2011; Brüns & Kroupa 2012); however it is unclear whether they can be formed in either the giant GC or tidal stripping scenario.

UCDs are typically approximately two times larger than dE nuclei at the same luminosity (Evstigneeva et al. 2008). This suggests that if nuclei are the UCD progenitors the nuclei must undergo expansion, or some other process, during tidal stripping. The situation is even more pronounced for nuclei and UCDs with $M_V > -11$: at this luminosity the typical half-light radius of nuclei is ~4 pc, while UCDs extend up to ~40 pc (Brodie et al. 2011).

All tidal stripping simulations to date have been performed in static, spherical galaxy potentials with a constant pericentre and apocentre (Bekki et al. 2001, 2003; Goerdt et al. 2008), thus it is uncertain what effect an evolving or triaxial potential has on the number and properties of the UCDs that form in this scenario. In addition, these studies did not investigate if tidal stripping of dwarf galaxies affects the nucleus size, thus the origin of the size difference between UCDs and dE nuclei is still uncertain.

In this paper we perform high-resolution *N*-body simulations of a nucleated dwarf galaxy being stripped via tidal interactions to test whether the extended, low-mass UCDs can be formed in the tidal stripping scenario. We simulate orbits with fixed pericentres and apocentres, as well as orbits that mimic 'box orbits' in an evolving or triaxial potential, to study the effect of the dwarf galaxy's orbit on the final size of the stripped dwarf galaxy.

2 THE SIMULATIONS

2.1 Simulation code

All simulations were performed with a graphics processing unit (GPU) enabled version of the particle-mesh code SUPERBOX (Fellhauer et al. 2000) on NVIDIA GPUs. SUPERBOX uses a leap-frog scheme to integrate the motion of particles and has high-resolution subgrids which stay focused on the simulated objects. In SUPER-BOX, the density grids are derived using a nearest-grid-point (NGP) scheme. Potentials are calculated from the density grids using a Fast Fourier Transformation, which are performed in parallel across the subgrids using multiple GPUs. The forces are calculated using an NGP scheme based on the second derivatives of the potential. We have increased the subgrid number from 2 to 4 in order to accurately resolve the innermost regions of our dE,N models and reduce edge

effects for particles crossing between subgrids. For the simulations we use 64^3 grid points for all subgrids with an innermost subgrid size of 0.013 kpc for model 1 and 0.025 kpc for models 2 and 3, and subsequent grid sizes of 0.05, 0.5, 4 and 40 kpc for all models. Time-steps are chosen such that no particle moves more than a grid cell length of the smallest subgrid per time-step. We use time-steps of 0.004 Myr, 0.008 Myr and 0.006 Myr for dE,N models 1, 2 and 3, respectively.

2.2 Cluster mass profile

In order to have a realistic mass profile for the galaxy cluster, we model M87, the central galaxy of the Virgo cluster, based on the observations of Kormendy et al. (2009) and Murphy, Gebhardt & Adams (2011) using Sérsic and logarithmic profiles for the stellar and dark matter components, respectively. The Sérsic (1963, 1968) surface brightness profile is given by

$$I(R) = I_0 e^{-b(R/R_e)^{1/n}} \tag{1}$$

where I_0, R_e and n are the central intensity, the effective half-light radius and the *Sérsic index* describing the curvature of the profile, respectively. The constant b is chosen such that R_e contains half the projected light and we use the relation between b and n found by Prugniel & Simien (1997). For the simulations the Sérsic surface brightness profile is converted into a potential using the method of Terzić & Graham (2005). We adopt for the stellar component a Sérsic index $n = 11.84$, an effective radius $R_e = 16.22$ kpc and a central intensity $I_0 = 2.732 \times 10^{17}$ L$_\odot$ kpc^{-2}, consistent with Kormendy et al. (2009), and a mass-to-light ratio $\Upsilon = 9.1$ (M/L)$_\odot$ consistent with Murphy et al. (2011).

The logarithmic potential of the dark matter halo is given by

$$\phi(r) = \frac{v_c^2}{2} \ln(r_c^2 + r^2) \tag{2}$$

where r_c is the core radius and v_c is the asymptotic circular velocity. We adopt a scale radius $r_c = 36$ kpc and a circular velocity of $v_c = 800$ km s^{-1} consistent with Murphy et al. (2011).

For the cluster potential we choose a static, spherical potential similar to what has been chosen by other authors (Bekki et al. 2001, 2003; Goerdt et al. 2008). In order to add a time varying or triaxial component to the cluster potential it would be necessary to add more parameters to the simulations. In addition, in order to take into account substructure in the cluster which could perturb the orbits of the dwarf galaxy, it would be necessary to simulate a full galaxy cluster. Therefore, to reduce unnecessary complexity in the simulations, we mimic these possible situations by changing the orbit of the dE,N during the simulations. We discuss the dwarf galaxy orbits in more detail in Section 2.4.

2.3 Nucleated dwarf ellipticals

We construct three models for dE, Ns according to values observed for dEs in the Virgo cluster. The model number for each simulation is shown in Column 3 of Table 1. The nucleus is modelled using a King (1962) profile with a concentration parameter $c = 1.5$, with the value of c chosen since it is a typical value for GCs (Trager, King & Djorgovski 1995) which are similar in size to dE nuclei. An absolute *V*-band magnitude $M_V = -10$ is used for the nucleus of dE,N models 1 and 2, and $M_V = -12$ is used for model 3. For dE,N model 1 we use a nucleus half-light radius $r_h = 4$ pc (the average radius at this luminosity; see Fig. 2), while for models 2 and 3 we use $r_h = 10$ pc. The magnitude $M_V = -10$ is chosen to be

Table 1. Parameters of the initial dwarf galaxy (Columns 2–5) and the resulting UCD (Columns 6–8) for all simulations. dE,N model 1 has a nucleus half-light radius $r_{\rm h} = 4$ pc and magnitude $M_V = -10$ (nucleus mass $M_{\rm nuc} = 2.56 \times 10^6$ M$_\odot$). dE,N model 2 has a nucleus half-light radius $r_{\rm h} = 10$ pc and magnitude $M_V = -10$ (nucleus mass $M_{\rm nuc} = 2.56 \times 10^6$ M$_\odot$). dE,N model 3 has a nucleus half-light radius $r_{\rm h} = 10$ pc and magnitude $M_V = -12$ (nucleus mass $M_{\rm nuc} = 1.62 \times 10^7$ M$_\odot$). Masses are converted to magnitudes assuming a mass-to-light ratio $\Upsilon = 3$ (M/L$_V$)$_\odot$.

Simulation no.	Orbit type	dE,N model	Apocentre (kpc)	Pericentre (kpc)	Close pericentre passages	Final $r_{\rm h}$ (pc)	Final M_V (mag)	Formation time (Gyr)	Simulation time (Gyr)
1	Elliptic	1	50	2	5	3.9	−9.77	0.9	2.2
2	Elliptic	1	50	5	7	5.5	−10.10	1.3	2.2
3	Elliptic	1	50	10	12	6.6	−10.12	2.3	4.2
4	Elliptic	1	50	20	27	8.6	−10.14	5.7	7.5
5	Elliptic	1	100	2	5	4.2	−9.71	1.6	3.9
6	Elliptic	1	100	5	9	6.1	−10.07	2.9	3.9
7	Elliptic	1	100	10	15	7.6	−10.14	5.0	5.9
8	Elliptic	2	50	2	6	5.6	−9.02	1.1	2.2
9	Elliptic	2	50	5	7	9.5	−9.86	1.3	2.2
10	Elliptic	2	50	10	11	11.7	−10.02	2.1	4.2
11	Elliptic	2	50	20	25	18.7	−10.32	5.2	7.5
12	Elliptic	2	100	2	6	5.9	−9.07	1.9	3.9
13	Elliptic	2	100	5	9	10.3	−9.90	2.9	3.9
14	Elliptic	2	100	10	17	15.2	−10.19	5.6	5.9
15	Elliptic	3	50	2	5	7.0	−11.43	0.9	2.2
16	Elliptic	3	50	5	6	12.0	−12.01	1.1	2.2
17	Elliptic	3	50	10	9	15.5	−12.13	1.7	4.2
18	Elliptic	3	50	20	15	24.3	−12.30	3.1	7.5
19	Elliptic	3	100	2	5	7.7	−11.31	1.6	3.9
20	Elliptic	3	100	5	6	13.9	−12.04	1.9	3.9
21	Elliptic	3	100	10	11	19.3	−12.16	3.6	5.9
22	Box	1	50	2	1	28.3	−10.84	2.0	2.2
23	Box	1	50	2	2	7.7	−10.30	1.3	2.2
24	Box	1	50	5	2	49.8	−11.10	1.1	2.2
25	Box	1	50	5	3	14.6	−10.61	1.1	2.2
26	Box	1	100	2	1	94.1	−11.36	1.9	3.9
27	Box	1	100	2	2	9.7	−10.33	2.2	3.9
28	Box	1	100	5	2	179.0	−12.22	1.6	3.9
29	Box	1	100	5	3	58.1	−11.11	2.6	3.9
30	Box	2	50	2	1	46.3	−10.86	1.2	2.2
31	Box	2	50	2	2	13.4	−10.09	1.4	2.2
32	Box	2	50	5	2	59.6	−11.10	0.9	2.2
33	Box	2	50	5	3	25.1	−10.58	1.1	2.2
34	Box	2	100	2	1	98.2	−11.37	1.9	3.9
35	Box	2	100	2	2	17.1	−10.21	2.2	3.9
36	Box	2	100	5	2	168.0	−12.13	1.7	3.9
37	Box	2	100	5	3	65.8	−11.12	2.0	3.9
38	Box	3	50	2	1	28.7	−12.50	1.2	2.2
39	Box	3	50	2	2	15.0	−12.15	0.5	2.2
40	Box	3	50	5	2	32.1	−12.59	1.3	2.2
41	Box	3	50	5	3	20.5	−12.38	0.7	2.2
42	Box	3	100	2	1	65.8	−12.80	1.9	3.9
43	Box	3	100	2	2	18.7	−12.21	1.0	3.9
44	Box	3	100	5	2	118.0	−13.08	2.2	3.9
45	Box	3	100	5	3	37.7	−12.60	1.6	3.9

comparable to the low-luminosity UCDs observed by Brodie et al. (2011), even though the least luminous UCDs observed by Brodie et al. have $M_V = -9$. We chose $M_V = -12$ to be comparable to a typical massive UCD. Note that the most massive UCDs have $M_V = -13$.

The main stellar component of the dwarf galaxy, referred to hereafter as the 'envelope', is modelled using a Sérsic profile. For dE,N models 1 and 2 we use a Sérsic index $n = 1.5$ and an effective radius $R_{\rm e} = 850$ pc, which are the average values observed by Grant, Kuipers & Phillipps (2005) and Geha, Guhathakurta & van der

Marel (2003) for dEs in the Virgo cluster, respectively, while for model 3 we use a Sérsic index $n = 1.5$ and an effective radius $R_{\rm e} = 2000$ pc. The central intensity is chosen such that the nucleus-to-envelope luminosity ratio is 0.3 per cent, the mean value for dEs in Virgo (Côté et al. 2006), giving an absolute V-band magnitude $M_V = -16.3$ for dE,N models 1 and 2, and $M_V = -18.3$ for dE,N model 3.

A mass-to-light ratio $\Upsilon = 3$ (M/L$_V$)$_\odot$ is set for both the nucleus and envelope, which is consistent with the average values observed by Chilingarian (2009). In order to reduce the number of particles

needed, we do not include a dark matter halo for our dE,N models. We expect that including a cored dark matter profile in the models would not significantly affect our results for UCD sizes and masses since we are only interested in the centre of the model where the fraction of dark matter to stellar matter is lowest. This may not be the case if a cuspy dark matter profile was used since dwarf galaxies with cuspy dark matter profiles are more resilient to tidal stripping (Bekki et al. 2003; Peñarrubia et al. 2010). However, observations suggest dE galaxies do not have a significant amount of dark matter within one effective radius (Geha, Guhathakurta & van der Marel 2002), more consistent with a cored profile, justifying our neglect of a dark matter halo.

Although the simulated UCD sizes and masses would be unaffected by a dark matter halo, it is likely the inclusion of one would change the UCD formation time due to the dark matter shielding the stellar component from disruption (e.g. in Fig. 5 the envelope shields the nucleus during tidal stripping). Since a dark matter halo would be much more extended than the stellar component, we expect one to two close passages would be necessary to disrupt the halo and therefore add ~0.5 Gyr to the formation time. However, as a dwarf galaxy sized halo disrupts at a radius of a few hundred kpc in a galaxy cluster (Goerdt et al. 2008), it is possible that the halo is stripped before the dwarf galaxy reaches the centre of the cluster.

We create an *N*-body representation for the dwarf galaxies using the following method adapted from Hilker et al. (2007):

(i) Deprojection of the two-dimensional surface density profile by means of the Abel integral equation (see equation 1 B-57b of Binney & Tremaine 1987) into a three-dimensional density profile.

(ii) Calculation of the cumulative mass function $M(< r)$ and the potential energy $\phi(r)$ from the three-dimensional density profile. From these the energy distribution function $f(E)$ is then calculated with the help of equation (4-140a) from Binney & Tremaine (1987), assuming isotropic orbits for the stars.

(iii) Creation of an *N*-body representation of the dE using the deprojected density profile and the distribution function.

The modelling is based on the assumptions of spherical symmetry and an underlying isotropic velocity distribution. For all dE,N models 10^7 particles with equal masses were distributed, corresponding to particle masses of 85.7 $M_\odot$ with 2.56×10^6 $M_\odot$ contained in the nucleus for dE,N models 1 and 2, and particle masses of 541 $M_\odot$ with 1.62×10^7 $M_\odot$ contained in the nucleus for model 3.

To test the stability of the models they were evolved in isolation for 2 Gyr. For model 2 the Lagrange radii are conserved to better than 4 per cent. For model 1 the half-light radius of the nucleus increases by 13 per cent due to numerical relaxation; however outside the central 30 pc the maximum radial change is less than 4 per cent. For model 3 the half-light radius of the nucleus increases by 12 per cent due to numerical relaxation while outside the central 45 pc the maximum radial change is less than 4 per cent.

2.4 Dwarf galaxy orbits

We test for nucleus expansion in the tidal stripping scenario with two types of orbits. First we assume that dE galaxies orbit the central galaxy on elliptic orbits with fixed apocentre and pericentre distances. For all dE,N models we test orbits with apocentres of 50 and 100 kpc and pericentres of 2, 5, 10 and 20 kpc. Such highly eccentric orbits are predicted by ΛCDM simulations for sub-haloes orbiting larger haloes (Ghigna et al. 1998).

Since elliptical galaxies are expected to reside in triaxial potentials and form through galaxy mergers, galaxy cluster potentials will

be neither static nor spherical. The orbits of dwarf galaxies in such clusters may be chaotic with strongly varying pericentres distances during successive passages, due to either the triaxial potential or encounters with other galaxies during the orbit. Thus in addition to the elliptic orbit, we consider the case where only a few encounters between the dE and central galaxy will happen with very small pericentre distances, and at all other times the dE is far from the central galaxy so that tidal effects are not important. We mimic such a scenario by simulating 1–3 pericentre passages and then placing the object on a circular orbit at apocentre to allow enough time for unbound particles to escape. This is referred to hereafter as the 'box' orbit. For all dE,N models we test box orbits with apocentres of 50 and 100 kpc and pericentres of 2 and 5 kpc. Note that we do not require that the orbits are circular (which is highly unlikely in ΛCDM), but only that the pericentre increases to $\gtrsim$10–20 kpc.

These two orbits represent the most extreme cases in the tidal stripping scenario, i.e. galaxies may have either many pericentre passages at small radii, or many passages at large radii and very few at small radii. It is probable that real UCDs will be on orbits somewhere in between these extremes.

The full list of simulations performed is shown in Table 1. The UCD formation time is defined as the time when the change in half-mass radius and mass within the tidal radius (calculated according to King 1962) of the resulting object fall below 10 per cent between successive passages, while the final half-light radius and mass of the object is calculated at the end of the simulation (Column 10 in Table 1). Since the change in the model is small at the end of the simulation (see Fig. 5) we can be confident that a longer simulation time will not significantly change our results. For the elliptic orbits the number of pericentre passages is the number before formation occurs and not the total number during the simulation.

3 RESULTS

3.1 Evolution of galaxy size

Fig. 1 shows a comparison of the final half-light radii for the simulated UCDs. Except for models on an elliptic orbit with a 2 kpc pericentre, all simulated UCDs have sizes larger than the initial model nucleus. All simulations, except for models on a box orbit with a 100 kpc apocentre and two pericentre passages at 5 kpc (simulations 26, 34 and 42), form objects with half-light radii less than 100 pc. For both elliptic and box orbits the half-light radius increases with pericentre distance since models with a small pericentre distance suffer more tidal stripping than those with a large pericentre distance. For a given pericentre distance, 100 kpc apocentres tend to produce larger half-light radii than 50 kpc apocentres because particles require more energy to escape the dwarf galaxy at a large galactocentric radius than at a small radius. Models on box orbits produce both larger half-light radii and a larger range of half-light radii than those on elliptic orbits ($10 \lesssim r_{\rm h}/{\rm pc} \lesssim 170$ for box orbits compared to $4 \lesssim r_{\rm h}/{\rm pc} \lesssim 25$ for elliptic orbits) due to box orbits having fewer close pericentre passages and therefore suffering less tidal stripping. In the box orbit scenario, an increase in the number of close pericentre passages results in a decrease in half-light radius due to the inner region of the model becoming more susceptible to tidal effects once the outer region has been removed.

Comparison of *V*-band magnitude and half-light radius between the simulated UCDs and observed GCs, UCDs and dE nuclei is shown in Fig. 2. Note that the final UCD in the simulations is a combination of the remaining particles from both the nucleus and the envelope and therefore can be more massive than the initial
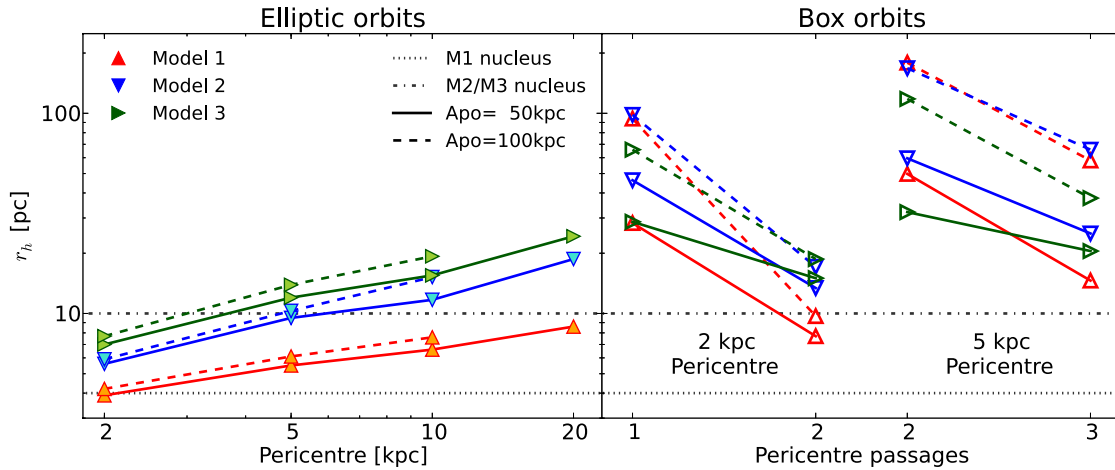
Figure 1. Comparison of the final half-light radii for all simulated UCDs in dependence of orbital type, dE,N model and apocentre distance. The left-hand panel shows the effect of pericentre distance for models on elliptic orbits, while the right-hand panel shows the effect of pericentre distance and number of close pericentre passages for models on box orbits. Symbols are as in the legend, where triangle-up (red), triangle-down (blue) and triangle-right (green) denote dE,N model 1 (nucleus $r_h = 4\,\mathrm{pc}$, $M_V = -10\,\mathrm{mag}$), model 2 (nucleus $r_h = 10\,\mathrm{pc}$, $M_V = -10\,\mathrm{mag}$) and model 3 (nucleus $r_h = 10\,\mathrm{pc}$, $M_V = -12\,\mathrm{mag}$), respectively, and orbits with a 50 (100) kpc apocentre are represented by a solid (dashed) line. The dotted and dash–dotted lines show the initial half-light radius of the nucleus for dE,N models 1 and 2/3, respectively.
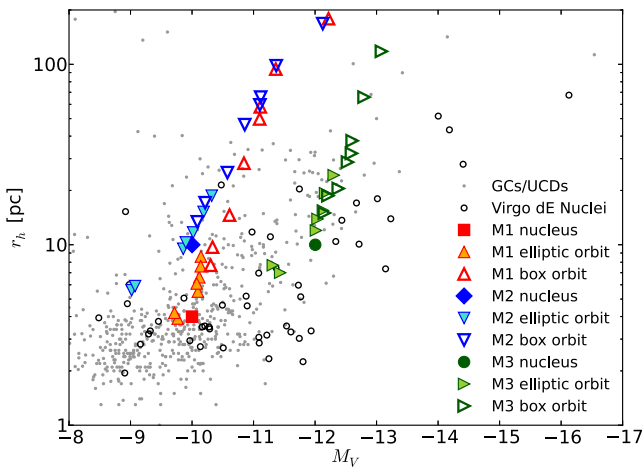

Figure 2. Final *V*-band magnitude and half-light radius for the simulated UCDs compared with GCs and UCDs from the nearby Universe (Brodie et al. 2011, grey points), and Virgo dwarf elliptical nuclei (Côté et al. 2006, open black circles). The nuclei are converted to *V*-band photometry from *g* and *z* bands using the relation derived for M87 GCs by Peng et al. (2006). Symbols and colours are as in the legend, where M1, M2 and M3 are dE,N models 1, 2 and 3 runs, respectively, and the original model nuclei sizes are represented by a red square (M1), blue diamond (M2) and green circle (M3). The simulations are converted to a luminosity assuming a mass-to-light ratio $\Upsilon = 3\,(\mathrm{M/L_V})_\odot$.

nucleus. For dE nuclei with $M_V > -11$ the median half-light radius is 3.5 pc, and thus our model with a nucleus $r_h = 4\,\mathrm{pc}$ (model 1) is more comparable to present-day nuclei than the model with $r_h = 10\,\mathrm{pc}$ (model 2). For dE nuclei with $M_V < -11$ the median half-light radius is 7.5 pc and thus comparable to the model with a nucleus $M_V = -12$ and $r_h = 10\,\mathrm{pc}$ (model 3). In the elliptic orbit scenario the models have a maximum final half-light radius approximately less than two times the original nucleus size, and therefore can only match observed UCDs if dE nuclei have initial half-light radii $r_h \gtrsim 10\,\mathrm{pc}$. In principle the extended UCDs could be formed on elliptic orbits with pericentres larger than 20 kpc, however as formation time scales exponentially with pericentre distance, while UCD half-light

radius scales as a power law with exponent ~ 0.5 with pericentre distance, the formation time required becomes much larger than a Hubble time for a dE,N with a nucleus size of $r_h \sim 4\,\mathrm{pc}$. In contrast, box orbits can produce half-light radii up to 40 times initial size of the model nucleus, and can produce the full range of observed UCD half-light radii with a nucleus half-light radius of either 4 or 10 pc. For model 3 the UCD sequence closely matches the most extended and massive UCDs ($-14 < M_V < -12.5$ and $60 < r_h/\mathrm{pc} < 100$).

The morphological evolution from dE to UCD for models 1 and 3 on elliptic orbits is shown in Fig. 3. Model 2 simulations take a similar path in $r_h - M_V$ space as model 1 due to the models having an identical enclosed mass profile for the dE envelope. All simulations for a given dE,N model take a similar path in $r_h - M_V$ space, first towards lower mass and then towards lower radius, with only the end-point along the sequence differing depending upon the orbital parameters. The figure shows that some objects classified as dwarf galaxies (i.e. objects with $r_h > 100\,\mathrm{pc}$) could have undergone some tidal stripping or are still being tidally stripped.

Figs 2 and 3 also show that our simulations predict the existence of objects with half-light radii between 50 and 200 pc and luminosities smaller than $M_V \sim -12$, while the catalogue from Brodie et al. (2011) lacks such objects. It is unclear whether this is a real effect or due to selection effects or selection bias, but note the catalogue compiled by Brüns & Kroupa (2012) contains unconfirmed candidates in this region. If the extended, low-mass UCDs form by tidal stripping, one would expect to see transition objects in the size gap. The absence or small number of objects in this region might imply different situations for UCD formation by tidal stripping: either the formation time is very short, or the tidal stripping occurred long ago, i.e. when the cluster formed. Our results show that UCDs on box orbits, which are necessary to form the extended UCDs, have typical formation times of 1–2 Gyr (see Table 1), in agreement with the first scenario. However, since most UCDs are ~ 10–11 Gyr old (Evstigneeva et al. 2007a; Francis et al. 2012), while most dE nuclei are a few Gyr old (Paudel, Lisker & Kuntschner 2011), this implies that most UCDs formed before the young dE nuclei were formed, otherwise one could expect to find more young UCDs. But note that dE nuclei with young ages might not be young at all, they might have formed long ago but had ongoing star formation or new star
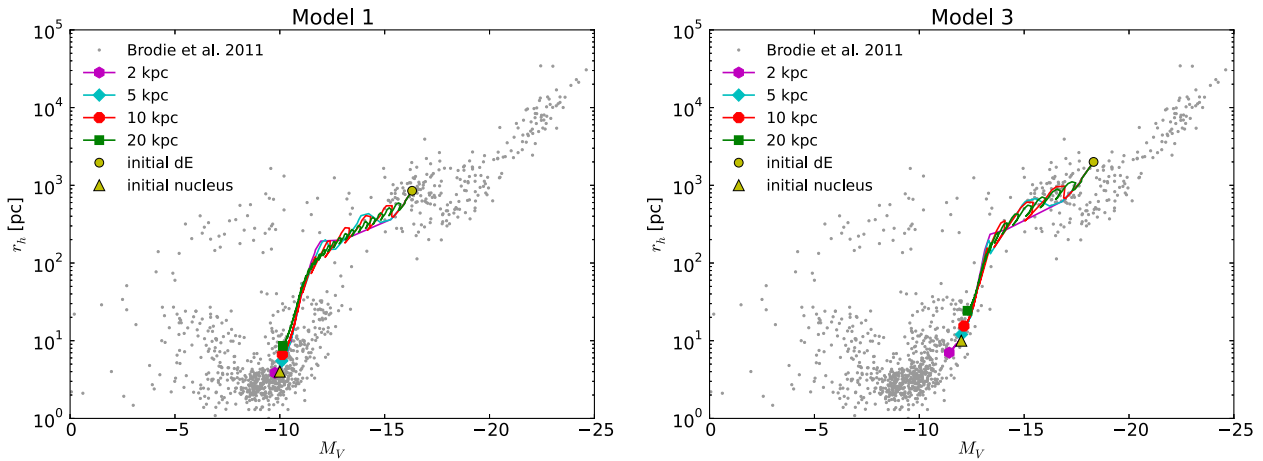
Figure 3. Morphology evolution of simulations on elliptic orbits with a 50 kpc apocentre for dE,N model 1 (left-hand panel) and dE,N model 3 (right-hand panel) compared to GCs, UCDs, dEs, dwarf spheroidals, compact ellipticals and giant ellipticals from the nearby Universe (Brodie et al. 2011, grey points). The *V*-band magnitude and half-light radius evolution of the models are shown as solid lines with a marker showing final UCD at the end of the simulation. The marker type and line colour for each simulation are as in the legend. The yellow circle and triangle mark the initial position of the dwarf galaxy and nucleus of the model, respectively.

formation events at recent times. Therefore either of these points, or a combination of the two, may explain the lack of transition objects between dwarf galaxies and UCDs.

Fig. 4 shows a comparison of final half-mass radius and half the object mass for the simulations with the initial cumulative mass profile of the models and the final cumulative mass profile for box orbits with one pericentre passage at 2 kpc and a 50 kpc apocentre/circular orbit. If the origin of the size difference between UCDs and dE nuclei is due to expansion of the nucleus during tidal stripping the cumulative mass profiles of the final UCDs should differ from that of the initial nucleus of the model. Fig. 4 shows that the final UCD profiles differ little from nucleus of the initial models, and the mass and half-mass radius of the simulated UCDs trace the initial model nucleus, with the exception of the most massive UCDs for each model which have a significant stellar halo. This indicates expansion plays little role in the final UCD sizes. Although the model 1 elliptic orbit simulations show some deviation from the
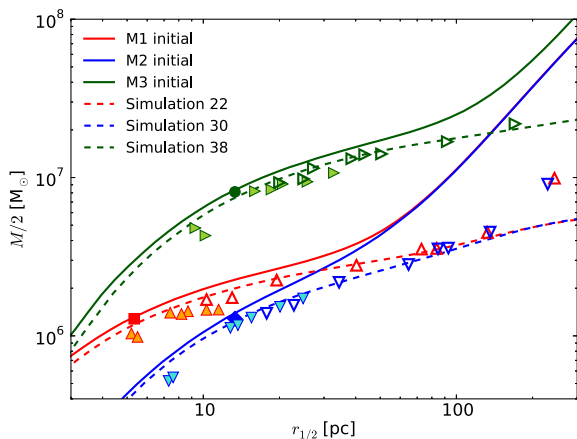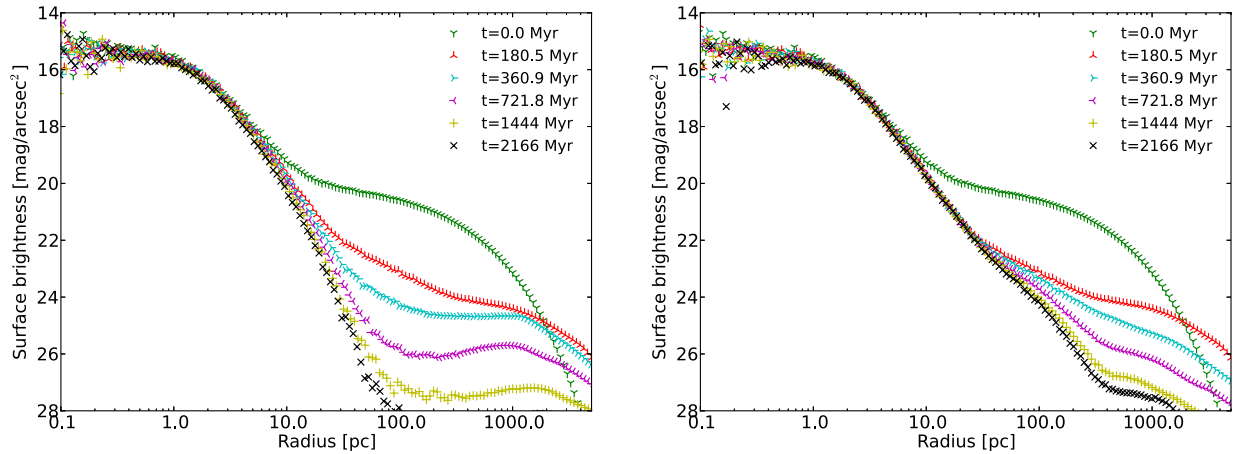
mass profile with increasing radius, this is most likely caused by numerical relaxation and not a real effect. Based on this result we expect that UCDs outside our sequence can be formed by models with different luminosities for the nucleus. Given the range of luminosities for dE nuclei in Fig. 2, the whole range of UCD sizes and luminosities could be produced by dE,N on box orbits.

3.2 UCD surface brightness profiles

As an example, Fig. 5 shows the surface brightness evolution for dE,N model 1 on an elliptic orbit with a 2 kpc pericentre and a 50 kpc apocentre (left-hand panel) compared to the same model on a box orbit which has one close pericentre passage at 2 kpc and then continues on a circular orbit at 50 kpc (right-hand panel). For the elliptic orbit, the dE,N is strongly stripped by the first two pericentre passages at 90 and 270 Myr and the final UCD has a size and mass resembling the initial nucleus of the model. For the box orbit, most of the envelope becomes unbound due to the pericentre passage at 90 Myr and subsequently escapes during the orbit at apocentre, while the nucleus remains unaffected by the encounter. The final mass of the object is approximately twice that of the initial nucleus. Since our set-up procedure does not distinguish between nucleus and envelope particles we are unable to determine which particles escape; however, naively one would expect the envelope particles to become unbound before the nucleus particles. Under this assumption all particles in the nucleus would be retained while 50 per cent of the final UCD mass comes from the envelope.

In the right-hand panel of Fig. 5 the final profile has a stellar halo, which is visible as a deviation from a single-component profile at a surface brightness of $\sim$23 mag arcsec^{-2}. In general, for models with a nucleus $r_h = 4$ pc (model 1) stellar haloes become visible for UCDs with sizes larger than $r_h \sim 30$ pc, while for models with a nucleus $r_h = 10$ pc (model 2 and 3) stellar haloes become visible for UCDs with sizes larger than $r_h \sim 50$-60 pc. For all simulations the halo does not become apparent until a surface brightness of 22–23 mag arcsec^{-2}. For simulation 22 (right-hand panel in Fig. 5), it is unclear whether a halo would be observable because if random Gaussian noise with a standard deviation of

Figure 4. Final 3D half-mass radius ($r_{1/2}$) and half the object mass for all simulated UCDs compared with the initial cumulative mass profiles for the models (solid lines) and final cumulative mass profiles for simulations 22, 30 and 38 (box orbits with one pericentre passage at 2 kpc and a 50 kpc apocentre/circular orbit for models 1, 2 and 3, respectively, dashed lines). Colours and symbols are as in Fig. 2.

Figure 5. Surface brightness profile evolution over time for dE,N model 1. Left: an elliptic with a 2 kpc pericentre and 50 kpc apocentre (Simulation 1 in Table 1, final $r_h = 3.9$ pc, $M_V = -9.77$). Right: a box orbit with one pericentre passage at 2 kpc and a 50 kpc apocentre/circular orbit (Simulation 22 in Table 1, final $r_h = 28.3$ pc, $M_V = -10.84$). The surface brightness profile symbols and colours are as in the legend, showing the time since the start of simulation.

0.2 mag arcsec^{-2} is added to simulate observational uncertainties, the profile is fit well by both a King profile and a two-component profile (King profile with a Sérsic profile for the halo). This indicates that some UCDs which only have a single-component surface brightness profile could be composed of the nucleus and remaining envelope from the initial dE,N. However, for the more massive and extended simulated UCDs the stellar halo is clearly visible.

The result that UCDs formed by tidal stripping are composed of stars from both the nucleus and envelope of the progenitor dE,N has an important implication. Nuclei of dE,Ns often have different metallicities from the envelope (Paudel et al. 2011), which suggests that UCDs with two-components, as well as some that have only a single-component profile (e.g. right-hand panel in Fig. 5), most likely contain populations with different metallicities or a metallicity gradient. This prediction may be tested with future observations.

Tidal streams are an inevitable consequence of the tidal stripping scenario and therefore must be present if UCDs form in this way. In the right-hand panel of Fig. 5 the final profile is embedded in a tidal stream, which becomes dominant in the surface brightness profile at a surface brightness of ~27 mag arcsec^{-2} and a radius of ~400 pc. For all simulations the tidal streams have surface brightnesses fainter than ~27 mag arcsec^{-2} after 2 Gyr. Only box orbit simulations with 50 kpc apocentres have tidal streams with surface brightnesses brighter than 28 mag arcsec^{-2} in the final profiles, while all other simulations have tidal streams with surface brightnesses fainter than 28 mag arcsec^{-2}. It is probable the tidal streams would disperse faster in reality due to substructure in the galaxy cluster and thus tidal streams are only likely to be observed around UCDs still undergoing significant stripping.

For both the elliptic and box orbit in Fig. 5 the inner region (within ~5–10 pc) changes little throughout the simulation. By fitting a King profile to the innermost region of the final surface brightness profiles for all models we find the core radius typically changes by less than 10 per cent of the initial core radius of the nucleus (dE,N model 1 has a nucleus core radius of 1.5 pc while dE,N models 2 and 3 both have a nucleus core radius of 3.7 pc). This suggests the surface brightness profiles of UCDs formed by tidal stripping should have the same core radius as their progenitor dE nucleus.

4 DISCUSSION

We have performed simulations of nucleated dwarf galaxies undergoing tidal stripping in a Virgo-like galaxy cluster to form UCDs. Using the particle-mesh code SUPERBOX, we have performed 45 simulations with varying orbital parameters to test the effect of the dwarf galaxy's orbit on the size of the UCD formed due to the stripping of the dwarf's outer envelope.

We find that repeated close passages which occur during elliptic orbits lead to the formation of compact star clusters/UCDs, and elliptic orbits can only reproduce the full range of UCD sizes if the dE nuclei have half-light radii $r_h > 10$ pc. Given a large fraction of dE nuclei have half-light radii $r_h \sim 4$ pc (including almost all nuclei with luminosities $M_V > -11$), we consider tidal stripping on elliptic orbits unlikely to be the dominant mechanism for UCD formation. In contrast, orbital motion in box orbits, or other orbits where very close pericentre passages happen only once or twice and at all other times the stripped dwarf galaxy is far from the centre of a major galaxy, leads to the formation of extended objects resembling UCDs regardless of the nucleus half-light radius. For such box orbits the dwarf galaxies need close pericentre passages with distances less than 10 kpc to undergo strong enough stripping so that UCD formation is possible.

Observations suggest that the nuclei must expand by a factor of 2 to account for the size difference between UCDs and dE nuclei (Evstigneeva et al. 2008); however we find the nuclei expand little during the tidal stripping process. Instead, the stripped dE,N galaxies can resemble the extended UCDs by retaining more mass than contained within the initial nucleus, causing the UCDs to be more extended. During the stripping process, the envelope profile steepens, and in some cases the UCD can appear to have a single-component profile despite being composed of both the nucleus and remnant envelope. For all orbits considered in our simulations, the typical UCD size is two to three times the initial dE nucleus size, in agreement with the findings of Evstigneeva et al. (2008).

Despite the simulated UCDs having more mass than the initial nucleus, we find only the extended UCDs have stellar haloes. For the dE,N models with a compact nucleus ($r_h = 4$ pc) we find haloes only become visible for objects with a half-light radius greater than ~30 pc, while for dE,N models with a larger nucleus ($r_h = 10$ pc) a halo becomes visible for a half-light radius larger than ~50–60 pc. For both nuclei sizes the halo tends to become

visible in the surface brightness profile at $\sim$22–23 mag arcsec^{-2} and between $\sim$10 and 100 pc; however, the position this occurs at for a given UCD will depend strongly on the mass profile of the progenitor dE,N (in particular on the King concentration for the nucleus and Sérsic index for the envelope) and remaining mass in the envelope. Some observed UCDs, in particular the most extended ones, are better fit by two-component models (Evstigneeva et al. 2008), while deviations from single-component King models at a surface brightness of $\sim$22–23 mag arcsec^{-2} can be seen qualitatively in some of the observed surface brightness profiles of UCDs (e.g. the profiles for UCD16 and UCD33), in agreement with our results.

Given our results suggesting the nuclei undergo little expansion and retain the core radius of their progenitor dE nucleus, we predict that high-mass UCDs ($M_V < -11$) should have cores ranging up to $\sim$20 pc due to the large range in nuclei sizes at higher luminosities, assuming most progenitor nuclei have half-light radii below 20 pc. In contrast, most low-mass UCDs should have profiles with cores up to a few parsec, since most nuclei in this range have half-light radii of $\sim$4 pc. This range is consistent for the UCDs in the Fornax and Virgo clusters which have King core radii in the range 2–7 pc (Evstigneeva et al. 2008). No surface brightness profiles are available for the extended, low-luminosity UCDs ($r_h \sim$ 40 pc, $M_V \sim -9$) as yet but this prediction may be tested with future observations.

Although we simulated a dE with a nucleus of $M_V = -12$ and $r_h = 10$ pc (model 3) there also exist many compact nuclei with $M_V = -12$ and $r_h = 4$ pc, as shown in Fig. 2. If the envelope for both dE,Ns is similar, our results from Fig. 4 imply a dE,N with a nucleus of $M_V = -12$ and $r_h = 4$ pc will evolve during tidal stripping in a similar way to model 3, up until $r_h \sim 100$ pc when the nucleus starts to become dominant in the mass profile. After this point the UCD would be more compact than model 3 for a given luminosity, similar to the situation between models 1 and 2. The most massive nuclei in Fig. 2 have $M_V < -14$ and $r_h \sim 40$ pc, however no UCDs are observed at these sizes. Our simulations show that tidally stripped dE,Ns resulting in UCDs less massive and less extended than the initial nucleus require many (more than 5) pericentre passages with distances less than 5 kpc. We consider such orbits with many close pericentre passages unlikely since a small perturbation could increase the pericentre distance. As the typical UCD size is two to three times the initial nucleus size, UCDs formed from such massive nuclei would likely have sizes of $r_h \sim 100$ pc and luminosities of $M_V \sim -15$. Since the host galaxies of the most massive nuclei are lenticular (S0) or elliptical galaxies, and therefore more massive than dEs, the number of close pericentre passages required to tidally strip the galaxy is likely much larger. The extreme orbits required for formation, and the rarity of objects with such massive nuclei, may explain the lack of objects in this region. An extremely massive nucleus with $M_V = -16$ would most likely resemble a compact elliptical galaxy, rather than a UCD, after tidal stripping.

Two questions that remain unanswered are whether orbits with only one to two close passages required for extended UCD formation occur in real galaxy clusters, and whether dwarf galaxies are destroyed in sufficient numbers to explain all UCDs. For the first question a possible scenario in which such orbits may occur is if the first few passages of a dwarf galaxy in a galaxy cluster are highly radial, due to infall on low-angular momentum orbits, after which the pericentre increases due to a triaxial potential or interactions with other galaxies. A detailed answer to the first question, however, requires following the orbits of dwarf galaxies in cosmological

simulations and we defer this, along with more accurate predictions of UCD numbers and spatial distributions, to a future paper.

For the second question, there already exists some previous work constraining the number of possible progenitor galaxies for UCDs. Mieske et al. (2012) compared the specific frequencies of GCs and UCDs around various clusters and found no more than 50 per cent of UCDs may be formed by tidal stripping (based on the error bars of the specific frequencies derived for GCs). In the central $\sim$50–70 kpc of the galaxy clusters they find $\gtrsim$90 per cent of possible progenitor dwarfs need to be disrupted to account for half of the UCDs. As tidal stripping will be most efficient near the centre of a galaxy cluster we consider it entirely possible that such a high fraction of dwarfs in this region have been tidally disrupted.

To date, there have been 34 UCDs discovered in M87, with possibly more than 50 still undiscovered out to a distance of 200 kpc (Brodie et al. 2011). Following Mieske et al. (2012), we assume 50 per cent of the UCDs, $\sim$40, to be formed by tidal stripping. According to the catalogue of Binggeli, Sandage & Tammann (1985), about 50 dEs are located within a projected distance of 200 kpc from the centre of M87 (Peng et al. 2008). Given approximately 70 per cent of dEs are nucleated (Côté et al. 2006; Turner et al. 2012), this leaves 35 dE,Ns to be possible UCD progenitors. Therefore, approximately $\frac{40}{40+35} \approx 53$ per cent of possible UCD progenitor galaxies within 200 kpc of M87 need to be tidally stripped to account for half of the UCDs. It is possible that observations are consistent with a population in which all dwarf galaxies are nucleated (Thomas, Drinkwater & Evstigneeva 2008), which would lower the fraction needed to be stripped by 10 per cent. This estimate is consistent with calculations from cosmological simulations which suggest half of satellite galaxies get disrupted and/or accreted to their host haloes (Henriques, Bertone & Thomas 2008).

Alternatively, one could obtain an estimate of accreted dwarf galaxy numbers by looking at the GC systems of elliptical galaxies. Giant elliptical galaxies contain very rich GC systems which are almost universally bimodal in the colour distributions due to differences in metallicity (Brodie & Strader 2006). Dwarf elliptical galaxies on the other hand contain GC systems which are predominantly metal-poor (Peng et al. 2008). One explanation for this bimodallity of giant elliptical GCs is that the metal-rich GCs are the intrinsic GC population of the galaxy, or were formed in starbursts triggered by gas-rich mergers, while the metal-poor GCs are provided by accretion of dwarf galaxies (e.g. see the review by Richtler 2012). This explanation is strengthened by current theories of giant elliptical formation where the dominant growth mechanism for the galaxies from $z = 1$ to $z = 0$ is accretion through minor mergers (Naab, Johansson & Ostriker 2009). Two previous studies have investigated the build-up of the GC systems of giant ellipticals via accretion of galaxies: Côté, Marzke & West (1998) for NGC 4472, and Hilker, Infante & Richtler (1999b) for NGC 1399, although using slightly different methods. These techniques provide a useful way to study the accretion of dwarf galaxies by giant ellipticals; however such an analysis is beyond the scope of this paper.

A common origin of accretion and tidal stripping of dwarf galaxies for UCDs and blue GCs in giant ellipticals also places a constraint on the spatial distribution of UCDs. If this scenario is correct, due to their common origin, we expect UCDs far from the centre of M87 to have a similar spatial distribution as the blue GCs. However at small distances UCDs should be underrepresented compared to GCs due to the ongoing tidal stripping converting UCDs into GC-like objects. Some evidence for a more extended distribution of UCDs compared to GCs in the inner regions of galaxy clusters has

been found (Hilker 2011; Mieske et al. 2012), in agreement with our expectations.

In summary, we have demonstrated that the extended, low-mass UCDs found by Brodie et al. (2011) can be formed in the tidal stripping scenario providing the dwarf galaxies have one or two pericentre passages with distances less than 10 kpc. Given the observed range of dE nuclei sizes and luminosities, the full range of UCD sizes can be produced within the tidal stripping scenario.

REFERENCES

Bassino L. P., Muzzio J. C., Rabolli M., 1994, ApJ, 431, 634
Bekki K., Couch W. J., Drinkwater M. J., 2001, ApJ, 552, L105
Bekki K., Couch W. J., Drinkwater M. J., Shioya Y., 2003, MNRAS, 344, 399
Binggeli B., Sandage A., Tammann G. A., 1985, AJ, 90, 1681
Binney J., Tremaine S., 1987, Galactic Dynamics. Princeton Univ. Press, Princeton, NJ
Brodie J. P., Strader J., 2006, ARA&A, 44, 193
Brodie J. P., Romanowsky A. J., Strader J., Forbes D. A., 2011, AJ, 142, 199
Brüns R. C., Kroupa P., 2012, A&A, 547, A65
Brüns R. C., Kroupa P., Fellhauer M., Metz M., Assmann P., 2011, A&A, 529, A138
Chiboucas K. et al., 2011, ApJ, 737, 86
Chilingarian I. V., 2009, MNRAS, 394, 1229
Chilingarian I. V., Mamon G. A., 2008, MNRAS, 385, L83
Chilingarian I. V., Mieske S., Hilker M., Infante L., 2011, MNRAS, 412, 1627
Côté P., Marzke R. O., West M. J., 1998, ApJ, 501, 554
Côté P. et al., 2006, ApJS, 165, 57
Da Rocha C., Mieske S., Georgiev I. Y., Hilker M., Ziegler B. L., Mendes de Oliveira C., 2011, A&A, 525, A86
Drinkwater M. J., Jones J. B., Gregg M. D., Phillipps S., 2000, Publ. Astron. Soc. Aust., 17, 227
Drinkwater M. J., Gregg M. D., Hilker M., Bekki K., Couch W. J., Ferguson H. C., Jones J. B., Phillipps S., 2003, Nat, 423, 519
Evstigneeva E. A., Gregg M. D., Drinkwater M. J., Hilker M., 2007a, AJ, 133, 1722
Evstigneeva E. A., Drinkwater M. J., Jurek R., Firth P., Jones J. B., Gregg M. D., Phillipps S., 2007b, MNRAS, 378, 1036
Evstigneeva E. A. et al., 2008, AJ, 136, 461
Fellhauer M., Kroupa P., 2002, MNRAS, 330, 642
Fellhauer M., Kroupa P., Baumgardt H., Bien R., Boily C. M., Spurzem R., Wassmer N., 2000, New Astron., 5, 305
Francis K. J., Drinkwater M. J., Chilingarian I. V., Bolt A. M., Firth P., 2012, MNRAS, 425, 325
Geha M., Guhathakurta P., van der Marel R. P., 2002, AJ, 124, 3073
Geha M., Guhathakurta P., van der Marel R. P., 2003, AJ, 126, 1794
Ghigna S., Moore B., Governato F., Lake G., Quinn T., Stadel J., 1998, MNRAS, 300, 146
Goerdt T., Moore B., Kazantzidis S., Kaufmann T., Macciò A. V., Stadel J., 2008, MNRAS, 385, 2136
Grant N. I., Kuipers J. A., Phillipps S., 2005, MNRAS, 363, 1019
Hau G. K. T., Spitler L. R., Forbes D. A., Proctor R. N., Strader J., Mendel J. T., Brodie J. P., Harris W. E., 2009, MNRAS, 394, L97
Haşegan M. et al., 2005, ApJ, 627, 203
Henriques B. M., Bertone S., Thomas P. A., 2008, MNRAS, 383, 1649
Hilker M., 2011, EAS Publ. Ser., 48, 219
Hilker M., Infante L., Vieira G., Kissler-Patig M., Richtler T., 1999a, A&AS, 134, 75
Hilker M., Infante L., Richtler T., 1999b, A&AS, 138, 55
Hilker M., Baumgardt H., Infante L., Drinkwater M., Evstigneeva E., Gregg M., 2007, A&A, 463, 119
Jones J. B. et al., 2006, AJ, 131, 312
King I., 1962, AJ, 67, 471
Kormendy J., Fisher D. B., Cornell M. E., Bender R., 2009, ApJS, 182, 216
Kroupa P., 1998, MNRAS, 300, 200
Madrid J. P., 2011, ApJ, 737, L13
Mieske S., Hilker M., Infante L., 2002, A&A, 383, 823
Mieske S. et al., 2004, AJ, 128, 1529
Mieske S., Hilker M., Infante L., Jordán A., 2006, AJ, 131, 2442
Mieske S., Hilker M., Jordán A., Infante L., Kissler-Patig M., 2007, A&A, 472, 111
Mieske S. et al., 2008, A&A, 487, 921
Mieske S., Hilker M., Misgeld I., 2012, A&A, 537, A3
Misgeld I., Mieske S., Hilker M., Richtler T., Georgiev I. Y., Schuberth Y., 2011, A&A, 531, A4
Murphy J. D., Gebhardt K., Adams J. J., 2011, ApJ, 729, 129
Naab T., Johansson P. H., Ostriker J. P., 2009, ApJ, 699, L178
Norris M. A., Kannappan S. J., 2011, MNRAS, 414, 739
Paudel S., Lisker T., Kuntschner H., 2011, MNRAS, 413, 1764
Peñarrubia J., Benson A. J., Walker M. G., Gilmore G., McConnachie A. W., Mayer L., 2010, MNRAS, 406, 1290
Peng E. W. et al., 2006, ApJ, 639, 838
Peng E. W. et al., 2008, ApJ, 681, 197
Penny S. J., Forbes D. A., Conselice C. J., 2012, MNRAS, 422, 885
Prugniel P., Simien F., 1997, A&A, 321, 111
Richtler T., 2012, preprint (arXiv:1210.0045)
Richtler T., Dirsch B., Larsen S., Hilker M., Infante L., 2005, A&A, 439, 533
Sérsic J. L., 1963, Boletin de la Asociacion Argentina de Astronomia, 6, 41
Sérsic J. L., 1968, Atlas de Galaxias Australes. Observatorio Astronomico, Cordoba
Terzić B., Graham A. W., 2005, MNRAS, 362, 197
Thomas P. A., Drinkwater M. J., Evstigneeva E., 2008, MNRAS, 389, 102
Trager S. C., King I. R., Djorgovski S., 1995, AJ, 109, 218
Turner M. L., Cote P., Ferrarese L., Jordan A., Blakeslee J. P., Mei S., Peng E. W., West M. J., 2012, ApJS, 203, 5

This paper has been typeset from a TeX/LaTeX file prepared by the author.

3

Dynamical masses of ultra-compact dwarf galaxies formed by tidal stripping

It has recently been suggested that tidal stripping may be responsible for the elevated dynamical-to-stellar mass ratios of some UCDs. However, in the previous chapter we did not investigate the mass-to-light ratios of UCDs formed by tidal stripping. In this Chapter, we reanalyse the simulations from Chapter 2 to investigate the velocity dispersions and dynamical-to-stellar mass ratios of UCDs formed by tidal stripping.

3.1   Introduction

A key feature of UCDs, and a topic that has received significant attention in the literature, is their elevated dynamical mass-to-light ratios compared to the mass-to-light ratio

expected based on their metallicities and ages (Haşegan et al. 2005; Dabringhausen, Kroupa, & Baumgardt 2009; Dabringhausen, Fellhauer, & Kroupa 2010; Dabringhausen et al. 2012; Baumgardt & Mieske 2008; Mieske & Kroupa 2008; Mieske et al. 2008, 2013; Taylor et al. 2010; Frank et al. 2011; Strader et al. 2013). A number of possible explanations for this have been suggested, including a non-standard initial mass function (Mieske & Kroupa 2008; Murray 2009; Dabringhausen et al. 2009, 2010), remnant dark matter halos (Baumgardt & Mieske 2008; Goerdt et al. 2008) and central supermassive black holes (SMBHs; Mieske et al. 2013) from tidally stripped galaxies. Recently, Seth et al. (2014) discovered the first UCD (M60-UCD1) to host a SMBH, providing direct support for SMBHs as a possible explanation for the elevated dynamical mass-to-light ratios of UCDs (although interestingly the dynamical mass of M60-UCD1 is consistent with the stellar mass predicted from stellar population synthesis models, Strader et al. 2013).

The most recent suggestion is that the elevated dynamical masses of UCDs are due to tidal stripping (Forbes et al. 2014). Under the assumption that the central velocity dispersion and virial coefficient (see Equation 3.1 and relating text) are largely unchanged in the process, they find that the dynamical-to-stellar mass ratios of UCDs formed from tidally stripped dE,Ns in the simulations from Chapter 2 are in reasonable agreement with the typical observed values for UCDs.

Here we reassess this claim by reanalysing the tidal stripping simulations from Chapter 2 to investigate the dynamical masses of UCDs formed by tidal stripping. We compare two different methods for determining the dynamical masses of UCDs, calculating central velocity dispersions and calculating velocity dispersions as seen by an observer, in order to compare with virial theorem estimates and the dynamical-to-stellar masses of observed UCDs. We caution however that as we did not include a dark matter halo in the simulations of Chapter 2 we may underestimate the dynamical-to-stellar mass ratios of UCDs formed by tidal stripping.
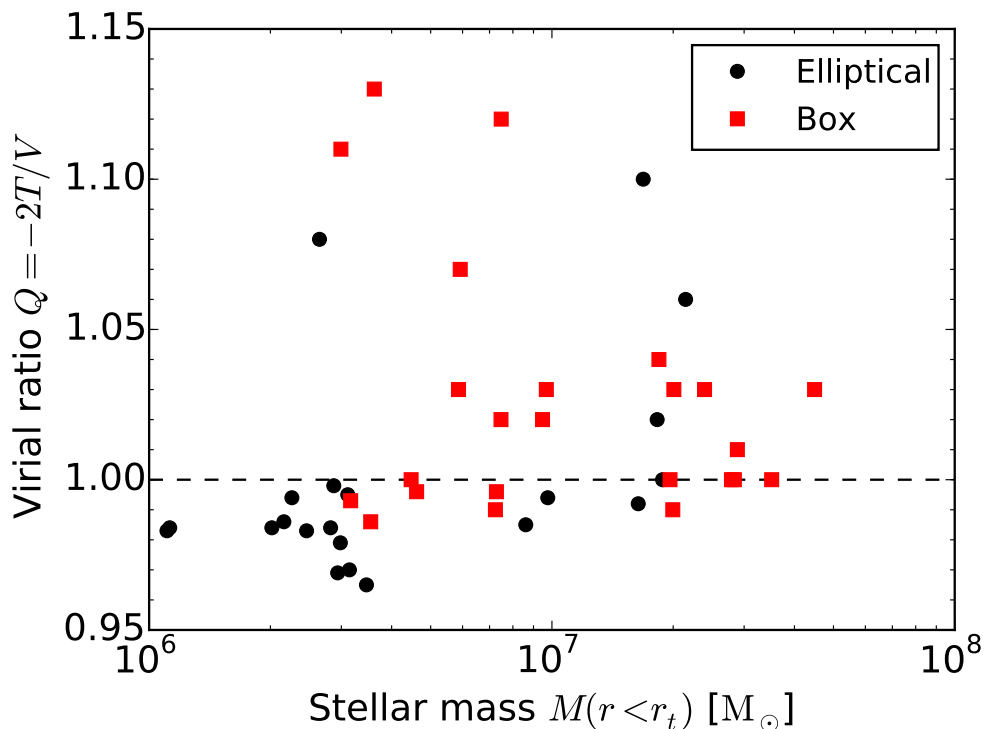
FIGURE 3.1: Virial ratios of the simulated UCDs formed by tidal stripping compared with their stellar masses within the tidal radius. UCDs formed on elliptical and box orbits are given by circles and squares, respectively. A virial ratio $Q = 1$ indicates a system in virial equilibrium.

3.2 Virial ratios

A first test of whether the elevated dynamical masses of UCDs are due to tidal stripping is to test if UCDs formed by this mechanism are in virial equilibrium. For a stable system of particles under gravitational attraction the virial theorem states that the average kinetic energy equals half of the average negative potential energy $T = -\frac{1}{2}V$. Thus a useful quantity to determine the state of a gravitationally bound system is the virial ratio $Q = -2T/V$, the ratio of kinetic to potential energy[1]. Virial ratios of unity indicate a stable system, while virial ratios larger than unity indicate an expanding system and less than unity a contracting system. If a system has $Q > 2$ it is unbound and the virial theorem is not applicable.

We calculate the virial ratios Q of the simulated UCDs for all particles within the tidal radius $r_t = (GM_{\mathrm{UCD}}/2v_{\mathrm{circ}}^2)^{1/3}r_{\mathrm{G}}^{2/3}$ where M_{UCD} is the mass of the UCD, v_{circ} is the circular

---

[1]This differs slightly from the alternative definition $Q = -T/V$, where a system in virial equilibrium has $Q = 0.5$.

velocity for the cluster potential and r_G is the distance of the UCD from the cluster centre. The virial ratios for the UCDs at the apocentre of their orbits are shown in Figure 3.1 compared to the stellar mass within the tidal radius of the UCDs. The UCDs have virial ratios close to unity, indicating stable systems. A number of UCDs have virial ratios above 1.05 indicating unbound material associated with the tidal tails. If the simulations were run for a longer time (most of these simulations had simulation times of 2-4 Gyr) we expect the tidal tails of these UCDs would further disperse and the virial ratios would drop to unity. As r_t depends upon r_G for the UCD, Q will therefore depend slightly upon at what point in the UCD's orbit the virial ratio is calculated. To determine the extent of this effect, we calculated Q at pericentre for the elliptical orbit simulations and found at pericentre objects have Q very close to unity (within 1 per cent). Since we calculated Q for the UCDs at the apocentre of their orbits, this means Q of the UCDs is at the maximum from unity it can possibly be. Since the virial ratios for nearly all simulations are approximately unity (with the exception of the few where the tidal tails still affect the virial ratio), the elevated dynamical masses of the observed UCDs are not due to the UCDs formed by tidal stripping being out of virial equilibrium.

3.3 UCD properties in projection

In Chapter 2 the properties of the simulated UCDs were determined only for particles within the three-dimensional tidal radius. In order to allow comparisons with the dynamical masses of observed UCDs we reanalyse the simulated UCDs in projection. To determine the effect of the line-of-sight on UCD properties we 'observe' the simulated UCDs from three different sight-lines along the x-, y- and z-axes of the simulations. The z-axis is perpendicular to the orbital plane of the UCDs while the x- and y-axes are in the orbital plane.

The mass and effective radius of the UCDs were determined by fitting surface density profiles to the UCDs. Surface density profiles were fitted via the following method:

(i) The surface density profiles of the UCDs were binned into 100 logarithmically spaced bins (between ~ 0.1 and $\sim$40,000 pc).

TABLE 3.1: Initial dE,N model parameters. Columns 2-5 give the mass, effective radius, 'observed' velocity dispersion and central velocity dispersion of the total dE,N, respectively. Columns 6-9 give the mass, effective radius, 'observed' velocity dispersion and central velocity dispersion of the nucleus of the model, respectively.

dE,N model	$M_{\rm tot}$ (log $M_\odot$)	$R_{e,{\rm tot}}$ (pc)	$\sigma_{\rm obs,tot}$ (km/s)	$\sigma_{0,{\rm tot}}$ (km/s)	$M_{\rm nuc}$ (log $M_\odot$)	$R_{e,{\rm nuc}}$ (pc)	$\sigma_{\rm obs,nuc}$ (km/s)	$\sigma_{0,{\rm nuc}}$ (km/s)
1	8.93	848.2	23.58	21.17	6.40	4	16.36	19.15
2	8.93	848.1	23.16	21.20	6.40	10	10.46	12.20
3	9.73	1996.3	35.18	34.79	7.21	10	26.25	30.79

(ii) To approximate what is seen by an observer we assume the deepest that can be observed is $\mu_V = 26$ mag arcsec^{-2} (or 4.3 $M_\odot$ pc^{-2} for $M/L_V = 3\,(M/L)_\odot$) and subtract this surface density from all bins.

(iii) The surface density profiles were fitted in log-space using the least-squares method for bins with more than 20 particles. We first try fitting for all bins. If a fit cannot be found we fit only for bins with surface densities more than twice that of the tidal streams, where the surface density of the tidal streams was taken to be the surface density at the three-dimensional tidal radius.

We fit the UCDs with a two component King (1962) plus Sérsic (1968) profile to account for the UCDs generally retaining a stellar envelope around the nucleus (see Figure 5 of Chapter 2). Although allowed to vary freely, the King component in all the fits recovered well the parameters for the nuclei of the original dE,N models (after accounting for numerical relaxation). We show the sizes and stellar masses of the simulated UCDs from the surface density profile fitting in Figure 3.2. Depending on the surface density of the tidal tails and their geometry in each projection the stellar masses of the UCDs can vary by up to a factor of ~1.35 and effective radii by up to a factor of ~1.75. The sizes and masses of the UCDs measured in projection are generally in agreement with those determined in Chapter 2 for particles within the three-dimensional tidal radius, except where the projected tidal tails make a significant contribution to the sizes and masses of the UCDs determined from the surface density fits.

To allow for later comparison, in Table 3.1 we give the properties of the initial dE,N models. The velocity dispersions of the dE,N models and the nuclei as seen by an observer
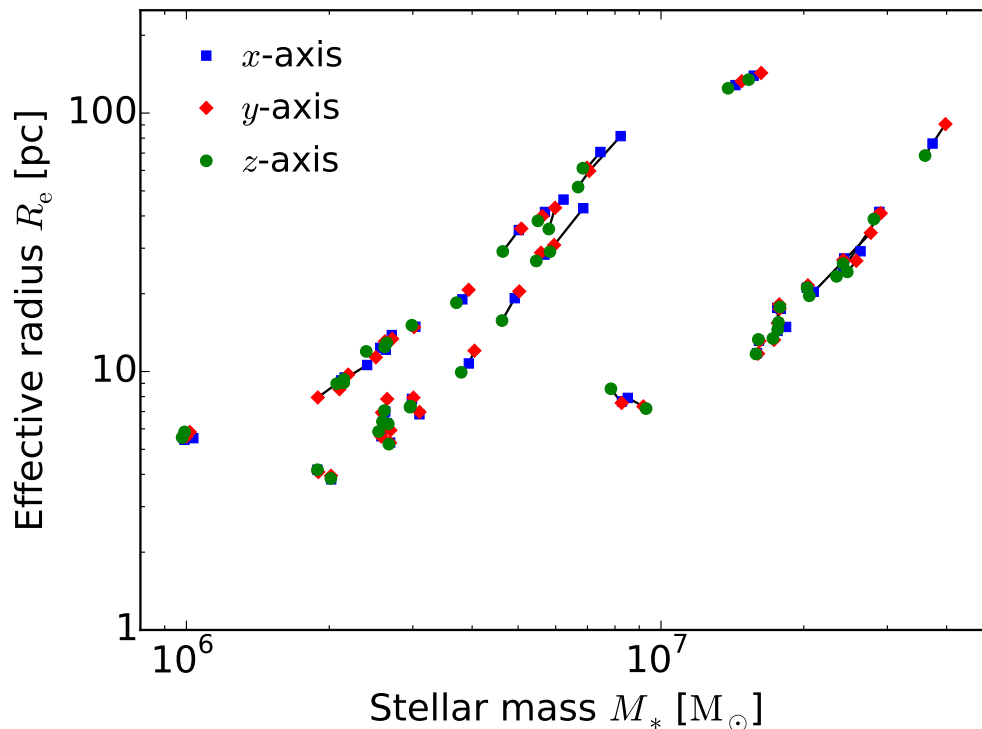
FIGURE 3.2: Sizes and masses of the simulated UCDs from surface density profile fitting for three sight-lines for each simulation (the x-, y- and z-axes of the simulations). The values for a given UCD in each projection are connected by black lines.

are calculated using the method of Hilker et al. (2007) assuming they are at the distance of the Virgo cluster. We give further details of this method in Section 3.4.1. The velocity dispersions were calculated within an aperture of $R_e/10$. The central velocity dispersions for the nuclei were determined by setting up N-body models with the parameters of the nuclei for the models using the method detailed in Section 2.3 of Chapter 2.

3.4   Dynamical mass estimates

A common method to estimate the dynamical mass of a galaxy is the scalar virial theorem

$$M_{\mathrm{dyn}} = CG^{-1}\sigma^2 R_e, \tag{3.1}$$

where R_e is the effective radius, σ is the projected velocity dispersion and C is the virial coefficient that takes into account projection effects, the orbital distribution of particles and

the mass distribution of the system.

In general the virial coefficient of the system is not known. Therefore one can create a model of the system with the same structural parameters of the galaxy in question which then obeys $M_{\mathrm{mod}} = CG^{-1}\sigma_{\mathrm{mod}}{}^2 R_e$, where σ_{mod} is the projected velocity dispersion of the model and $M_{\mathrm{mod}} = M_*$ is the mass of the model (equal to the stellar mass of the galaxy). The dynamical mass of the galaxy with the observed velocity dispersion σ_{obs} can then be determined as

$$M_{\mathrm{dyn}} = (\sigma_{\mathrm{obs}}/\sigma_{\mathrm{mod}})^2 M_{\mathrm{mod}}. \tag{3.2}$$

This is the typical method used to determine the dynamical masses of UCDs (e.g. Hilker et al. 2007).

The projected velocity dispersion in Equation 3.1 is typically taken to be the central velocity dispersion σ_0 (which is usually calculated within $R_e/10$, e.g. Bertin, Ciotti, & Del Principe 2002; Forbes et al. 2014). At the distance of the Virgo and Fornax clusters (for which most measurements of UCD masses have been made) it is not currently possible to measure the central velocity dispersions of UCDs directly. Instead most velocity dispersion measurements are made within a slit of $\sim 1''$ (depending on the instrument used). At the distances of the Fornax (19 Mpc, Freedman et al. 2001) and Virgo (16.5 Mpc, Mei et al. 2007) clusters this corresponds to ~ 90 and ~ 80 pc, respectively. For typical GCs ($R_e \sim 4$ pc) and the most compact UCDs ($R_e \sim 7$ pc, depending on the definition of a UCD) this effectively measures the global velocity dispersion. Here we determine the dynamical masses of the simulated UCDs by measuring both the projected velocity dispersions as seen by an observer (Section 3.4.1) and the projected central velocity dispersions (Section 3.4.2). As in Section 3.3 we calculate σ along the sight-lines of the x-, y- and z-axes of the simulations to take into account line-of-sight in the dynamical mass determinations.

Idealised models of the UCDs in each projection, from which the model velocity dispersions were determined, were set up using the following method (which is a modified version of the algorithm outlined in Hilker et al. 2007):

(i) The fitted surface density profiles of the simulated UCDs in Section 3.3 were converted to three-dimensional profiles (where we use the deprojected form of the Sérsic profile

as given by Terzić & Graham 2005).

(ii) Setting up N-body models with the fitted parameters, using a similar method to that in Chapter 2. Namely, calculating the potential energy and distribution function from the density profile, then creating the N-body representation using the density profile and the distribution function assuming isotropic orbits for the stars. We use 1,000,000 particles for each model.

For two simulations, 3 and 17, we also determine the dynamical mass at every snapshot in the simulation to investigate the evolution of the dynamical-to-stellar mass ratios of UCDs during tidal stripping. We observe from the y- and z-axis sight-lines to take into account line-of-sight and use both $\sigma_{\rm obs}$ and σ_0 to determine $M_{\rm dyn}$. Here we use a minimum of 30,000 particles for the King component (nucleus) of the fit and a minimum of 100,000 particles in total.

3.4.1   Dynamical masses from observed velocity dispersions

In this section we calculate the velocity dispersions of the simulated UCDs as seen by an observer using the method of Hilker et al. (2007):

(i) All test are convolved with a Gaussian whose full-width at half-maximum (FWHM) corresponds to the observed seeing.

(ii) The fraction of the "light" (Gaussian) that falls into the slit at the projected distance of the observed object is calculated.

(iii) These fractions are used as weighting factors for the velocities. All weighted velocities that fall into the slit region are then used to calculate the "mimicked" observed velocity dispersion $\sigma_{\rm mod}$.

We assume the UCDs are at a distance of 16.5 Mpc, similar to the Virgo cluster (Mei et al. 2007) and use a slit of 1×3 arcsec (80×240 pc at Virgo distance) and seeing of 0.8 arcsec, which we take as typical parameters for UCD observations (e.g. Hilker et al. 2007).
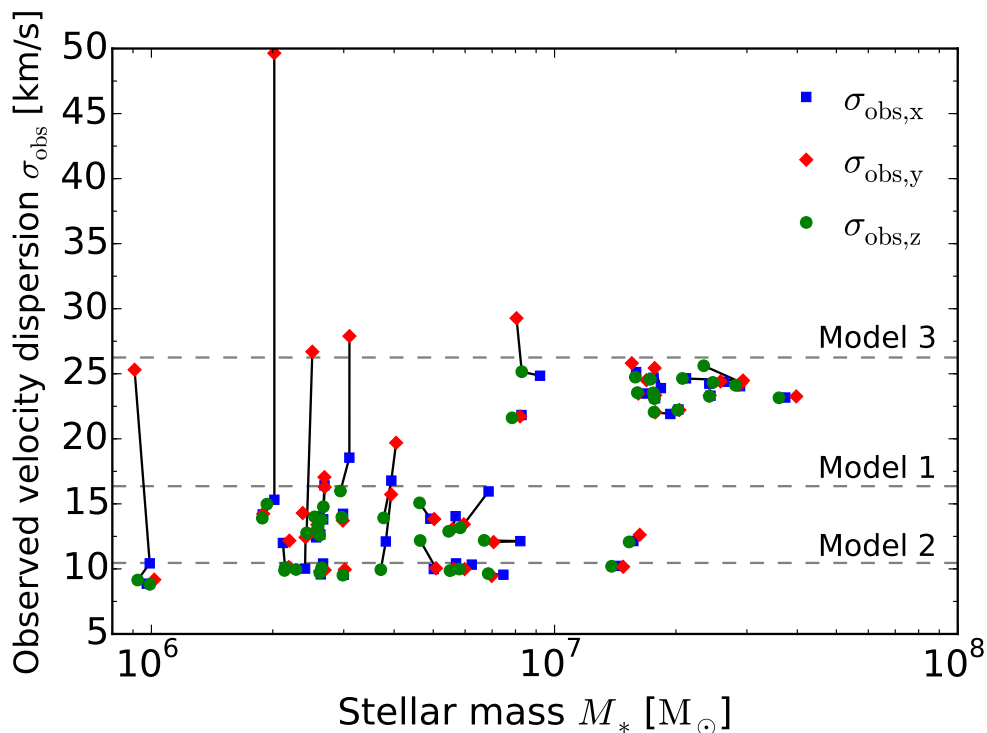
FIGURE 3.3: Velocity dispersions of the simulated UCDs as seen by an observer compared with stellar masses of the UCDs determined from the fitted surface density profiles. The results for each sight-line (x-, y- and z-axes of the simulations) are given by squares, diamonds and circles with the results for a given UCD connected by a black line. The dashed lines show the observed velocity dispersions of the model nuclei.

In Figure 3.3 we show the velocity dispersion as seen by an observer σ_{obs} for the simulated UCDs in each projection. With the exception of a few models with very elevated σ_{obs} that we discuss below, σ_{obs} is generally close to that of the model nucleus and relatively insensitive to the line-of-sight. For each dE,N model σ_{obs} is very similar for all UCDs (i.e. constant over all masses) with deviations between models largely due to numerical relaxation and differing simulation times. The UCDs generally have a smaller σ_{obs} than that of the model nucleus due to numerical relaxation in the centre of the models. In the dE,N model 2 simulations where relaxation is less pronounced (as the velocity dispersions are smaller compared to the other models due to the low mass and large size of the nucleus) the UCDs have very similar velocity dispersions to the model nucleus.

A number of simulations (1, 8, 23 and 31), generally the least massive and most compact UCDs of each dE,N model, have very elevated σ_{obs} along the y-axis line-of-sight compared

to the other sight-lines. When rotating the UCDs, the velocity dispersions remain elevated within ~45 degrees of the y-axis line-of-sight. Two of these simulations (23 and 31) have virial ratios larger than 1.1 while the other two simulations (1 and 8) have virial ratios close to unity. Simulation 1 has the largest elevation in σ_{obs} while Q closest to unity (0.986) out of the four simulations. Given this we suggest the very elevated velocity dispersions are due to extra-tidal stars in the tidal tails being projected onto the UCDs. These simulations all result in compact objects ($R_{\mathrm{eff}} < 12$ pc) and thus the slits are larger than the UCDs and pick up many particles from the tidal tails. Additionally, because of the position of the UCDs in their orbits, in the y-axis projection we view through more of the tidal tails than in other projections which significantly increase the velocity dispersion. The tidal tails of these UCDs would be visible in the surface brightness profile at surface brightnesses of $\mu_V \sim 27\text{-}28$ mag arcsec^{-2} assuming a mass-to-light ratio $M/L_V = 3\,(\mathrm{M/L})_\odot$. These simulations also all have short simulation times of 2.2 Gyr (which would correspond to recent mergers) and if these simulations were run for a longer time the tidal tails would further disperse and reduce the elevation of the velocity dispersions.

In Figure 3.4 we show the dynamical-to-stellar mass ratios determined from their observed velocity dispersions $M_{\mathrm{dyn}}(\sigma_{\mathrm{obs}})/M_*$ for the simulated UCDs. Overall we find no correlation between virial ratio Q and $M_{\mathrm{dyn}}(\sigma_{\mathrm{obs}})/M_*$; only two simulations have both an elevated Q and $M_{\mathrm{dyn}}(\sigma_{\mathrm{obs}})/M_*$. On average the dynamical masses are increased by 11, 76 and 6 per cent for x-, y- and z-axis projections, respectively (16 per cent for the y-axis projection when excluding the four simulations with the largest mass ratios). For the simulated UCDs with masses $M_* > 10^7\,\mathrm{M}_\odot$ the average increases are less than 5 per cent for all projections. Such an increase is not sufficient to explain the dynamical-to-stellar mass ratios of the observed UCDs which have an average $M_{\mathrm{dyn}}/M_* \sim 1.7$ for UCDs with masses $M > 10^7\,\mathrm{M}_\odot$ (Mieske et al. 2013).

In contrast to the M_{dyn}/M_* trend of observed UCDs which increases with UCD mass (Mieske et al. 2013; Forbes et al. 2014), we find the most massive of the simulated UCDs have M_{dyn}/M_* close to unity. This is because the most massive UCDs have larger sizes and therefore stars from the centre of the UCDs dominate the velocity dispersion measurements, making the contribution of extra-tidal stars negligible.
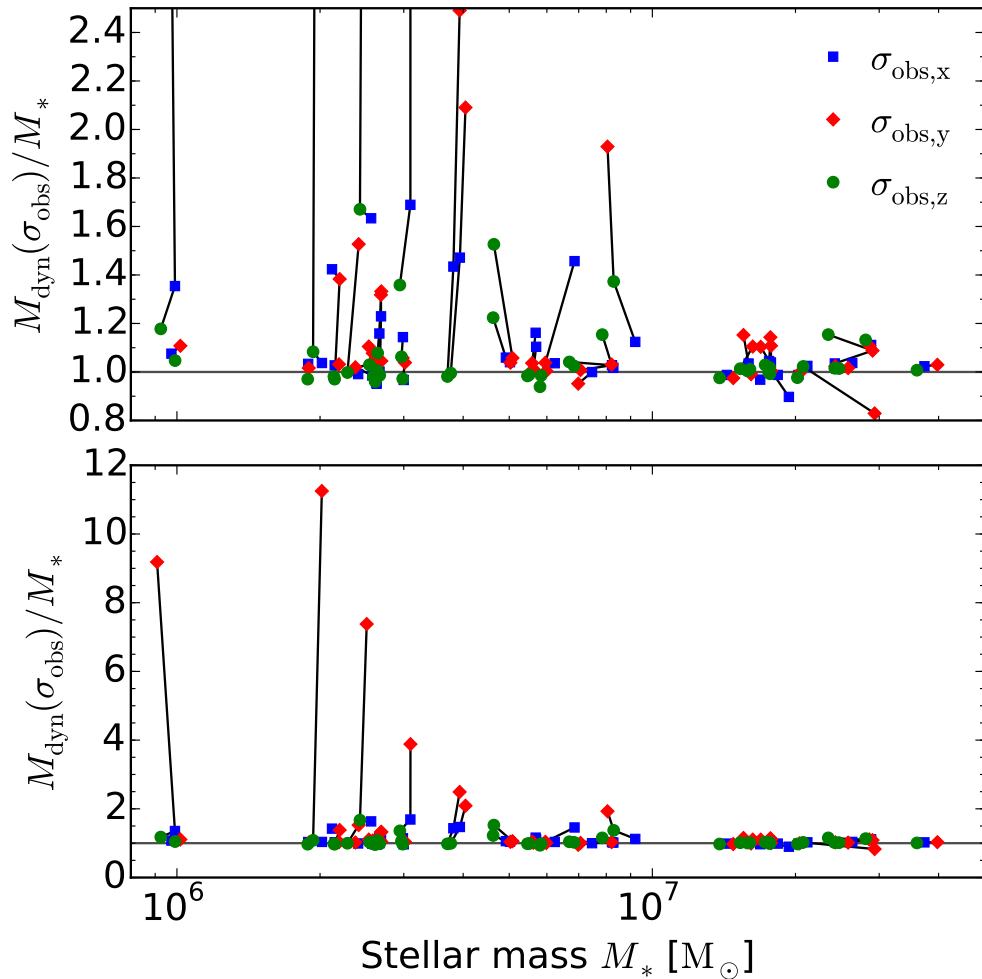
FIGURE 3.4: Dynamical-to-stellar mass ratios of the simulated UCDs determined from their observed velocity dispersions compared with stellar masses of the UCDs determined from the fitted surface density profiles. The results for each sight-line (x-, y- and z-axes of the simulations) are given by squares, diamonds and circles with the results for a given UCD connected by a black line.

3.4.2 Dynamical masses from central velocity dispersions

In Figure 3.5 we show σ_0, determined within $R_e/10$, in each projection compared with the stellar mass of the UCD determined from the fitted surface density profiles. We find that σ_0 for the UCDs is relatively insensitive to the line-of-sight, with a mean difference of 1.5 per cent and a maximum difference of 8 per cent from the average over the three sight-lines. This is because σ_0 is calculated within a small aperture and the tidal tails have sufficiently dispersed such that they do not have a large effect on σ_0. The velocity dispersions of the UCDs for each dE,N model are generally lower than that of the nucleus of each model which
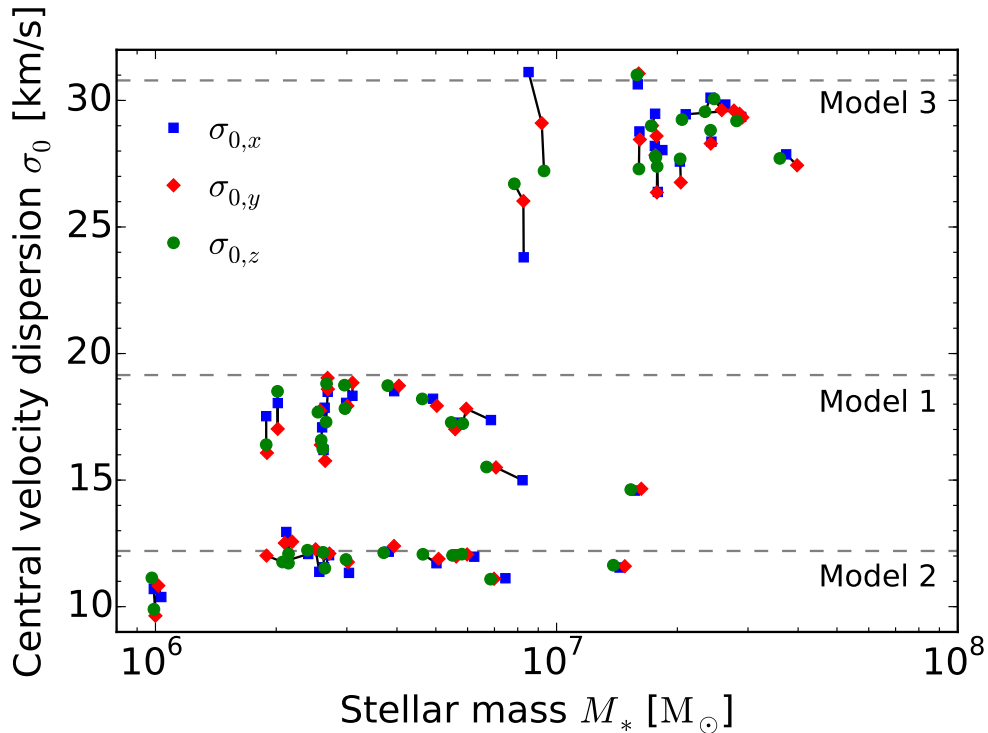
FIGURE 3.5: Central velocity dispersions for the simulated UCDs compared with their stellar masses determined from surface density fitting. σ_0 is calculated along three sight-lines for each simulation (the x-, y- and z-axes of the simulations) with the values for a given UCD connected by black lines. The dashed lines show the central velocity dispersions of the nuclei of each dE,N model.

is cause by relaxation in the centre of each model. However there is also a trend with mass (particularly evident for the dE,N model 1 simulations; see also Figure 3.11) that is due to the radius within which σ_0 is calculated. Since σ_0 is calculated within $R_e/10$, as the mass of the UCD (and thus size, see Figure 3.2) increases more particles from the stellar envelope are included which have a lower velocity dispersion than particles at the centre of the UCD.

One of the assumptions made by Forbes et al. (2014) when comparing our tidal stripping simulations from Chapter 2 against the observed UCDs was that the central velocity dispersions were constant throughout the simulations. The ratio of the final-to-initial central velocity dispersions for all simulations along the three sight-lines in shown in Figure 3.6. dE,N model 1, 2 and 3 simulations decrease to values of σ_0 that are $\sim$85, 55 and 80 per cent of the initial values, respectively. The reason for the decrease in σ_0 is the decrease of the aperture within which σ_0 is calculated. At the start of the simulations σ_0 is effectively that
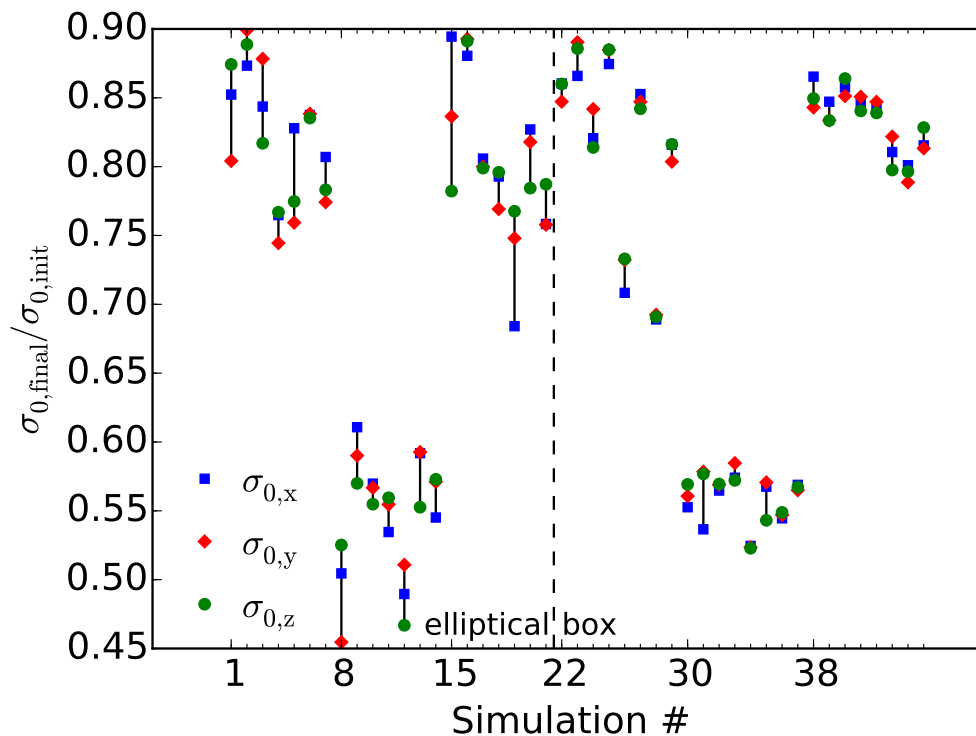
FIGURE 3.6: Ratio of final-to-initial central velocity dispersions for all simulations, where $\sigma_{0,\mathrm{final}}$ is the central velocity dispersion of the UCD formed at the end of the simulation. σ_0 is calculated along three sight-lines for each simulation (the x-, y- and z-axes of the simulations). The dashed line shows the division between elliptical and box orbit simulations.

of the main galaxy since stars from the galaxy far outnumber those of the nucleus that are included in the calculation. As the effective radius of the galaxy, and therefore the aperture, decreases due to stripping, σ_0 decreases approximately to that of the nucleus. The amount that σ_0 decreases by after tidal stripping is not constant for all galaxies but depends upon the specific parameters for the galaxy and nucleus. For the model 2 simulations σ_0 decreases by a larger amount than the model 1 simulations (the galaxies of both models have the same parameters) because the model 2 nucleus has a lower central density and therefore lower velocity dispersion. The assumption of a constant σ_0 throughout the simulations therefore does not hold. This conclusion is in contrast to the expectations of Bender, Burstein, & Faber (1992) who suggested that to a first approximation σ_0 is unchanged by the tidal stripping of the outer stars of a galaxy. However this only applies to non-nucleated galaxies since, as we have found, for nucleated galaxies σ_0 changes from that of the galaxy to that of the nucleus as the outer stars of a galaxy are removed. It is also in conflict with the results
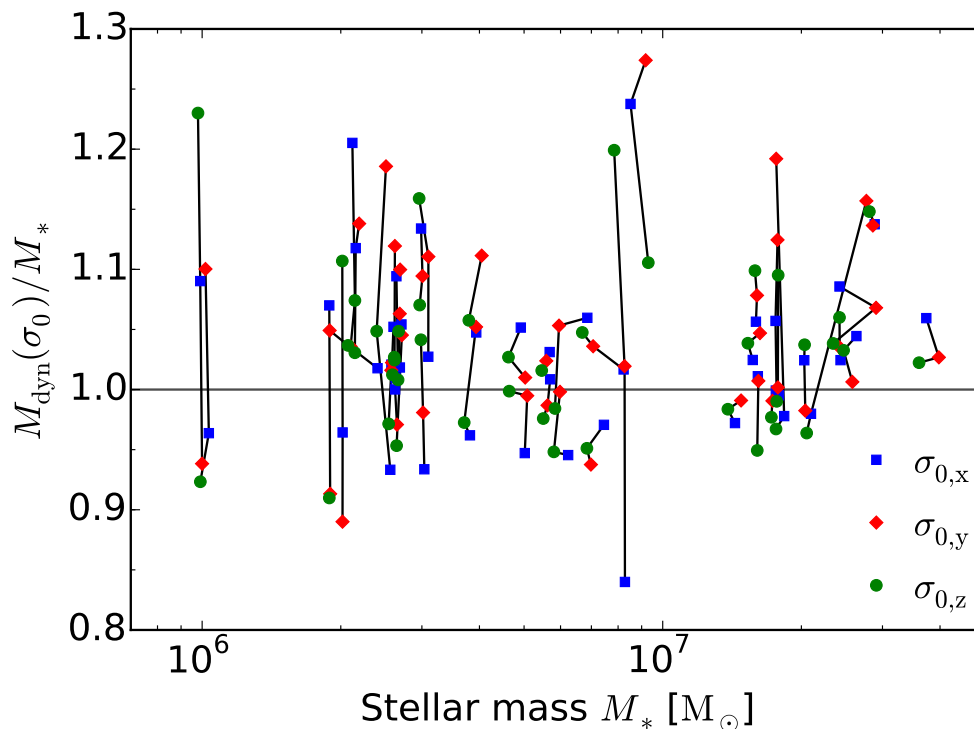
Figure 3.7: Dynamical-to-stellar mass ratios calculated from the virial theorem and using models from surface density profile fitting of the UCDs. The results for each sight-line (x-, y- and z-axes of the simulations) are given by squares, diamonds and circles with the results for a given UCD connected by a black line.

of simulations performed by Chilingarian (2009) of compact ellipticals being formed by the tidal stripping of disc galaxies with a central bulge. Their results show σ_0 is approximately constant during this process. We suggest this is due to the bulge of the galaxy having a much larger contribution to σ_0 in a disc galaxy than does the nucleus of a dwarf galaxy.

The variation of σ_0 during the simulations partially explains why Forbes et al. (2014) found final values of $M_{\mathrm{dyn}}/M_* \sim 2$ for our simulations. A reduction of σ_0 by a factor 0.85 (which applies to both our simulations that Forbes et al. investigated, simulations 3 and 39) would reduce the dynamical masses calculated via the scalar virial theorem with a constant virial coefficient by a factor 0.7. The variation of σ_0 with time is however not a complete explanation of the extreme dynamical-to-stellar mass ratios (~ 10) found for our simulations by Forbes et al.. We suggest this can be explained by a varying virial coefficient, as we discuss below.

In Figure 3.7 we show the dynamical-to-stellar mass ratios determined from their central
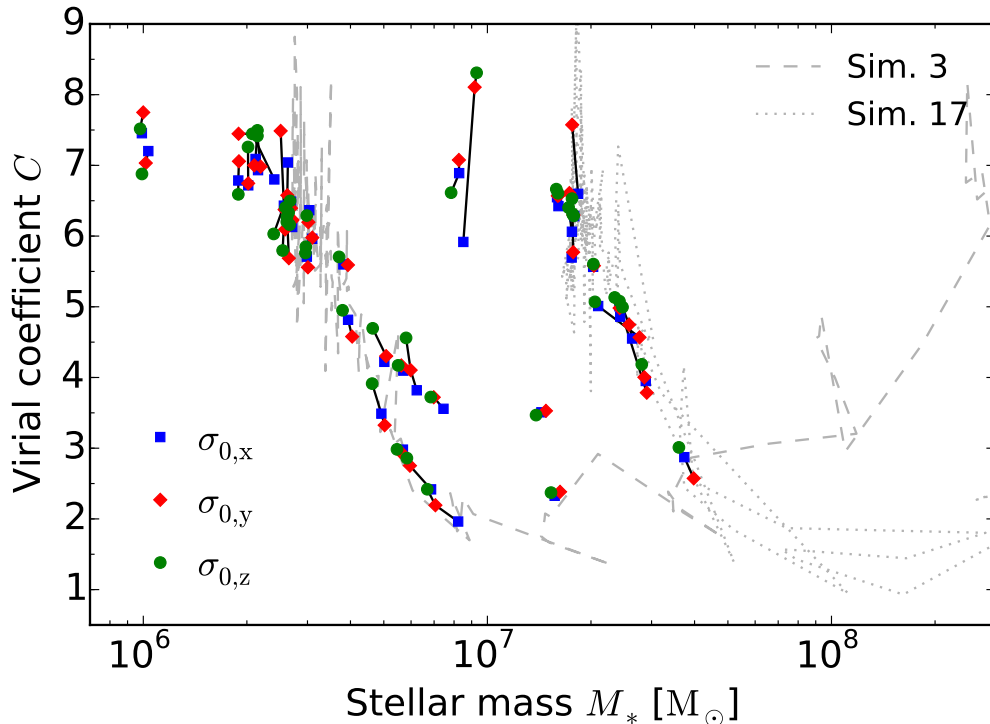
FIGURE 3.8: Virial coefficients for the idealised models of our simulated UCDs compared with their stellar masses. The results for each sight-line (x-, y- and z-axes of the simulations) are given by squares, diamonds and circles with the results for a given UCD connected by a black line. The virial coefficients over time (in the z-axis projection) for simulations 3 and 17 are shown as dashed and dotted grey lines, respectively.

velocity dispersions $M_{\mathrm{dyn}}(\sigma_0)/M_*$ for the simulated UCDs. We find on average the dynamical masses are increased by ~ 5 per cent for all projections. In contrast to $M_{\mathrm{dyn}}(\sigma_{\mathrm{obs}})/M_*$, $M_{\mathrm{dyn}}(\sigma_0)/M_*$ is relatively insensitive to the projection direction, differing by a maximum of 50 per cent between projections. As with $M_{\mathrm{dyn}}(\sigma_{\mathrm{obs}})/M_*$, we find no correlation between virial ratio Q and $M_{\mathrm{dyn}}(\sigma_0)/M_*$. We also find no correlation between $M_{\mathrm{dyn}}(\sigma_{\mathrm{obs}})/M_*$ and $M_{\mathrm{dyn}}(\sigma_0)/M_*$.

In Figure 3.8 we show the virial coefficients determined from the idealised models of the simulated UCDs (where $M_{dyn} = M_*$ by construction) compared with their stellar masses. Depending on the geometry of the tidal tails in each projection the virial coefficients of the UCDs can vary by up to a factor of 2. The virial coefficients determined from the models are generally much smaller than the virial coefficients of the initial dE,Ns (9.70, 9.67 and 9.63 for dE,N models 1, 2 and 3, respectively, determined from the parameters in Table 3.1).

The models with masses similar to the nucleus for each dE,N model have the highest virial coefficients and reach a peak with values similar to the nuclei of the dEs (7.36, 7.26 and 7.36 for models 1, 2 and 3, respectively). UCDs more massive than the model nucleus have lower virial coefficients due to the UCDs having a larger size than the nucleus. When comparing the time evolution of C for simulations 3 and 17, both simulations reach a minimum $C \sim 1$ at masses ~ 10 times that of the nucleus mass for the dE,N model. We attribute this similar trend with mass for each dE,N model to the models having the same King concentration ($c = 1.5$) for the nucleus and Sérsic index ($n = 1.5$) for the galaxy. Models with different parameters will also differ in position for the minimum of C.

As well as a decrease in σ_0 during the simulations, a changing virial coefficient as mass is stripped from the dE,N/UCD explains why Forbes et al. (2014) found very high dynamical-to-stellar mass ratios for our simulations from Chapter 2. At its minimum, the virial coefficient of the UCD differs from the initial virial coefficient of the galaxy by a factor of ~ 10. As seen in Figure 3.7 after taking this into account we find $M_{\mathrm{dyn}}/M_* \approx 1$ for the simulated UCDs. We further investigate the time evolution of M_{dyn}/M_* in the next section.

3.5 Dynamical-to-stellar mass ratios over time

For simulations 3 and 17 (dE,N model 1 and 3, respectively) we determined the dynamical masses at every snapshot from the y- and z-axis sight-lines. These simulations have the same orbit with an apocentre of 50 kpc and pericentre of 10 kpc. In Figure 3.9 we show the stellar mass at every snapshot determined from surface density fitting using the method described in Section 3.3. When tidal stripping is strongest (< 1.5 Gyr for these simulations) the mass, and similarly the effective radius, determined from surface density fitting can vary significantly depending on the line-of-sight, in this case up to a factor of ~ 10. This is due to the tidal tails being projected onto the galaxy/UCD and appearing as an extra extended component in the surface density profile (e.g. see Figure 5 of Chapter 2).

In Figure 3.10 we show σ_{obs} and $M_{\mathrm{dyn}}(\sigma_{\mathrm{obs}})/M_*$ over time for simulations 3 and 17. In the z-axis projection (perpendicular to the orbital plane) σ_{obs} decreases from that of the galaxy to that of the nucleus and quickly reaches a stable value. The simulations never reach extreme
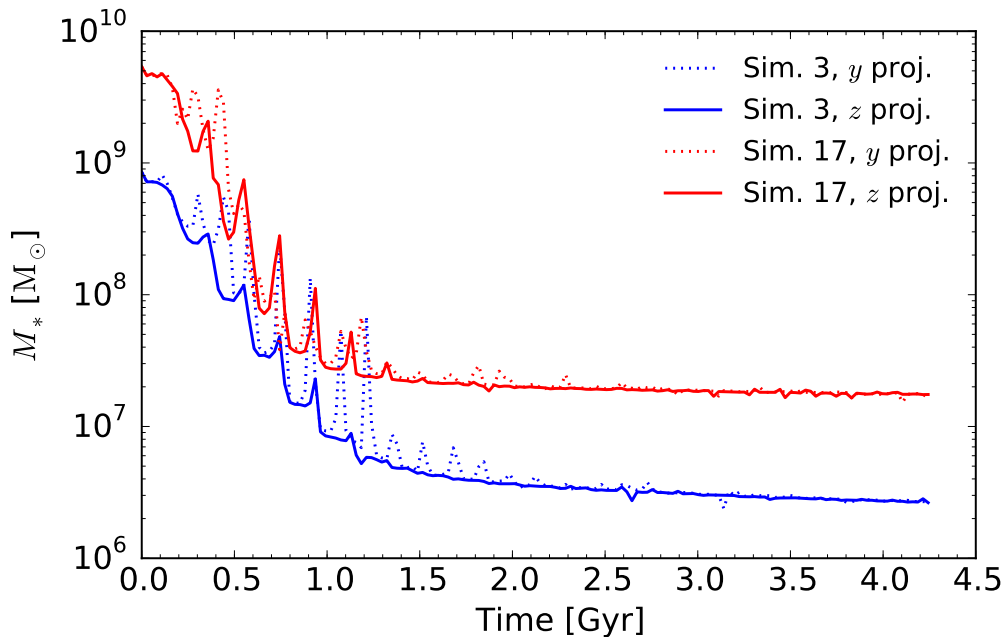
FIGURE 3.9: Time evolution of the stellar mass for simulations 3 and 17 determined from surface density fitting. Simulation 3 is shown by blue lines and simulation 17 by red line. The y-axis line-of-sight is shown by dotted lines and the z-axis line-of-sight by solid lines.

dynamical-to-stellar mass ratios and have $M_{\mathrm{dyn}}(\sigma_{\mathrm{obs}})/M_* < 2$ at all times. However in the y-axis projection (within the orbital plane) the simulations periodically have very high peaks in σ_{obs} and $M_{\mathrm{dyn}}(\sigma_{\mathrm{obs}})/M_*$ due to the changing velocity vector relative to the line-of-sight. When the velocity of the UCD is perpendicular to the line-of-sight $M_{\mathrm{dyn}}(\sigma_{\mathrm{obs}})/M_* \sim 1$. When the velocity of the UCD parallels the line-of-sight σ_{obs} is increased by the tidal tails being projected onto the UCD. Over time the magnitude of the peaks decrease as the tidal tails becomes dispersed. Simulation 3 reaches a maximum of $M_{\mathrm{dyn}}(\sigma_{\mathrm{obs}})/M_* = 33$ and simulation 17 a maximum of $M_{\mathrm{dyn}}(\sigma_{\mathrm{obs}})/M_* = 8$, both occuring at $\sim$1.2 Gyr in the simulation. At this time tidal tails would still be visible around the UCDs. Overall simulation 17 peaks at much lower $M_{\mathrm{dyn}}(\sigma_{\mathrm{obs}})/M_*$ values than simulation 3 due to the size and mass of the UCD formed, meaning the UCD fills more of the slit and the tidal tail particles are less important to the velocity dispersion calculation. After $\sim$2 Gyr the UCD in simulation 17 has $M_{\mathrm{dyn}}(\sigma_{\mathrm{obs}})/M_* < 2$.

In Figure 3.11 we show σ_0 and $M_{\mathrm{dyn}}(\sigma_0)/M_*$ over time for simulations 3 and 17. As in the previous figure, in the z-axis projection $M_{\mathrm{dyn}}(\sigma_0)/M_*$ never becomes significantly
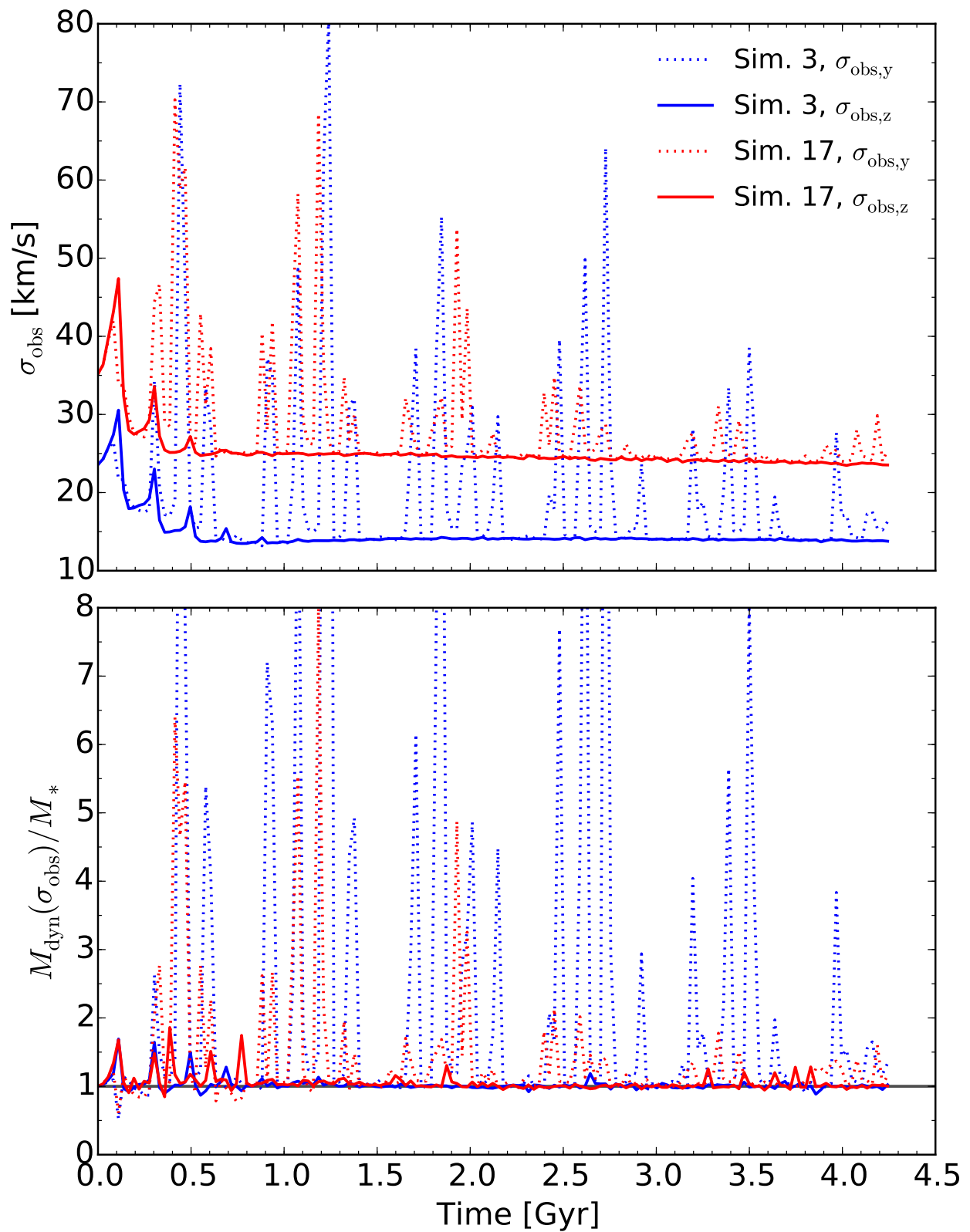
FIGURE 3.10: Time evolution of the observed velocity dispersion σ_{obs} and the dynamical-to-stellar mass ratio M_{dyn}/M_* determined from σ_{obs} for simulations 3 and 17. Simulation 3 is shown by blue lines and simulation 17 by red line. The y-axis line-of-sight is shown by dotted lines and the z-axis line-of-sight by solid lines.
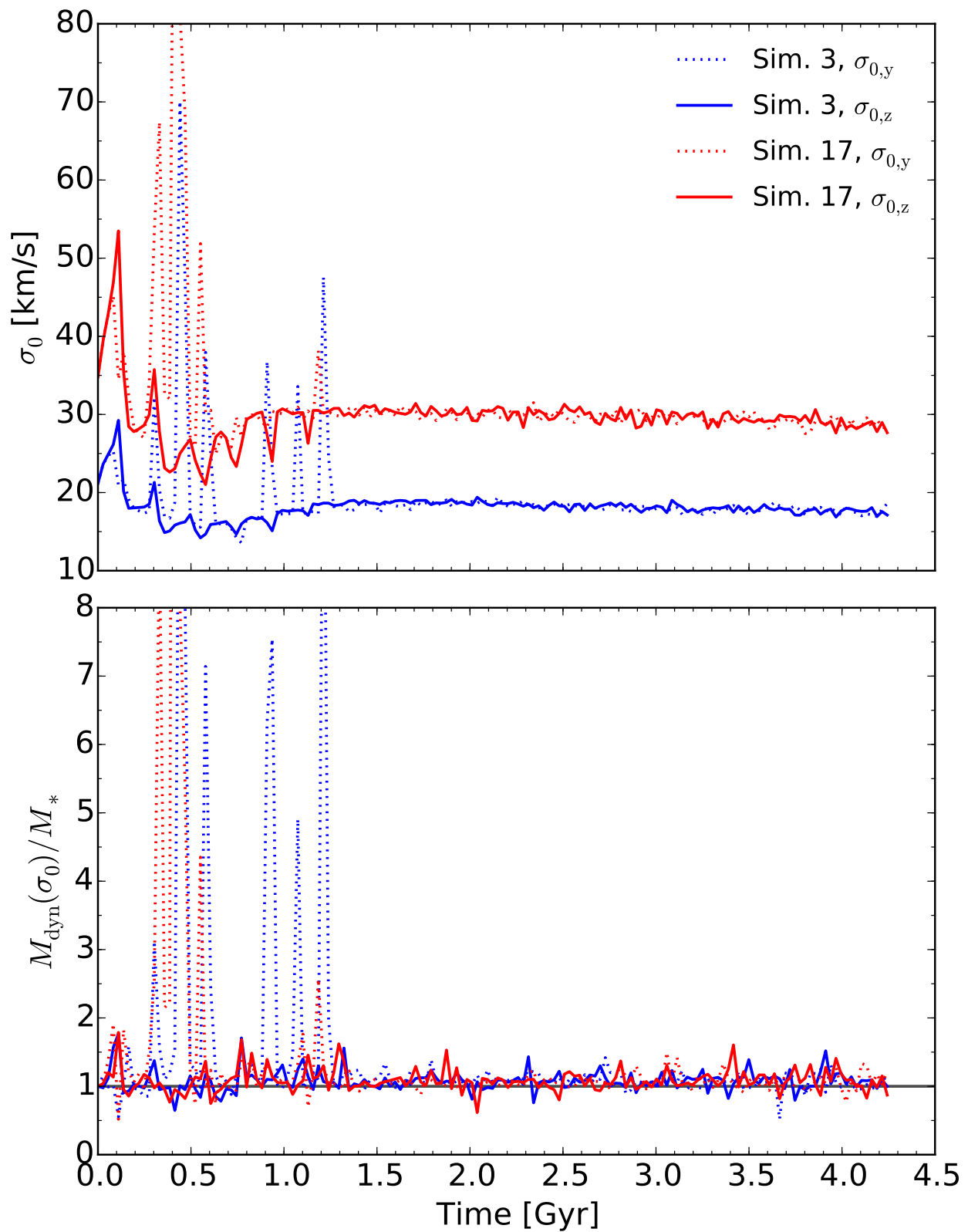
FIGURE 3.11: Time evolution of the central velocity dispersion σ_0 and the dynamical-to-stellar mass ratio M_{dyn}/M_* determined from σ_0 for simulations 3 and 17. Simulation 3 is shown by blue lines and simulation 17 by red line. The y-axis line-of-sight is shown by dotted lines and the z-axis line-of-sight by solid lines.

elevated for either simulation and at all times $M_{\mathrm{dyn}}(\sigma_0)/M_* < 2$. In the y-axis projection σ_0, and thus also $M_{\mathrm{dyn}}(\sigma_0)/M_*$, becomes very elevated during the period where mass loss is strongest (< 1.5 Gyr). This is due to the high velocity dispersion of the tidal tails in projection and also the changing aperture within which σ_0 is calculated ($R_e/10$) due to the tidal tails increasing the size of the galaxy/UCD in the surface density fitting. After the high mass-loss phase $M_{\mathrm{dyn}}(\sigma_0)/M_*$ becomes stable at ~ 1.

3.6   Conclusions

It has recently been suggested that the elevated dynamical-to-stellar mass ratios of UCDs may be explained by the tidal stripping of nucleated galaxies. In this chapter we reanalysed the tidal stripping simulations from Chapter 2 to determine the dynamical-to-stellar mass ratios of UCDs formed by tidal stripping. We measure both the velocity dispersion as seen by an observer and the central velocity dispersion in order to compare the mass ratios with observed UCDs and virial theorem estimates. We also observed all UCDs from three different projections to investigate the importance of line-of-sight on dynamical-to-stellar mass ratios. For two simulations we measured the dynamical-to-stellar mass ratios at every snapshot to investigate the evolution of the mass ratios during tidal stripping. We stress here that we did not include a dark matter halo for the dwarf galaxies in our simulations so our results are subject to the caveat that we may be underestimating the dynamical-to-stellar mass ratios of UCDs formed by tidal stripping. Observations of dE galaxies suggest they do not contain a significant amount of dark matter within an effective radius (Geha et al. 2002) consistent with a cored dark matter profile. In this case stars dominate the centre of the dwarf galaxy and a dark matter halo is not likely to have significant effect on the velocity dispersion of the UCD. This would not be the case for a very concentrated NFW profile (Navarro, Frenk & White 1996) where the formed UCD may remain dark matter dominated (Goerdt et al. 2008).

Our main conclusions are summarised as follows.

(i) Provided the tidal tails formed during tidal stripping have sufficiently dispersed, UCDs formed via this mechanism have virial ratios close to unity and are therefore in virial

equilibrium.

(ii) After tidal stripping, UCDs have velocity dispersions approximately that of the nucleus of the progenitor galaxy. Velocity dispersion is therefore not constant during tidal stripping but decreases from that of the galaxy to that of the nucleus.

(iii) Dynamical-to-stellar mass ratios determined from observed velocity dispersions are generally close to $M_{\mathrm{dyn}}/M_* = 1$ and when observing perpendicular to the orbit of the UCDs' the mass ratios are elevated by 6 per cent on average. However for recent mergers ($\lesssim 2$ Gyr) and compact UCDs where the UCD is smaller than the slit used to measure the velocity dispersion the line-of-sight becomes important. When observing nearly parallel with the velocity of the UCD, UCDs can have $M_{\mathrm{dyn}}/M_* \sim 10$ due to extra-tidal stars projected onto the UCD. For massive and extended UCDs where the UCD fills much of the slit dynamical-to-stellar mass ratios are elevated by less than 5 per cent.

(iv) For dynamical-to-stellar mass ratios determined from central velocity dispersions the line-of-sight is unimportant and the mass ratios are increased by less than 5 per cent in all projections. We also determined virial coefficients for the UCDs and found the virial coefficient evolves with the mass of the UCD, reaching a minimum $C \sim 1$ when the UCD has $\sim$10 times the mass of the model nucleus. The change in virial coefficient with mass explains why Forbes et al. (2014) found elevated mass ratios for our simulations from Chapter 2 while we find mass ratios close to unity.

(v) The time evolution of the dynamical-to-stellar mass ratios varies depending on the line-of-sight and velocity dispersion used. When observing perpendicular to the orbital plane the galaxy/UCD has $M_{\mathrm{dyn}}/M_* < 2$ at all times for both the observed and central velocity dispersions. When observing in the orbital plane dynamical-to-stellar mass ratios determined from observed velocity dispersions periodically reach extreme mass ratios ($M_{\mathrm{dyn}}/M_* > 8$) with the magnitude decreasing over time as the tidal tails disperse. When using central velocity dispersions and observing in the orbital plane the dynamical-to-stellar mass ratios are only elevated during the period of strongest

mass-loss (< 1.5 Gyr in this case) and afterwards decrease to $M_{\mathrm{dyn}}/M_* \sim 1$.

Overall our results suggest that tidal stripping is not the cause of the elevated dynamical-to-stellar mass ratios for most UCDs, especially for the most massive UCDs. Due to their larger sizes and internal velocity dispersions, we find the observed velocity dispersions of massive UCDs (10^7-10^8 M$_\odot$) are less affected by extra-tidal stars. For low-mass UCDs where the slit covers a significant fraction the UCD (e.g. S999, Janz et al. 2015) extra-tidal stars from tidal stripping may elevate the velocity dispersion if one happens to observe the UCD with a line-of-sight nearly parallel to the orbital direction of the UCD and therefore observe along the length of the tidal tails. This will be particularly important for recent mergers where the tidal tails haven't had time to significantly disperse, although in this case other effects may also be visible (e.g. low surface brightness shells, Penny, Forbes & Conselice 2012). Therefore, other explanations (e.g. central black holes, non-standard initial mass functions or dark matter) are needed to account for the dynamical-to-stellar mass ratios of UCDs.

4

Paper two: Contribution of stripped nuclear clusters to globular cluster and ultra-compact dwarf galaxy populations

Contribution of stripped nuclear clusters to globular cluster and ultracompact dwarf galaxy populations

J. Pfeffer,[1,2]★ B. F. Griffen,[3] H. Baumgardt[1] and M. Hilker[2]

[1]*School of Mathematics and Physics, The University of Queensland, Brisbane, QLD 4072, Australia*
[2]*European Southern Observatory (ESO), Karl-Schwarzschild-Strasse 2, D-85748 Garching, Germany*
[3]*Massachusetts Institute of Technology, Kavli Institute for Astrophysics and Space Research, 77 Massachusetts Avenue, Cambridge, MA 02139, USA*

ABSTRACT

We use the Millennium II cosmological simulation combined with the semi-analytic galaxy formation model of Guo et al. to predict the contribution of galactic nuclei formed by the tidal stripping of nucleated dwarf galaxies to globular cluster (GC) and ultracompact dwarf galaxy (UCD) populations of galaxies. We follow the merger trees of galaxies in clusters back in time and determine the absolute number and stellar masses of disrupted galaxies. We assume that at all times nuclei have a distribution in nucleus-to-galaxy mass and nucleation fraction of galaxies similar to that observed in the present day Universe. Our results show stripped nuclei follow a mass function $N(M) \sim M^{-1.5}$ in the mass range $10^6 < M/\mathrm{M_\odot} < 10^8$, significantly flatter than found for globular clusters. The contribution of stripped nuclei will therefore be most important among high-mass GCs and UCDs. For the Milky Way we predict between one and three star clusters more massive than $10^5\,\mathrm{M_\odot}$ come from tidally disrupted dwarf galaxies, with the most massive cluster formed having a typical mass of a few times $10^6\,\mathrm{M_\odot}$, like ω Centauri. For a galaxy cluster with a mass $7 \times 10^{13}\,\mathrm{M_\odot}$, similar to Fornax, we predict $\sim$19 UCDs more massive than $2 \times 10^6\,\mathrm{M_\odot}$ and $\sim$9 UCDs more massive than $10^7\,\mathrm{M_\odot}$ within a projected distance of 300 kpc come from tidally stripped dwarf galaxies. The observed number of UCDs are $\sim$200 and 23, respectively. We conclude that most UCDs in galaxy clusters are probably simply the high-mass end of the GC mass function.

Key words: methods: numerical – galaxies: dwarf – galaxies: formation – galaxies: interactions – galaxies: star clusters: general.

1 INTRODUCTION

Ultracompact dwarf galaxies (UCDs) are a class of stellar systems that was discovered more than a decade ago in spectroscopic surveys of the Fornax cluster (Hilker, Infante & Richtler 1999; Drinkwater et al. 2000). They have since been discovered in other galaxy clusters (Mieske et al. 2004, 2007; Haşegan et al. 2005; Jones et al. 2006; Madrid 2011; Misgeld et al. 2011; Penny, Forbes & Conselice 2012), galaxy groups (Evstigneeva et al. 2007b; Da Rocha et al. 2011), as well as isolated spiral galaxies (Hau et al. 2009). UCDs have typical ages of 10–11 Gyr (Evstigneeva et al. 2007a; Francis et al. 2012) and are typically defined to have half-light radii $7 \lesssim r_{\mathrm{h}}\,\mathrm{pc}^{-1} \lesssim 100$ and masses $M \gtrsim 2 \times 10^6\,\mathrm{M_\odot}$, making them an intermediate object between globular clusters (GCs) and dwarf galaxies.

The exact formation mechanism of UCDs and their relation to GCs and dwarf galaxies is unknown and under much debate, although a number of scenarios have been proposed. The simplest explanation is that they are the high-mass end of the GC mass func-

tion observed around galaxies with rich GC systems (Mieske, Hilker & Infante 2002; Mieske, Hilker & Misgeld 2012) where a physical mechanism causes an increasing lower size limit with increasing mass (e.g. Murray 2009). Since UCDs have larger sizes than typical GCs, they may be formed from the merger of many GCs in star cluster complexes (Kroupa 1998; Fellhauer & Kroupa 2002; Brüns et al. 2011; Brüns & Kroupa 2012). Alternatively, they could be nucleated dwarf galaxies stripped by tidal interactions such that only their compact central region remains, referred to as the tidal stripping or 'threshing' scenario (Bassino, Muzzio & Rabolli 1994; Bekki, Couch & Drinkwater 2001; Bekki et al. 2003; Drinkwater et al. 2003; Pfeffer & Baumgardt 2013). There is also evidence suggesting UCDs are a mix of stellar systems from different formation scenarios rather than a single one (Mieske et al. 2006; Brodie et al. 2011; Chilingarian et al. 2011; Da Rocha et al. 2011; Norris & Kannappan 2011).

In general, it is impossible to determine the formation mechanism of a given UCD because the predictions of internal UCD properties (size, mass, colour, velocity dispersion and metallicity) are very similar between the formation scenarios (although there are exceptions, such as NGC 4546-UCD1 which is evidently the

★ E-mail: j.pfeffer@uq.edu.au

result of tidal stripping; Norris & Kannappan 2011). Given this, comparison of UCD ages, numbers and spatial distributions with those of genuine GCs and dwarf galaxies are needed to determine the relative importance of the different UCD formation scenarios.

In this work, we concentrate on the tidal stripping scenario. Tidal stripping of nucleated dwarf galaxies is a likely origin for at least some part of the UCD population for a number of reasons: observational studies show UCDs and early-type galaxy nuclei have many common properties (Evstigneeva et al. 2008; Brodie et al. 2011). Theoretical work has also demonstrated that the sizes, masses and internal velocity dispersions of stripped nuclei and UCDs are very similar (Bekki et al. 2003; Pfeffer & Baumgardt 2013). Irregular objects with asymmetric extensions have been found which may be dwarf galaxy nuclei undergoing tidal stripping (Richtler et al. 2005; Brodie et al. 2011). Current theories of giant elliptical formation in galaxy clusters suggest the dominant growth mechanism for the galaxies from $z = 1$ to 0 is accretion through minor mergers (e.g. Naab, Johansson & Ostriker 2009). Finally, in any hierarchical galaxy formation scenario, dwarf galaxies are tidally disrupted and UCD or GC formation has to occur since the nuclei of dwarf galaxies are too compact to be destroyed (Pfeffer & Baumgardt 2013). In the Milky Way, objects such as ω Cen (Lee et al. 1999; Hilker & Richtler 2000) are thought to form via such a process and may be considered as 'low-mass' UCDs, while the ongoing formation of a 'low-mass' UCD may be observed in the M54–Sagittarius dwarf galaxy system (Ibata et al. 1997).

Previous work predicting UCD numbers and spatial distributions from tidal stripping was performed by Bekki et al. (2003) and Thomas, Drinkwater & Evstigneeva (2008), who modelled dwarf galaxies as test particles in a static potential and used a 'threshing radius' to decide if a UCD has formed or not, and Goerdt et al. (2008), who used the orbits of particles in a cosmological simulation combined with simulations of disc galaxies and dark matter haloes being disrupted in a static galaxy cluster. Both Bekki et al. and Goerdt et al. found their predictions matched observations, however, these studies were based on a very small sample of UCDs known at the time. Thomas et al., using a larger UCD sample, extended the analysis to lower luminosity UCDs and dwarf galaxies and found a static threshing model underpredicts UCDs at radii greater than 30 kpc for the Fornax cluster. Mieske et al. (2012) calculated the fraction of GCs that contribute to the UCD population based on the specific frequencies of GCs around galaxies. They found at most 50 per cent of UCDs were formed by tidal stripping.

Although they are simple to implement, static models of UCD formation in galaxy clusters have a number of disadvantages. As noted by Thomas et al. (2008), static models do not take into account UCD formation that may have occurred within smaller subclusters that later fell into the main cluster and account for the extended spatial distribution of UCDs. Galaxy clusters may have triaxial potentials, thus dwarf galaxies may be on box orbits or other chaotic orbits which provide a few close passages necessary for UCD formation but orbit at large radii at other times (Pfeffer & Baumgardt 2013). Galaxy clusters are expected to undergo many mergers with subclusters during formation, which in the process may change the radial distributions of UCDs. Therefore, predictions of UCD properties within the context of cosmologically motivated galaxy cluster formation are needed to provide a definite answer on the feasibility of the tidal stripping scenario.

In this paper we use the high-resolution Millennium II cosmological simulation combined with a state-of-the-art semi-analytic galaxy formation model (described in Section 2.1) to predict the properties of objects formed by tidal stripping of nucleated galaxies.

Throughout the paper we refer to objects formed in the simulation by tidal stripping as *stripped nuclei* since such objects may resemble both GCs and UCDs and because the observed UCD populations may be the result of more than one formation channel. This paper is organized as follows. Section 2 describes how we identify stripped nuclei in the cosmological simulation and Section 3 presents the results following from our methods. In Section 4 we compare our results with observations. In Section 5 we discuss the implications of our work for UCD formation scenarios and summarize our results in Section 6.

2 METHOD

In this section we provide an overview of the cosmological simulations we make use of and our method for defining and identifying stripped nuclei within the simulations.

2.1 Overview of simulations

Semi-analytic models (SAMs) of galaxy formation allow one to predict the properties of galaxies and how they evolve over cosmic time by applying analytic recipes to the dark matter merger trees of cosmological simulations. We make use of the state-of-the-art SAM of Guo et al. (2011) which was applied to the high-resolution Millennium II simulation (MS-II; Boylan-Kolchin et al. 2009). The MS-II has a resolution 125 times that of the Millennium simulation (Springel et al. 2005) and has a box size of 137 Mpc and a particle mass of $9.42 \times 10^6 \, M_\odot$. The SAM is constrained by low-redshift abundance and clustering in the Sloan Digital Sky Survey and is tuned to reproduce the $z = 0$ mass distribution of galaxies down to stellar masses of $10^{7.5} \, M_\odot$. For data associated with the MS-II run, we assume a cosmology consistent with the *Wilkinson Microwave Anisotropy Probe* 1-year data (*WMAP*1) results (Spergel et al. 2003) and assume $h = 0.73$ for all masses and distances. In addition, we also consider the scaled Millennium II simulation and SAM (MSII-SW7; Guo et al. 2013), which was scaled to parameters consistent with a *WMAP* 7-year cosmology (*WMAP*7; Komatsu et al. 2011), to test the importance of the assumed cosmology on our results. For data associated with the MSII-SW7 run we assume parameters consistent with a *WMAP*7 cosmology and assume $h = 0.704$ for all masses and distances. The best fit for *WMAP*7 is close to the best fit from *Planck* data (Planck Collaboration XVI 2013) and therefore results would not change significantly in this cosmology.

2.2 Simulated galaxy cluster selection

Since UCDs are mainly found in massive galaxy clusters (such as the Fornax and Virgo clusters which have virial masses of 7×10^{13} and $4 \times 10^{14} \, M_\odot$, respectively; McLaughlin 1999; Drinkwater, Gregg & Colless 2001), we only consider SAM galaxy clusters with virial masses greater than $10^{13} \, M_\odot \, h^{-1}$ ($1.37 \times 10^{13} \, M_\odot$ in MS-II, $1.42 \times 10^{13} \, M_\odot$ in MSII-SW7). From this selection we obtain 301 clusters in MS-II and 298 clusters in MSII-SW7. However, we exclude 12 clusters in MS-II and nine clusters in MSII-SW7 due to their proximity to the edge of the simulation box (where the edge of the box is within twice the virial radius of the cluster). We define SAM galaxy clusters at $z = 0$ as all galaxies that are located within twice the clusters' virial radius from the central galaxy (i.e. the galaxy at the potential minimum for the cluster). To mimic observations of galaxy clusters a better choice would be to define cluster membership by the line-of-sight velocity of a galaxy. However, since we only use the SAM galaxy clusters (and
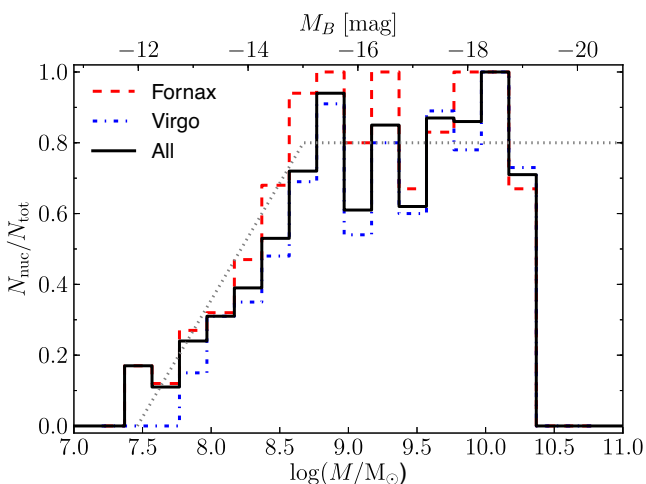
their merger histories, as discussed in Section 2.3) to choose the progenitors of the stripped nuclei, this makes little difference since there are typically few haloes beyond the virial radius large enough to form stripped nuclei.

2.3 Identifying stripped nuclei

In order to identify galaxies in the simulations which may form stripped nuclei we search the galaxy merger trees of all galaxies in the SAM galaxy clusters at $z = 0$. We define a galaxy as a possible stripped nucleus progenitor (hereafter referred to as candidate galaxies and the dark matter halo of the galaxies as candidate haloes) when the stellar mass first exceeds $10^{7.5}\,M_\odot$ (i.e. all progenitors of the candidate galaxy have a stellar mass less than this limit). We choose this lower mass cut based on the nucleation fraction observed for galaxies (see Fig. 1) where galaxies below this mass do not host nuclei. To decide if a candidate galaxy forms a stripped nucleus we search the galaxy merger tree and find when the candidates are completely disrupted according to the galaxy disruption criteria in the SAM (equation 30 of Guo et al. 2011). A stripped nucleus is formed in such a merger under following conditions.

(i) The merger was a minor merger, where we define minor mergers as those with 'dynamical' mass ratios smaller than 1:3 (as in Hopkins et al. 2010). The dynamical mass M_{dyn} is defined as $M_{dyn} = M_* + M_{gas} + M_{DM}(<r_s)$, where M_* is the stellar mass of the galaxy, M_{gas} is the cold gas mass and $M_{DM}(<r_s)$ is the mass of the dark matter halo within the Navarro–Frenk–White (NFW) scale radius. About 9 per cent of candidates have major mergers.

(ii) The merger happened at least 2 Gyr ago so there is enough time to form a UCD (Pfeffer & Baumgardt 2013). About 5 per cent of candidates merged less than 2 Gyr ago. The number of objects that we remove can also give a measure of the number of recently formed objects per galaxy cluster mass (i.e. recent mergers that may be observable): for mergers within 2 Gyr we find an average of 0.65 objects per $10^{13}\,M_\odot$ and for mergers within 1 Gyr we find an average of 0.30 per $10^{13}\,M_\odot$. These values decrease to 0.53 per $10^{13}\,M_\odot$ and 0.25 per $10^{13}\,M_\odot$, respectively, when only considering nucleated objects.

(iii) The dynamical friction time, calculated using equations (7)–(26) from Binney & Tremaine (1987), is shorter than the time the stripped nucleus has been orbiting within the halo it is associated with at $z = 0$. About 13 per cent of candidates will have inspiralled via dynamical friction.

Since the particle mass ($9.42 \times 10^6\,M_\odot$ in MS-II, $1.21 \times 10^7\,M_\odot$ in MSII-SW7) is similar to the mass of UCDs, the most bound particle of the candidate halo in the snapshot before merging is defined as the stripped nucleus that formed after the galaxy merges. We assign the stripped nucleus a mass randomly chosen from a log-normal mass function for the nucleus-to-galaxy mass ratio with a mean of 0.3 per cent and a log-normal standard deviation of 0.5 dex, based on fig. 1 4 from Côté et al. (2006). Note we do not take into account tidal stripping for the stripped nuclei (i.e. once a stripped nucleus has formed it does not lose mass).

The fraction of galaxies that are nucleated is taken from observations of galaxies in the Virgo and Fornax clusters. For galaxies more luminous than $M_B \leq -15$ mag the nuclear fraction was calculated from the properties of galaxies and nuclei in the ACS Fornax Cluster Survey (Turner et al. 2012) and ACS Virgo Cluster Survey (ACSVCS; Côté et al. 2006).[1] For the fainter galaxies, $M_B > -15$ mag, we take the compilation of Fornax galaxies from Thomas et al. (2008). The nuclear classification is based on the Fornax Cluster Catalog (Ferguson 1989). The faint Virgo galaxies are taken from the work and classification of Lisker et al. (2007, updated catalogue, private communication). For the magnitude range $-15 > M_B > -15.5$ the nucleation classification of the ACSVCS (Côté et al. 2006) was taken into account. We are confident that for the low surface brightness early-type dwarf galaxies the detection of nuclear clusters essentially is complete because the compact nuclei have a high contrast on top of the faint, extended stellar body of the galaxy. The fraction of nucleated galaxies according to their stellar mass is shown in Fig. 1. To convert from B-band luminosity to stellar mass, we choose a mass-to-light ratio of $(M/L)_B = 3\,(M/L)_\odot$ for all galaxies, the average observed for dwarf galaxies in the Virgo cluster (Chilingarian 2009). We take an average nucleation fraction of 80 per cent for galaxies more massive than $M = 4.7 \times 10^8\,M_\odot$ ($M_B = -15$ mag). For galaxies less massive than this, we choose a fraction that varies linearly (in log-space) between 80 per cent at $M = 4.7 \times 10^8\,M_\odot$ and 0 per cent at $M = 3.0 \times 10^7\,M_\odot$ ($M_B = -12$ mag). For galaxies with masses larger than $10^{11}\,M_\odot$ we assume nuclei no longer exist due to destruction by supermassive black holes (Graham & Spitler 2009). Note that the lack of nucleated galaxies with masses $10^{10.5} < M_*/M_\odot < 10^{11}$ in Fig. 1 is due to a small sample size. We make no distinction between early- and late-type galaxies since similar nucleated fractions are observed for both (e.g. Carollo et al. 1997; Böker et al. 2002; Côté et al. 2006; Seth et al. 2006). Where possible we work with fractions of stripped nuclei instead of randomly choosing galaxies to satisfy the nucleated fraction (e.g. instead of letting only 80 per cent of disrupted galaxies form a stripped nuclei we let every galaxy create 0.8 stripped nuclei). This improves our statistics.

Two possible problems related to studying UCD formation in MS-II and MSII-SW7 are the simulation mass resolution and lack of a stellar component. The first problem relates to using a single particle to represent the nucleus of a galaxy. By using a single particle, it is possible that during a merger the particle is ejected

Figure 1. Fraction of early-type galaxies with nuclear clusters in the Fornax and Virgo clusters. The data sets used for the calculation are described in Section 2.3. The grey, dotted line shows the adopted function for the nucleation fraction of galaxies.

---

[1] We used the online version of the ACSVCS nuclei catalogue which is based on Sérsic fits: https://www.astrosci.ca/users/VCSFCS/Data_Products_files/acsvcs_nuclei_sersic.dat
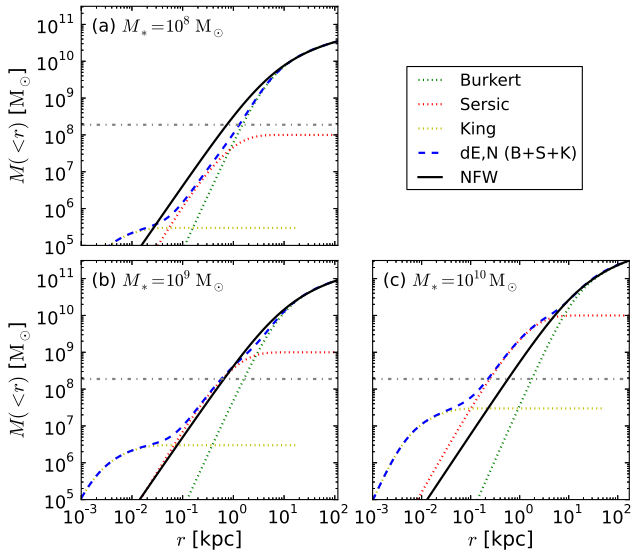
Figure 2. Cumulative mass distributions for combined King, Sérsic and Burkert models of nucleated dwarf elliptical galaxies compared with NFW models of the same total mass from MS-II. For reference, the lowest mass halo resolved in MS-II (a halo with 20 particles) is shown by a dash–dotted line.

before the merger is complete and therefore no longer accurately tracks the path of a stripped nucleus. By choosing the most bound particle of the halo just before merging as the stripped nucleus, we expect such an effect is negligible.

The second problem relates to the mass distribution of haloes in dark matter only simulations. The mass distribution of a galaxy has important implications for stripped nucleus formation since it determines how close a galaxy has to pass to the galaxy cluster centre to be disrupted (i.e. for a given mass, objects with extended mass distributions will be disrupted at larger radii than objects with more concentrated mass distributions). Haloes in dark matter only simulations are well fit by cuspy profiles (e.g. NFW profiles; Navarro, Frenk & White 1996), while the dark matter haloes of galaxies are better fit by cored profiles (Oh et al. 2011). The matter in a cuspy profile is more centrally concentrated compared to a cored profile, therefore making cuspy dark matter haloes harder to disrupt. However, the baryonic matter located within haloes is typically more concentrated than the dark matter and potentially acts as a compensating effect within cored haloes. It is uncertain how a combined stellar matter and cored dark matter profile compares with that of a cuspy dark matter profile and how this affects the number of stripped nuclei that are able to form in the simulations.

To see how differences in halo mass profiles are likely to affect our results, in Fig. 2 we compare realistic mass profiles for nucleated dwarf elliptical galaxies (dE,Ns) with NFW profiles (Navarro et al. 1996) of the same total mass. In Fig. 2(b) we show the results for a dE,N with stellar mass $10^9 \, \mathrm{M_\odot}$ which we take to be an average dE,N. For the dwarf elliptical we chose a King profile (King 1962) for the nucleus (with parameters $c = 1.5$, $R_\mathrm{h} = 4$ pc, $M = 3 \times 10^6 \, \mathrm{M_\odot}$), a Sérsic profile (Sérsic 1963) for the stellar envelope of the galaxy (with parameters $n = 1.5$, $R_\mathrm{e} = 1.0$ kpc, $M = 1 \times 10^9 \, \mathrm{M_\odot}$) and a Burkert profile (Burkert 1995) for the dark matter halo (with mass $M = 9 \times 10^{10} \, \mathrm{M_\odot}$). The parameters for the King profile are chosen to be comparable to a typical dwarf elliptical nucleus with the mass chosen to satisfy the nucleus-to-envelope luminosity ratio of 0.3 per cent for dwarf ellipticals in the Virgo cluster (Côté et al. 2006). For the stellar envelope the effec-

tive radius R_e is typical for a dwarf elliptical of this mass (Misgeld & Hilker 2011) while the Sérsic index n is chosen based on the observed M_V–n relation for early-type galaxies (Misgeld, Mieske & Hilker 2008). The dark matter mass is chosen based on the average halo virial mass for galaxies in the SAM with the same stellar mass. The concentration for the NFW profile ($c_\mathrm{NFW} = 19.3$) is chosen using the relation for subhaloes derived by Klypin, Trujillo-Gomez & Primack (2011). Remarkably, the mass profiles of the dE,N and the NFW profile in Fig. 2(b) match reasonably well above a mass of $10^7 \, \mathrm{M_\odot}$ (or a radius of 0.1 kpc), below which the nucleus dominates the mass profile of the dwarf galaxy. Therefore a dE,N with a stellar mass $10^9 \, \mathrm{M_\odot}$ and a halo with an NFW profile would likely be disrupted at a similar radius in a galaxy cluster.

If we repeat the same procedure for dE,Ns of other masses the situation is slightly different. In Fig. 2(a) we show the comparison for a dE,N with stellar mass $10^8 \, \mathrm{M_\odot}$ with King profile parameters $c = 1.5$, $R_\mathrm{h} = 4$ pc and $M = 3 \times 10^5 \, \mathrm{M_\odot}$, Sérsic profile parameters $n = 1.5$, $R_\mathrm{e} = 0.8$ kpc and $M = 1 \times 10^8 \, \mathrm{M_\odot}$ and a dark matter mass of $M = 3 \times 10^{10} \, \mathrm{M_\odot}$. In Fig. 2(c) we show the comparison for a dE,N with stellar mass $10^{10} \, \mathrm{M_\odot}$ with King profile parameters $c = 1.5$, $R_\mathrm{h} = 4$ pc and $M = 3 \times 10^7 \, \mathrm{M_\odot}$, Sérsic profile parameters $n = 1.5$, $R_\mathrm{e} = 1.5$ kpc and $M = 1 \times 10^{10} \, \mathrm{M_\odot}$ and a dark matter mass of $M = 3 \times 10^{11} \, \mathrm{M_\odot}$. For a dE,N with a stellar mass $10^8 \, \mathrm{M_\odot}$ we find the NFW profile is more concentrated than the dE,N profile, while for a dE,N with a stellar mass $10^{10} \, \mathrm{M_\odot}$ we find the dE,N profile is more concentrated than the NFW profile. Therefore it is likely we underestimate formation of stripped nuclei at the low-mass end (nuclei masses less than $10^6 \, \mathrm{M_\odot}$) and overestimate formation of stripped nuclei at the high-mass end (nuclei masses greater than $10^7 \, \mathrm{M_\odot}$).

3 RESULTS

In this section we present the results from the analysis of the simulations described in Section 2. Where not indicated otherwise, we show results from MS-II plus SAM (*WMAP*1 cosmology) where galaxy clusters are selected by cluster virial mass and work with fractions of stripped nuclei instead of randomly choosing galaxies to satisfy the nucleated fractions of progenitor galaxies (see Section 2.3).

In Fig. 3 we show the projected distribution of stripped nuclei formed in a Virgo-sized galaxy cluster (for the simulated cluster the virial mass is $1.86 \times 10^{14} \, \mathrm{M_\odot}$ and the virial radius is 1.15 Mpc). Here we randomly choose galaxies to satisfy nucleated fractions instead of working with fractions. The cluster has 200 (169) stripped nuclei in total (within the box); 103 (91) more massive than $10^6 \, \mathrm{M_\odot}$ and 35 (32) more massive than $10^7 \, \mathrm{M_\odot}$. Most of the stripped nuclei, ∼80 per cent, are located within the cluster virial radius since there are few haloes beyond this radius large enough to form them. Around 60 per cent of the stripped nuclei are located within half the cluster virial radius, with most of these associated with the central galaxy. Of the stripped nuclei associated with the central galaxy, 90 per cent are located within half the cluster virial radius. These numbers are typical for most clusters.

3.1 Number of stripped nuclei formed

3.1.1 Total number in clusters

In Fig. 4 we show the total number of stripped nuclei formed by $z = 0$ for each galaxy cluster in the SAM compared to the cluster
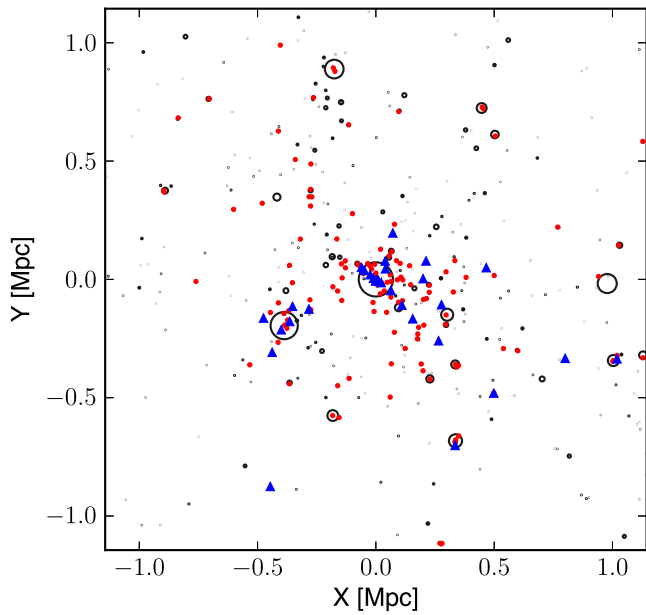
Figure 3. Projected distribution of stripped nuclei in one of the Virgo-sized galaxy clusters at $z = 0$. The stripped nuclei with masses $M_{nuc} \leq 10^7$ M$_\odot$ are shown as red points and those more massive than 10^7 M$_\odot$ are shown as blue triangles, while galaxies are shown as black circles with radii scaling with the stellar mass. The central galaxy (the galaxy at the centre of the cluster potential) is located at (0,0) and the cluster virial radius is $r_{vir} = 1.15$ Mpc, equal to the width of the box. In total there are 200 stripped nuclei in the cluster (169 within this box).

virial mass, along with the least-squares best fit and the standard deviation of the data points from the best-fitting relation for each population. For each cluster we average the number of stripped nuclei within the projected virial radius over three sightlines (the x-, y- and z-axis of the simulation). There is very little difference between using the projected and 3D virial radius. The data show an increase in scatter from the best-fitting lines for decreasing cluster masses and increasing nuclei masses which can be attributed to
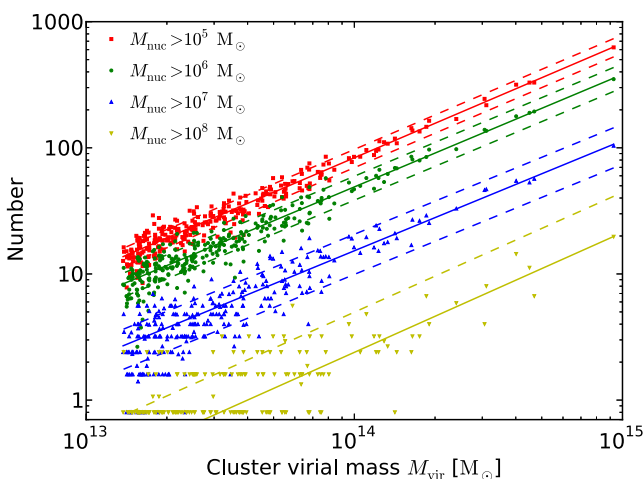
Figure 4. The number of stripped nuclei formed above a given mass located within the projected cluster virial radius at $z = 0$ for individual galaxy clusters. The least-squares best fit for each population is shown by a solid line and the standard deviation of the data points from the best fit are shown by a dashed line (we do not show the error in the best fit since this is small). The equation of best fit for each population is given in the text.

Poisson scatter and an increasing sample size. We find the best-fitting relations of the number of stripped nuclei for a given lower mass cut to be

$$N(M_{nuc} > 10^5 \, \mathrm{M}_\odot) = 10 \pm 1.7 \left(\frac{M_{vir}}{10^{13} \, \mathrm{M}_\odot} \right)^{0.91}, \qquad (1)$$

$$N(M_{nuc} > 10^6 \, \mathrm{M}_\odot) = 6.3 \pm 1.4 \left(\frac{M_{vir}}{10^{13} \, \mathrm{M}_\odot} \right)^{0.89}, \qquad (2)$$

$$N(M_{nuc} > 10^7 \, \mathrm{M}_\odot) = 2 \pm 0.71 \left(\frac{M_{vir}}{10^{13} \, \mathrm{M}_\odot} \right)^{0.87}, \qquad (3)$$

$$N(M_{nuc} > 10^8 \, \mathrm{M}_\odot) = 0.27 \pm 0.29 \left(\frac{M_{vir}}{10^{13} \, \mathrm{M}_\odot} \right)^{0.95}, \qquad (4)$$

where M_{vir} is the virial mass for the cluster and the error in the relation is the standard deviation of the data points from the mean. Interestingly the slopes of the best-fitting lines are slightly less than linear: formation of stripped nuclei is slightly more efficient in low-mass clusters than high-mass ones. This could be due to the fact that satellite galaxies have higher velocities in high-mass clusters, so that they are less likely to be on orbits needed for disruption. In MSII-SW7 the number of stripped nuclei predicted for clusters of similar mass is 5–10 per cent larger than in MS-II. However, the slopes of the fits in MSII-SW7 are almost identical to those in MS-II.

The average number of stripped nuclei associated with satellite galaxies in clusters is 36 per cent and therefore central galaxies typically have 64 per cent of stripped nuclei. The average number associated with satellite galaxies varies with cluster mass: from 34 per cent at the low-mass end ($M_{vir} < 10^{14}$ M$_\odot$) to 58 per cent at the high-mass end ($M_{vir} > 10^{14}$ M$_\odot$).

On average 22 per cent of stripped nuclei were formed in haloes which then merged into another halo. When looking only at the central galaxies in galaxy clusters, this jumps to 29 per cent on average, 28 per cent for clusters with virial masses $M_{vir} < 10^{14}$ M$_\odot$ and 35 per cent for clusters with virial masses $M_{vir} > 10^{14}$ M$_\odot$.

3.1.2 Numbers in individual galaxies

In this section we compare the number of stripped nuclei that form around individual galaxies. Specifically, we compare the numbers around central and satellite galaxies in the galaxy clusters and compare how the numbers correlate with the halo virial mass and the stellar mass of the galaxy. To determine which galaxy and halo each stripped nucleus is associated with, we trace the galaxy and halo merger trees of the candidate galaxies and haloes to the descendants at $z = 0$. We assume that when a galaxy or halo becomes disrupted by its host galaxy or halo, any stripped nuclei from the satellite are transferred to the host. Before a satellite is disrupted we assume that all stripped nuclei it hosted before infall are still associated with it, even though some nuclei may have been unbound during tidal stripping. For all satellite halo masses in this section we take the virial mass before infall into the host halo (and subsequent tidal stripping). This allows us to directly compare the number of stripped nuclei for central and satellite galaxies.

As we selected the sample of galaxy clusters from the SAM by virial mass only (see Section 2.2), our original sample of clusters only has a complete sample of central galaxies above stellar masses
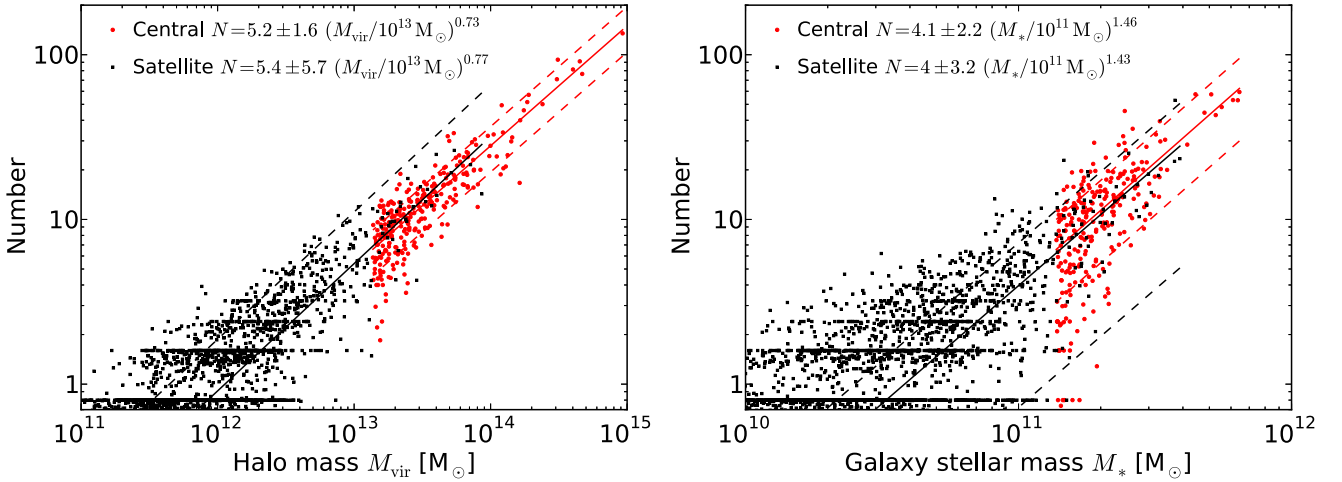
Figure 5. Number of stripped nuclei with masses larger than 10^6 M$_\odot$ formed for individual galaxies in the simulated galaxy clusters compared to the halo virial mass of the galaxy (left) and galaxy stellar mass from the SAM (right). Central galaxies (galaxies at the centre of a galaxy cluster) are shown as red dots, while satellite galaxies (all other galaxies) are shown as black squares. For satellite halo masses we take the virial mass before infall into a cluster. The least-squares best fit for each population is shown by a solid line and the standard deviation of the data points from the best-fitting line is shown by a dashed line (we do not show the error in the best fit since this is small). The equation of best fit for each population is shown in the legend of the figures. In the right-hand panel we select galaxy clusters in the SAM by central galaxy mass (described in Section 3.1.2), rather than cluster virial mass, so that the number of central galaxies is complete above 10^{11} M$_\odot$ h^{-1}.

of $\sim 3 \times 10^{11}$ M$_\odot$. Therefore, in order to obtain a complete sample to lower masses we create a new sample of clusters which are selected to have a central galaxy stellar mass larger than 10^{11} M$_\odot$ h^{-1}. This gives us a sample of 271 clusters which we analyse using the method described in Section 2.3. The new sample of clusters is therefore used for the right-hand panel in Fig. 5, while the original sample is used for the left-hand panel, where both panels are a *WMAP*1 cosmology.

In Fig. 5 we compare the number of stripped nuclei with masses larger than 10^6 M$_\odot$ that form for each galaxy against the halo virial mass and stellar mass of the galaxy. The left-hand panel of the Fig. 5 shows that the number of stripped nuclei which form for both central and satellite haloes follows a tight relation with halo mass. The best-fitting relation for each sample is almost identical, which suggests they are part of the same distribution and it is not necessary to make a distinction between central and satellite galaxies when comparing against halo mass. As in Fig. 4 most of the points in the figure are within a factor of 2 from the best-fitting relation, although there is slightly larger scatter at the low-mass end. Compared to Fig. 4, the best-fitting relation for the number of stripped nuclei with halo mass is slightly flatter (in Fig. 4 the power-law slope is $\alpha \approx 0.9$, compared to $\alpha \approx 0.75$ in Fig. 5). This can be attributed to more massive haloes having a higher proportion of satellites that can host stripped nuclei compared to lower mass haloes. In the right-hand panel of Fig. 5, as in the left-hand panel, the relations for centrals and satellites are almost identical, suggesting they are part of the same distribution. However, there is a much larger scatter in the number of stripped nuclei for a given stellar mass of a galaxy compared to the left-hand panel. We therefore suggest that the halo mass of a galaxy is a better predictor for the number of stripped nuclei formed by a galaxy than the galaxy stellar mass.

3.1.3 Most massive stripped nuclei formed

Given that galaxies and haloes of larger masses are able to tidally strip satellites of larger mass without undergoing a major merger,

it is expected that the most massive stripped nucleus for a halo should scale with halo mass. In the left-hand panel of Fig. 6 we compare the mass of the most massive stripped nucleus formed for each galaxy with the halo virial mass of the galaxy. We do not distinguish between central and satellite galaxies since we showed in Section 3.1.2 it is unnecessary when comparing against halo mass (halo mass before infall for satellite galaxies). Here we randomly choose galaxies to satisfy nucleated fractions instead of working with fractions. In the right-hand panel of Fig. 6 we compare the most massive stripped nucleus of a galaxy with the galaxy stellar mass. Again we do not distinguish between central and satellite galaxies. The maximum stripped nucleus mass is largely set by the major merger prescription and therefore scales with halo and galaxy mass. The large scatter in the maximum nucleus mass for a given halo or stellar mass can be attributed to the particular merger histories of each galaxy, as well as the distribution in the nucleus-to-galaxy mass ratio.

A tidal stripping origin has been suggested for the most massive GCs in the Milky Way and M31 and is also the most likely origin for the most massive UCDs in the Virgo and Fornax clusters. The most massive GCs in the Milky Way and M31 are ω Cen and G1, respectively. For the Virgo and Fornax clusters the most massive UCDs are M60-UCD1 and UCD3, respectively. These are shown in Fig. 6 and agree well with the predicted maximum nucleus masses for halo mass, but lie slightly under the prediction for stellar mass. We also show the most massive UCDs from NGC 3923, NGC 4546 and the Sombrero galaxy in the right-hand panel of Fig. 6. NGC 4546-UCD1 falls above the most massive nucleus we predict which may partially be caused by recent star formation (Norris & Kannappan 2011). A tidal stripping origin for these GCs and UCDs is therefore compatible with our results.

With the exception of the Virgo and Fornax clusters and NGC 4546, the masses of the most massive GCs and UCDs also agree well with that predicted from the GC luminosity functions (Hilker 2009; Norris & Kannappan 2011). Therefore an agreement between the predicted maximum stripped nucleus mass and that
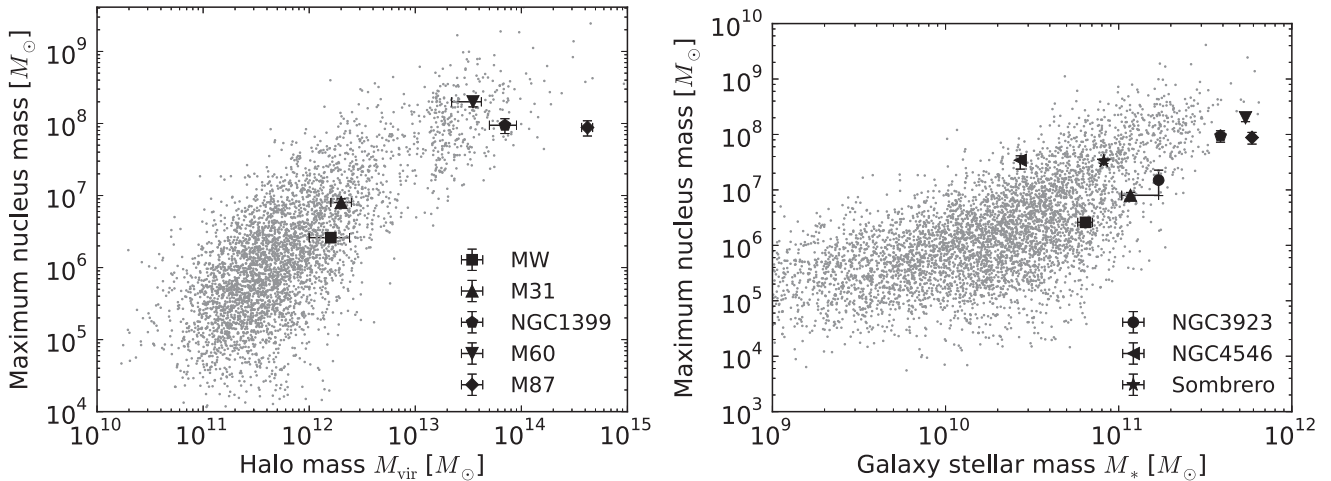
Figure 6. Maximum stripped nucleus mass for individual galaxies compared to the halo virial mass or halo mass before infall for satellite haloes (left) or galaxy stellar mass (right) of the galaxy. For the Milky Way, M31, NGC 1399, M87 and M60 the most massive GC or UCD (ω Cen, G1, UCD3, VUCD7 and M60-UCD1, respectively) are shown. The masses of ω Cen, G1, UCD3, VUCD7 and M60-UCD1 are taken from Jalali et al. (2012), Baumgardt et al. (2003), Hilker et al. (2007), Evstigneeva et al. (2007b) and Strader et al. (2013), respectively. The halo masses of the Milky Way, M31, NGC 1399, M87 and M60 are taken from Boylan-Kolchin et al. (2013), Fardal et al. (2013), Drinkwater et al. (2001), McLaughlin (1999) and Humphrey et al. (2006), respectively, where we assume NGC 1399 and M87 sit at the centre of the cluster potential. The stellar masses of the Milky Way and M31 are taken from McMillan (2011) and Geehan et al. (2006), respectively, and NGC 1399, M87 and M60 from Misgeld & Hilker (2011). In the right-hand panel we also include the most massive UCDs of NGC 3923, NGC 4546 and the Sombrero galaxy from Norris & Kannappan (2011).

observed for a galaxy does not necessarily imply a tidal stripping origin.

3.2 Mass function of stripped nuclei

In Fig. 7 we show the predicted mass function for the stripped nuclei from all clusters in MS-II compared to the mass function of GCs (a power law with a slope $\alpha \simeq -2$ for GCs more massive than $3 \times 10^5\,\mathrm{M_\odot}$; Jordán et al. 2007). For masses in the range $10^6 < M/\mathrm{M_\odot} < 10^8$ the nuclei follow a power law with a slope
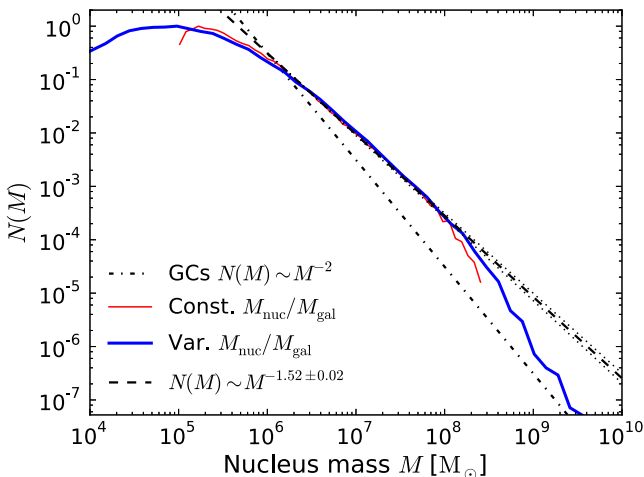

Figure 7. Normalized mass function of the stripped nuclei for all clusters with a constant nucleus mass fraction $M_{\mathrm{nuc}}/M_{\mathrm{gal}} = 0.3$ per cent (thin red solid line) and distribution in the mass fraction (thick blue solid line) compared with the mass function of GCs (dash–dotted line; arbitrarily scaled such that GCs have the same absolute number at $10^6\,\mathrm{M_\odot}$). The best-fitting slope for the stripped nuclei with masses between 10^6 and $10^8\,\mathrm{M_\odot}$ for a constant nucleus mass fraction is shown by the dashed line, with the standard deviation in the slope shown by the dotted lines.

$\alpha = -1.52 \pm 0.02$. We find no systematic variation of the slope of the mass function with galaxy cluster mass. We also compared this result to the prediction from the MSII-SW7 run and found the result is unchanged. For low-mass galaxy clusters ($M_{\mathrm{vir}} \sim 10^{13}\,\mathrm{M_\odot}$) the slope can vary significantly due to low numbers of nuclei and Poisson scatter, however, high-mass clusters ($M_{\mathrm{vir}} > 10^{14}\,\mathrm{M_\odot}$) have little scatter from the average. Below masses of $10^6\,\mathrm{M_\odot}$ the mass function of the nuclei flattens due to the decreasing nucleation fraction of the progenitor galaxies. Above masses of $10^8\,\mathrm{M_\odot}$ the nuclei mass function steepens due to the steepening of the mass function of the progenitor galaxies with stellar masses above $10^{10.5}\,\mathrm{M_\odot}$ (see fig. 7 of Guo et al. 2011). Since stripped nuclei have a flatter mass function than GCs, the contribution of stripped nuclei to UCDs will be more important at the high-mass end.

We note that this result does not take into account that stripped nuclei may retain some stars from the main galaxy (Pfeffer & Baumgardt 2013). If the average difference in size between UCDs and the nuclei of the progenitor galaxies is a factor of 2 (Evstigneeva et al. 2008), this will increase the mass by 50 per cent and therefore will not be significantly different from our prediction (assuming the increase in size is due to stripped nuclei retaining some mass from the progenitor galaxy; Pfeffer & Baumgardt 2013). In addition, we do not include ongoing tidal stripping of the objects, which would act in the opposite direction. Assuming the efficiency of these processes does not depend on the mass of the progenitor galaxy the slope of the mass function would change little, although how they affect the absolute scale is unclear.

3.3 Ages of disrupted galaxies

In the upper panel of Fig. 8 we show the predicted mass-weighted ages and merger times for the galaxies which are disrupted to form stripped nuclei, as well as the mass-weighted ages of dwarf galaxies which survive to $z = 0$. The figure shows that galaxies which merge and become stripped nuclei mostly form very early (95 per cent
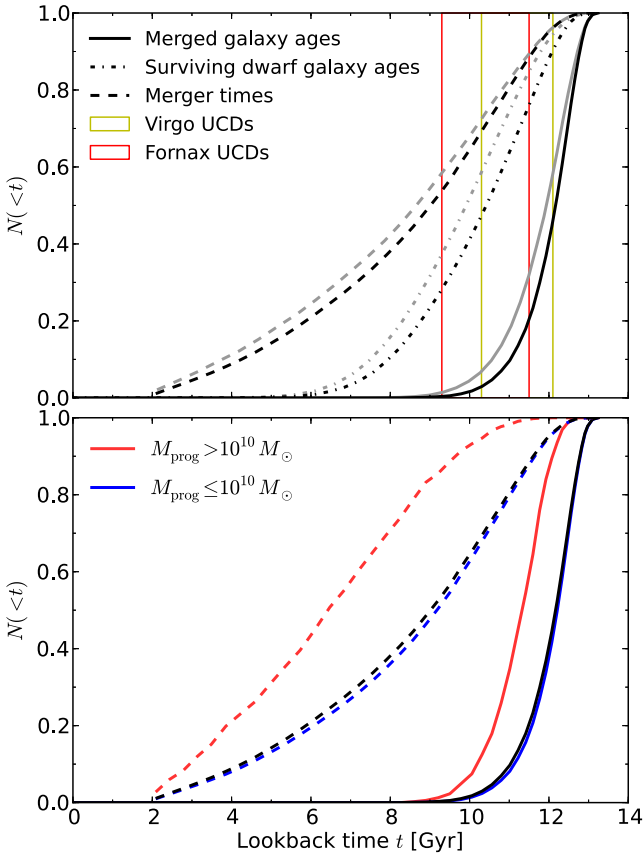
Figure 8. Normalized cumulative distribution of the predicted ages and merger times for disrupted galaxies. The *merged galaxy ages* are the mass-weighted ages of the galaxies from the SAM which are disrupted to form stripped nuclei in our model. The *surviving dwarf ages* are the mass-weighted ages of the dwarf galaxies (with masses between $10^{7.5}$ and $10^{10.5}\,\mathrm{M_\odot}$) which survive in the SAM galaxy clusters at $z = 0$. The *merger time* shows the time when the dark matter haloes of the progenitor galaxies which form stripped nuclei are no longer resolved. In the upper panel black lines show the results from a *WMAP*1 cosmology, while grey lines show results from a *WMAP*7 cosmology. We also show the standard deviation of ages of UCDs in the Virgo and Fornax clusters for comparison (Francis et al. 2012). In the lower panel we divide the progenitor galaxies into high- and low-mass groups and compare the galaxy ages and merger times for a *WMAP*1 cosmology. Since the low-mass group contains most of the galaxies its distributions are almost identical to that of the total population.

formed more than 10.5 Gyr ago), even though mergers happen up until 2 Gyr ago (the minimum time we require to form a stripped nucleus). The dwarf galaxies remaining at $z = 0$, however, are typically younger by about 2 Gyr than the dwarf galaxies that merge. This preferential disruption of old galaxies agrees well with the observation that typically only old dwarf galaxies are located near the centre of galaxy clusters (e.g. Paudel, Lisker & Kuntschner 2011). The plot also shows that there is very little difference between *WMAP*1 and *WMAP*7 cosmologies for the ages of galaxies which merge to form stripped nuclei and the merger times of disrupted galaxies. However the surviving dwarf galaxies are slightly younger (~0.5 Gyr) in a *WMAP*7 cosmology.

From the ages of the progenitor galaxies alone it is impossible to infer ages for the stripped nuclei since the ages of nuclei bear little relation to their host galaxies (Paudel et al. 2011). For our scenario we require that some part of the nucleus is built up with the formation of the galaxy or very soon afterwards (within 0.9 Gyr) in order to

explain 95 per cent of the stripped nuclei we predict. This would particularly affect the most massive nuclei since they may take a longer time to form than low-mass nuclei if they are built up by several star formation events. Therefore, in the lower panel of Fig. 8 we divide the galaxies into high-mass (galaxy stellar mass $M > 10^{10}\,\mathrm{M_\odot}$) and low-mass (galaxy stellar mass $M \leq 10^{10}\,\mathrm{M_\odot}$) groups. The figure shows that high-mass galaxies typically form about 0.8 Gyr later than low-mass galaxies, however, they also merge much later than low-mass galaxies (~2.5 Gyr later). To explain 95 per cent of the high-mass stripped nuclei (masses $M \gtrsim 10^7\,\mathrm{M_\odot}$) it is only required that the nuclei form within ~2 Gyr.

In the upper panel of Fig. 8 we also plot the mean ages of UCDs in the Virgo and Fornax clusters from Francis et al. (2012) for comparison. If nucleus formation happens (or continues to happen) sometime between the formation and the merging of the progenitor galaxy, the ages of stripped nuclei would fall well within the measured ages of UCDs.

3.4 Radial distribution of stripped nuclei

In Fig. 9 we show the projected cumulative radial distributions from the centre of a galaxy cluster for the stripped nuclei more massive than $10^6\,\mathrm{M_\odot}$, where the clusters are binned according to cluster mass. The number of simulated galaxy clusters in each mass range is 170, 58, 40 and 21, from least massive bin to most massive. For each cluster we average over three sightlines (the x-, y- and z-axis of the simulation) to calculate the radial distribution. Note that the radial distributions include stripped nuclei associated with satellite galaxies and not just those associated with the central galaxy. From least massive bin to most massive in panels (a)–(i) the percentage of stripped nuclei associated with satellite galaxies is approximately 18, 20, 25 and 28 per cent and in panel (j) it is approximately 17, 22, 30 and 43 per cent.

Panels (a)–(d) show the absolute numbers of stripped nuclei while panels (e)–(h) show the normalized radial distributions. Despite the large differences in the absolute numbers (the standard deviation for all mass bins is ~25 per cent of the mean) the normalized radial distributions have a small deviation from the mean (less than 5 per cent). In panels (i) and (j) we compare the normalized radial distributions for each mass bin. The radial profiles strongly depend on the cluster mass, with the radial profiles being more concentrated in low-mass clusters. This is partially explained by high-mass clusters having more stripped nuclei associated with satellite galaxies in the cluster, and therefore a larger number of stripped nuclei at larger projected distances. If we only plot the nuclei associated with the central galaxy panel (i) is almost unchanged, while in panel (j) the spread between the largest and smallest mass bins is reduced by about 50 per cent. The remaining difference can be explained by high-mass clusters having more mass within a given radius (or fraction of the virial radius) than low-mass clusters and can therefore tidally strip galaxies at a larger radius.

Comparing these results with observations is not trivial since one needs uniform observations that cover a significant fraction of a galaxy cluster. Such observations might become available with programs such as the Next Generation Virgo cluster Survey (NGVS; Ferrarese et al. 2012).

3.5 Orbits of stripped nuclei

One question that remains unanswered from Pfeffer & Baumgardt (2013) is whether the orbits that can explain the full size range of UCDs in galaxy clusters are likely to occur. Pfeffer & Baumgardt
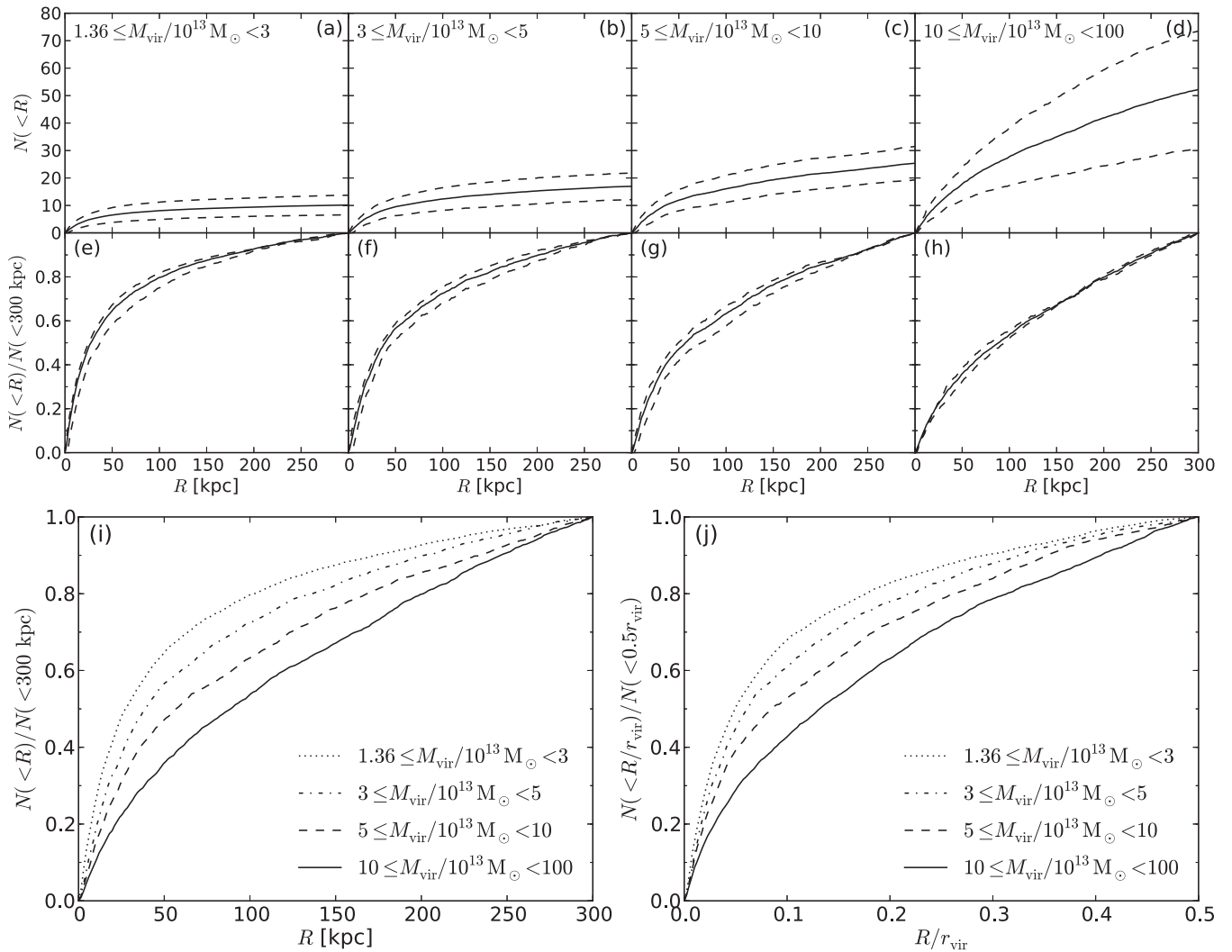
Figure 9. Projected cumulative radial distributions from the centre of the galaxy cluster for stripped nuclei with masses larger than $10^6 \, \mathrm{M_\odot}$. The panels (a)–(d) show the radial distributions within 300 kpc with the data stacked by the virial mass of the cluster (the mass ranges are indicated in each panel). The solid line shows the mean for each sample, while the dashed lines show the standard deviation. Panels (e)–(h) show the normalized distributions of panels (a)–(d). The mean and standard deviation for the absolute and normalized distributions were calculated separately. Panels (i) and (j) show the mean of the normalized radial distributions for each mass range. Panel (i) shows the radial distributions within 300 kpc, while panel (j) shows projected radius scaled by the virial radius for each cluster.

found that dwarf galaxies should have at most a few close passages within ∼10 kpc of the central galaxy in a rich galaxy cluster to form extended UCDs (those that are many times the size of dwarf galaxy nuclei of a similar mass) while those with many close passages form objects approximately the size of the nucleus. The orbits that progenitor galaxies take in galaxy clusters during the formation of GCs/UCDs therefore have strong implications for the size of objects that can form during tidal stripping.

The snapshot output times of MS-II (every 300 Myr on average between 0 and 12 Gyr in lookback time) is much too coarse to follow the orbits of galaxies which are likely to become stripped nuclei. Therefore in order to find when peri-/apocentres occur we advance the particles between snapshots based on their current position and velocity. For each candidate we find the snapshot at which the candidate halo first becomes a satellite in a larger halo, then at each snapshot until $z = 0$ we find the position and velocity of candidate halo or the most bound particle which we designated the stripped nucleus (once the candidate halo is disrupted). We use a

simple leapfrog method to advance the halo or particle between the snapshots with 1000 time steps. We take into account the gravitational potential of all subhaloes in the clusters for the potential calculation and assume an NFW profile for all haloes. The positions of all haloes are also advanced between snapshots. When determining the number of pericentre passages we assume only passages with the host halo are important for disrupting the galaxies. Since we do not know how the mass of the subhaloes change between the snapshots, we advanced the halo or particle at one time step forward, then at the next time step backward, and chose the orbit that fits the positions of the particles in the snapshots.

Since this is a rather simple and naïve analysis, there are a number of problems which may introduce significant errors. The two problems which will introduce the largest errors in the orbit calculations are not taking into account dynamical friction and not taking into account any triaxiality of haloes. Since the halo catalogues of MS-II do not include any information on triaxiality it is not

Table 1. Mean and median number of pericentre passages and fraction of objects with at least one pericentre passage less than a given distance.

Pericentre	Mean	Median	Fraction (per cent)
<5 kpc	23	9	81
<10 kpc	26	12	86
<20 kpc	28	15	91
<50 kpc	31	19	96

possible to include this effect in this work. We assume here that all pericentre passages are of equal importance to the formation of the stripped nuclei. However, since some passages may have occurred in smaller haloes before entering a galaxy cluster, we may overestimate the number of important pericentre passages to the stripped nuclei. Therefore the number of extended stripped nuclei may be larger than we predict. For these reasons we do not use the orbits to decide whether a stripped nucleus has formed and instead rely on the merger tree. The following results are therefore only approximate.

In Table 1 we show the typical number of pericentre passages for stripped nuclei with at least one passage less than a given distance. We find most candidates, 66 per cent, typically have more than three pericentre passages less than 10 kpc and therefore likely form compact objects similar to the size of the initial nucleus (within a factor of ∼2; Pfeffer & Baumgardt 2013). We also find 20 per cent of candidates have only between one and three pericentre passages less than 10 kpc and therefore satisfy the condition to form extended UCDs. Alternatively, candidates that have no pericentre passages less than 20 kpc may also form extended objects and which account for 9 per cent of candidates. However, these are mainly dwarf galaxies with stellar masses between $10^{7.5}$ and 10^9 M$_\odot$ (95 per cent of galaxies with stellar masses greater than 10^{10} M$_\odot$ have a least one orbit less than 20 kpc) and therefore will most likely still form compact objects since they will be disrupted at larger distances than more massive galaxies. This supports the view that there will be few intermediate objects between UCDs and dwarf galaxies since objects that form slowly are rare (e.g. Brodie et al. 2011; Brüns & Kroupa 2012). The final 5 per cent of candidates have no passages less than 10 kpc and at least one between 10 and 20 kpc. Since almost all of these galaxies have low masses (less than 5 per cent have masses larger than 10^{10} M$_\odot$) they will also likely form compact objects.

4 COMPARISON WITH OBSERVATIONS

4.1 Milky Way

In the Milky Way it has been suggested that the GCs ω Cen (Lee et al. 1999; Hilker & Richtler 2000), M22 (Marino et al. 2009), NGC 1851 (Han et al. 2009), Terzan 5 (Ferraro et al. 2009), NGC 2419 (Cohen et al. 2010), NGC 3201 (Simmerer et al. 2013) and NGC 5824 (Saviane et al. 2012) are the nuclei of disrupted dwarf galaxies due to either stellar populations with multiple ages or stellar populations with a spread in heavy element abundances. We use the GC luminosities from the online GC data base of Harris (1996) and the mass-to-light ratios from McLaughlin & van der Marel (2005), from which we use the Wilson fits since the fits are at least as good, and often better, than the King and power-law fits (with the exception of Terzan 5 where we take the mass from Lanzoni et al. 2010). This gives seven GCs with masses larger than 10^5 M$_\odot$ (all sug-

gested GCs) and two GCs more massive than 10^6 M$_\odot$ (ω Cen and Terzan 5) that are thought to be remnants of stripped dwarf galaxies. If we extrapolate equations (1)–(4) to the virial mass of the Milky Way $M_{\rm vir} = 1.6^{+0.8}_{-0.6} \times 10^{12}$ M$_\odot$ (90 per cent confidence interval from Boylan-Kolchin et al. 2013) we predict $1.9^{+1.3}_{-0.9}$ stripped nuclei have formed around the Milky Way with a mass larger than 10^5 M$_\odot$ and $1.2^{+0.9}_{-0.6}$ have formed with a mass larger than 10^6 M$_\odot$. Around 41^{+38}_{-23} per cent of Milky Way mass haloes are predicted to have a stripped nucleus more massive than 10^7 M$_\odot$ and 5^{+10}_{-5} per cent are predicted to have a stripped nucleus more massive than 10^8 M$_\odot$. The number of stripped nuclei predicted for the Milky Way in MSII-SW7 is very similar to that in MS-II. Therefore, given the errors from the fits in Fig. 4 and the virial mass estimates, the number of stripped nuclei that we predict with masses larger than 10^6 M$_\odot$ is completely consistent with the number that are observed in the Milky Way. For stripped nuclei with masses larger than 10^5 M$_\odot$ the number we predict is a factor of 3 lower than the number that are observed in the Milky Way. This does not necessarily imply tension with observations since the Poisson scatter is large for Milky Way-sized haloes and it is not clear whether these GCs in the Milky Way are definitely stripped nuclei or have formed via a different process. Alternatively this disagreement could be explained by low-mass dwarf galaxies having a higher nucleation fraction at early times.

4.2 M31

Four GCs around M31 have also been suggested to be the nuclei of disrupted dwarf galaxies: G1 (Meylan et al. 2001), G78, G213 and G280 (Fuentes-Carrera et al. 2008). These GCs all have masses larger than 10^6 M$_\odot$ (Strader, Caldwell & Seth 2011). Current estimates suggest a halo virial mass for M31 close to the upper bound for the Milky Way ($M_{\rm vir} = 2^{+0.5}_{-0.4} \times 10^{12}$ M$_\odot$; Fardal et al. 2013). Therefore we expect M31 to host $1.5^{+0.7}_{-0.5}$ stripped nuclei with masses larger than 10^6 M$_\odot$, a factor of 2 lower than the number suggested by observations. However in Fig. 5 some haloes with masses of $\sim 2 \times 10^{12}$ M$_\odot$ do host four stripped nuclei with masses larger than 10^6 M$_\odot$ and therefore M31 may have had more mergers than typical for its halo mass.

4.3 Fornax cluster

The Fornax cluster has the best studied UCD population of any galaxy cluster (e.g. Mieske et al. 2004; Gregg et al. 2009) and therefore offers the best possibility to compare our predictions with observations. The observed number of UCDs in Fornax and their luminosities and for some cases dynamical masses are taken from a compilation of confirmed UCDs from work by Hilker et al. (1999, 2007), Drinkwater et al. (2000), Mieske et al. (2002, 2004, 2008), Bergond et al. (2007), Firth et al. (2007), Gregg et al. (2009), Schuberth et al. (2010) and Chilingarian et al. (2011), where we assume UCDs are any objects with masses above 2×10^6 M$_\odot$. The masses were calculated from the V-band luminosity and $(V - I)$ colour of the UCDs, assuming a M/L_V–$(V - I)$ relation according to Maraston (2005) SSP models [Kroupa initial mass function (IMF), blue horizontal branch] for ages above 11 Gyr (see Misgeld & Hilker 2011).

Within a clustercentric radius of $0°9$, which corresponds to ~ 300 kpc at the Fornax distance of 19 Mpc (Ferrarese et al. 2000), the numbers of UCDs with masses above 10^7 M$_\odot$ is more than 95 per cent complete thanks to the all-targets approach by the 2dF Fornax surveys of Drinkwater et al. (2000) and Gregg et al. (2009). For UCDs with masses above 2×10^6 M$_\odot$ the completeness is

Table 2. Number of predicted stripped nuclei and the number of confirmed UCDs observed in the Fornax cluster within a given projected radius. The observed number of UCDs with masses $M > 2 \times 10^6$ M$_\odot$ represents lower limits because of incompleteness.

Mass (M$_\odot$)	$R < 83$ kpc		$R < 300$ kpc	
	Pred.	Obs.	Pred.	Obs.
$>2 \times 10^6$	$11.6^{+5.7}_{-4.9}$	>146	$19.0^{+8.9}_{-7.5}$	>193
$>10^7$	$5.6^{+3.5}_{-2.9}$	16	$8.5^{+5.0}_{-4.1}$	23
$>10^8$	$1.1^{+1.5}_{-1.1}$	0	$1.5^{+1.9}_{-1.4}$	0

not easy to access. Most spectroscopic surveys concentrated on the inner 15 arcmin from the cluster centre, i.e. a projected radius of <83 kpc at Fornax distance. Within 50 kpc the UCD number counts above 2×10^6 M$_\odot$ are nearly complete (see discussion in Mieske et al. 2012). Beyond this radius the spectroscopic coverage becomes patchy (see Schuberth et al. 2010) and the completeness drops below 70 per cent within 100 kpc and probably is even lower beyond that. In terms of the total number the effect is not that dramatic, since the radial number density profile of UCDs decreases rapidly with clustercentric distance.

In Table 2 we show the predicted number of stripped nuclei for a simulated cluster with the virial mass of the Fornax cluster as well as the observed number of UCDs in the Fornax cluster. The predicted number of stripped nuclei are taken from equations (2)–(4). We assume a virial mass for the Fornax cluster of $(7 \pm 2) \times 10^{13}$ M$_\odot$ (Drinkwater et al. 2001). We predict about one stripped nucleus with a mass $M > 10^8$ M$_\odot$ in the Fornax cluster, which agrees well with the observed most massive 'UCD3', which has a dynamical mass $M \approx 10^8$ M$_\odot$ (Hilker et al. 2007). The number of stripped nuclei with masses $M > 10^7$ M$_\odot$ we predict can account for 20–60 per cent of the UCDs in the Fornax cluster, with a mean of 40 per cent. For UCDs with masses $M > 2 \times 10^6$ M$_\odot$ stripped nuclei can only account for 5–12 per cent of the number observed. This fraction is likely slightly lower due to the incompleteness of observed UCDs. If we assume all stripped nuclei are twice the effective radius of the original nucleus due to retaining stars from the host galaxy, the stripped nuclei will have a mass 1.5 times that of the nucleus (Pfeffer & Baumgardt 2013). Taking this into account, we would predict $10.7^{+5.9}_{-4.9}$ stripped nuclei with masses $M > 10^7$ M$_\odot$. This would account for 25–70 per cent of the UCDs observed in Fornax with similar masses.

This means that most of the UCDs below 10^7 M$_\odot$ are most probably genuine globular clusters in accordance with the results of Mieske et al. (2012). For UCDs with masses above 10^7 M$_\odot$ a significant fraction is likely to be stripped nuclei.

5 DISCUSSION

5.1 Are UCDs stripped nuclei?

We find the contribution of stripped nuclei to UCD populations in galaxy clusters is only important for the most massive UCDs ($M > 10^7$ M$_\odot$). In the Fornax cluster stripped nuclei can only account for up to 26 per cent of UCDs more massive 2×10^6 M$_\odot$. Therefore our finding suggests most UCDs are part of the bright tail of the GC population in agreement with Mieske et al. (2012).

Many UCDs appear to have elevated dynamical mass-to-light ratios, implying notable amounts of dark mass in them (Mieske et al. 2013). Mieske et al. note that within their sample, two-thirds of high-mass UCDs ($M > 10^7$ M$_\odot$) and one-fifth of low-mass UCDs ($2 \times 10^6 < M/$M$_\odot < 10^7$) require at the 1σ level some additional dark mass to account for their elevated dynamical mass-to-light ratio. They suggest central black holes as relict tracers of massive progenitors are a plausible explanation for the elevated mass-to-light ratios, which implies many of the more massive UCDs are stripped nuclei. Within the errors, these fractions are in good agreement with the number of UCDs we predict to form via tidal stripping in the Fornax cluster.

The difference between the observed number of UCDs and the predicted number of stripped nuclei suggests GCs dominate the combined GC plus stripped nucleus mass function, with the exception of the most massive objects. This agrees well with the luminosity function of UCDs in the Fornax cluster (Gregg et al. 2009, see fig. 4) where the most luminous UCDs appear as a bright tail on top of the GC luminosity function. Interestingly, this is not seen in the GC mass function of Hilker (2009, see fig. 4). The origin of this difference is unclear. The difference in the slope of the power law for GCs, $\alpha = -2$ for masses $M > 3 \times 10^5$ M$_\odot$, and stripped nuclei, $\alpha = -1.4$ for masses $10^6 < M/$M$_\odot < 10^8$, may provide a way to further test our tidal stripping model observationally.

Other recent studies have investigated whether tidal stripping of dwarf galaxies in clusters can account for the UCDs observed in clusters. Mieske et al. (2012) calculated the fraction of GCs that contribute to the UCD population based on the specific frequencies of GCs around galaxies. They found at most 50 per cent of UCDs can have been formed by tidal stripping. Around NGC 1399, they found if tidal stripping contributes 50 per cent of the observed UCDs then $\gtrsim$ 90 per cent of primordial dwarf galaxies in the central ~50–70 kpc of the galaxy cluster must have been disrupted. However we find at most 12 per cent of UCDs are formed by tidal stripping. Repeating their calculation and taking this into account implies only ~40 per cent of primordial dwarf galaxies must have been disrupted. These calculations assume that any UCDs formed by tidal stripping must have formed at the centre of the galaxy cluster. In our model about 28 per cent of stripped nuclei associated with the central galaxy in a Fornax-sized galaxy cluster have been stripped from satellite galaxies which have since merged in the cluster. This would then imply only ~35 per cent of primordial dwarf galaxies in the centre of galaxy clusters have been disrupted.

Thomas et al. (2008) investigated a static model of tidal stripping in a Fornax-like galaxy cluster where dwarf galaxies are disrupted and form UCDs if they pass within a given radius. They found a static model predicts far too few UCDs at radii greater than about 30 kpc. Our model relieves some tension from the static models since not all UCDs must be formed in the cluster itself. Some UCDs are still associated with satellite galaxies within the clusters, while others have been stripped from satellite galaxies which have since merged in the cluster. We find approximately 36 per cent of stripped nuclei are associated with satellite galaxies in clusters. On average 22 per cent of stripped nuclei were formed around satellite galaxies that have since merged in the cluster. Stripped nuclei that are associated with satellites or formed around galaxies which later merged into the cluster will tend to be found at larger radii in clusters than those formed around the central galaxy and may therefore account for extended distribution of UCDs.

There are a number of further tests needed for our model. Comparing the absolute number of stripped nuclei predicted against

the numbers observed is the most direct test. In particular comparisons of the number of stripped nuclei around central and satellite galaxies, as well as clusters of different masses, are particularly important. We find that stripped nuclei should scale with the halo virial mass for the galaxy. However, determining whether an object is a stripped nucleus or a normal GC is difficult without resolved stellar populations (such as in the Milky Way). Alternatively, enhanced mass-to-light ratios, above that expected from stellar populations, may indicate a tidal stripping origin rather than a GC origin (e.g. if stripped nuclei host central black holes; Mieske et al. 2013).

We predict a minimum 20 per cent of stripped nuclei should be extended, with sizes more than twice that of the nucleus in the progenitor galaxy. It is likely the fraction is higher since interactions with satellite galaxies will have less affect on a dwarf galaxy than those with massive galaxy clusters. However, the observational completeness for such objects is relatively unknown and therefore more observations are required before a comparison can be made.

Since tidal tails of disrupting dwarf galaxies are expected to disperse and become unobservable on time-scales of $\sim$1 Gyr (Pfeffer & Baumgardt 2013) this gives constraints on the number of disrupting objects we can expect to observe in galaxy clusters. We find that an average of 0.3 objects (with stellar masses larger than $10^{7.5}$ M$_\odot$ before stripping) per 10^{13} M$_\odot$ have had mergers within the last 1 Gyr, or 0.25 per 10^{13} M$_\odot$ when only considering nucleated galaxies. Thus, given their halo virial masses, the Fornax and Virgo clusters are expected to have 2–3 and 11–14 disrupting galaxies which may be observable, and 2 and 9–12 disrupting nucleated galaxies, respectively.

5.2 Caveats

By far the largest source for error in our method is assuming that nuclei at high redshift adopt the same relations we observe at low redshift, in particular that the nucleus-to-galaxy mass ratio and the fraction of galaxies that host nuclei are constant at all times. If this is different in the early Universe it may significantly affect our predictions for the number of stripped nuclei and their mass function. If nuclei are mainly formed after their progenitor galaxy this may imply a steeper mass function than we predict (Fig. 7) due to galaxies that merge early having less massive nuclei than similar galaxies which merge later. If at least some part of the nucleus is formed with the galaxy than the total number of stripped nuclei will be largely unaffected. If most nuclei are formed well after their host galaxy this could reduce the total number of stripped nuclei significantly. Some evidence for the latter exist in observations. Paudel et al. (2011) find nuclei are typically much younger than their host galaxies (3.5 Gyr on average). However, since the nuclei are modelled as simple stellar populations, any recent star formation may bias the nuclei to lower ages and does not rule out the formation of part of the nuclei at early times.

Other sources of error follow from the SAM. Weinmann et al. (2011) find the dwarf-to-giant galaxy ratio in model clusters is too high by a factor of $\sim$50 per cent. They suggest tidal disruption of low-mass galaxies is not efficient enough in the SAM. Since the ratio of disrupted to non-disrupted galaxies in the model clusters is about 60 per cent, this means we may be underestimating the number of stripped nuclei formed by 50 per cent. Guo et al. (2011) note that the abundance of low-mass galaxies ($\sim 10^{10}$ M$_\odot$) is overproduced at early times ($z > 0.6$), indicating that star formation in low-mass galaxies may be too efficient at early times in their model. This may not be a significant problem for our model be-

cause dwarf galaxies merge at much later times than when they form (see Fig. 8). However, this may affect the amount of time a nucleus has to form if it forms after the host galaxy and therefore relates to the first caveat. Low-mass galaxies in the SAM are also too strongly clustered on scales below 1 Mpc: too large a fraction of the model galaxies are satellites, although the overall abundance of galaxies matches well (Guo et al. 2011). They suggest a lower value for the linear fluctuation amplitude σ_8 would reduce this clustering. This would affect our predictions little since the fraction of mass in a halo that was accreted in subhaloes of a given mass is relatively insensitive to the shape of the power spectrum (Zentner & Bullock 2003; Dooley et al. 2014). A lower value for σ_8 also results in subhaloes merging later which would allow more time for nuclei to form. There is only a slight improvement in these problems between MS-II and MSII-SW7 since the decrease in σ_8 between *WMAP*1 and *WMAP*7 is compensated by an increase in matter density Ω_m (Guo et al. 2013).

In our model we do not take into account continuous tidal stripping of the stripped nuclei or that some objects may retain part of the host galaxy after stripping. Continuous tidal stripping will mainly affect the most massive and more extended objects near the centre of haloes (or objects with very radial orbits, but these will be fewer) and may need to be taken into account when comparing radial distributions with observations. This effect will mainly decrease high-mass stripped nuclei and therefore slightly increase the low-mass numbers (assuming low-mass stripped nuclei will tend to be more compact and therefore largely unaffected). During the tidal stripping process, objects that have few close passages in galaxy clusters may retain some part of their host galaxy (Pfeffer & Baumgardt 2013). Objects that have many pericentre passages at distances larger than about 10 kpc may have an effective radius a factor of 2 larger than the isolated nucleus, or a factor of 1.5 in mass (e.g. their simulations 4, 11 and 18), while objects that have many passages less than 10 kpc will appear about the same size as the isolated nucleus. Objects which have only one to three passages less than about 10 kpc, but many at much larger distances, may appear more than twice the size of the nucleus (i.e. their 'box orbits'). In Section 3.5 we showed that the number of objects which have box orbits are likely to be few ($\sim$20 per cent) and most objects will have many passages less than 10 kpc ($\sim$54 per cent). Therefore for most objects retaining part of the host galaxy has little effect.

6 SUMMARY

In this paper we present the first work to study GC and UCD formation within the framework of cosmology. We use cosmological simulations combined with a semi-analytic galaxy formation model to predict the properties of stripped nuclei that form via tidal stripping. Our main conclusions are summarized as follows.

(i) The number of stripped nuclei scales with cluster virial mass slightly less than linearly ($N \sim M_{\rm vir}^{0.9}$): formation is slightly more efficient in low-mass clusters than high-mass ones. For individual galaxies it scales as $N \sim M_{\rm vir}^{0.7}$. Stripped nuclei numbers only scale with galaxy stellar mass in the sense that high-mass galaxies typically reside in high-mass haloes, therefore, there is large scatter. The average fraction of stripped nuclei associated with satellite galaxies in galaxy clusters is 35 per cent.

(ii) Between masses of 10^6 and 10^8 M$_\odot$, the mass function of stripped nuclei is approximately a power law with $N(M) \sim M^{-1.5}$. In order to compare the predicted mass function with observations

we require observations that are complete to masses of a few times $10^6\,\mathrm{M_\odot}$ for GCs and UCDs. We predict there should be a break in the combined GC and UCD mass function (although not at which mass) which changes from a GC-dominated regime with $N(M) \sim M^{-2}$ to a stripped-nucleus-dominate regime, unless GCs completely dominate the mass function.

(iii) The progenitor galaxies of stripped nuclei are typically very old ($\sim$12 Gyr), while the formation of stripped nuclei happens right up until 2 Gyr ago (our minimum time for formation). If nucleus formation happens, or continues to happen, sometime between the formation and merging of the progenitor galaxy (within 1 Gyr for low-mass galaxies, 2 Gyr for high-mass galaxies with masses larger than $10^{10}\,\mathrm{M_\odot}$) the ages of stripped nuclei agree well with those of observed UCDs.

(iv) When distances are scaled by the cluster virial radius, the radial distributions of stripped nuclei in low-mass clusters are more concentrated than distributions in high-mass clusters. Detailed comparison with observed radial distributions is needed to further test our model, but is beyond the scope of this paper. Comparisons may be possible with programs such as the NGVS.

(v) During the formation of stripped nuclei, most objects have many close pericentre passages less than 10 kpc, while 20 per cent have only between one and three passages less than 10 kpc which is required for extended UCD formation (objects more than two time the size of the nucleus). Therefore tidal stripping will preferentially result in compact objects similar in size to the initial nucleus.

(vi) We predict that between one and three stripped nuclei more massive than $10^5\,\mathrm{M_\odot}$ and one to two stripped nuclei more massive than $10^6\,\mathrm{M_\odot}$ will form for systems with the virial mass of the Milky Way. For nuclei with masses larger than $10^6\,\mathrm{M_\odot}$, this agrees well with the number of GCs in the Milky Way which have a spread in heavy element abundances and therefore were likely formed inside a dwarf galaxy. However for masses above $10^5\,\mathrm{M_\odot}$ the number predicted is a factor of 3 lower than the number of GCs suggested to be stripped nuclei. The most massive nuclei predicted to form in the Milky Way and M31 agree well with the masses of ω Cen and G1, the most massive GCs from each galaxy, respectively.

(vii) In the Fornax cluster stripped nuclei can only account for up to 12 per cent of UCDs more massive than $2 \times 10^6\,\mathrm{M_\odot}$. For UCDs more massive than $10^7\,\mathrm{M_\odot}$, between 20 and 60 per cent are likely to be stripped nuclei, or 25–70 per cent when taking into account stellar envelopes from tidal stripping. This agrees well with the result of Mieske et al. (2012) that most UCDs are part of the bright tail of the GC population.

ACKNOWLEDGEMENTS

REFERENCES

Bassino L. P., Muzzio J. C., Rabolli M., 1994, ApJ, 431, 634
Baumgardt H., Makino J., Hut P., McMillan S., Portegies Zwart S., 2003, ApJ, 589, L25
Bekki K., Couch W. J., Drinkwater M. J., 2001, ApJ, 552, L105
Bekki K., Couch W. J., Drinkwater M. J., Shioya Y., 2003, MNRAS, 344, 399
Bergond G. et al., 2007, A&A, 464, L21
Binney J., Tremaine S., 1987, Galactic Dynamics. Princeton Univ. Press, Princeton, NJ
Böker T., Laine S., van der Marel R. P., Sarzi M., Rix H.-W., Ho L. C., Shields J. C., 2002, AJ, 123, 1389
Boylan-Kolchin M., Springel V., White S. D. M., Jenkins A., Lemson G., 2009, MNRAS, 398, 1150
Boylan-Kolchin M., Bullock J. S., Sohn S. T., Besla G., van der Marel R. P., 2013, ApJ, 768, 140
Brodie J. P., Romanowsky A. J., Strader J., Forbes D. A., 2011, AJ, 142, 199
Brüns R. C., Kroupa P., 2012, A&A, 547, A65
Brüns R. C., Kroupa P., Fellhauer M., Metz M., Assmann P., 2011, A&A, 529, A138
Burkert A., 1995, ApJ, 447, L25
Carollo C. M., Stiavelli M., de Zeeuw P. T., Mack J., 1997, AJ, 114, 2366
Chilingarian I. V., 2009, MNRAS, 394, 1229
Chilingarian I. V., Mieske S., Hilker M., Infante L., 2011, MNRAS, 412, 1627
Cohen J. G., Kirby E. N., Simon J. D., Geha M., 2010, ApJ, 725, 288
Côté P. et al., 2006, ApJS, 165, 57
Da Rocha C., Mieske S., Georgiev I. Y., Hilker M., Ziegler B. L., Mendes de Oliveira C., 2011, A&A, 525, A86
Dooley G. A., Griffen B. F., Zukin P., Ji A. P., Vogelsberger M., Hernquist L. E., Frebel A., 2014, ApJ, 786, 50
Drinkwater M. J., Jones J. B., Gregg M. D., Phillipps S., 2000, Publ. Astron. Soc. Aust., 17, 227
Drinkwater M. J., Gregg M. D., Colless M., 2001, ApJ, 548, L139
Drinkwater M. J., Gregg M. D., Hilker M., Bekki K., Couch W. J., Ferguson H. C., Jones J. B., Phillipps S., 2003, Nature, 423, 519
Evstigneeva E. A., Gregg M. D., Drinkwater M. J., Hilker M., 2007a, AJ, 133, 1722
Evstigneeva E. A., Drinkwater M. J., Jurek R., Firth P., Jones J. B., Gregg M. D., Phillipps S., 2007b, MNRAS, 378, 1036
Evstigneeva E. A. et al., 2008, AJ, 136, 461
Fardal M. A. et al., 2013, MNRAS, 434, 2779
Fellhauer M., Kroupa P., 2002, MNRAS, 330, 642
Ferguson H. C., 1989, AJ, 98, 367
Ferrarese L. et al., 2000, ApJ, 529, 745
Ferrarese L. et al., 2012, ApJS, 200, 4
Ferraro F. R. et al., 2009, Nature, 462, 483
Firth P., Drinkwater M. J., Evstigneeva E. A., Gregg M. D., Karick A. M., Jones J. B., Phillipps S., 2007, MNRAS, 382, 1342
Francis K. J., Drinkwater M. J., Chilingarian I. V., Bolt A. M., Firth P., 2012, MNRAS, 425, 325
Fuentes-Carrera I., Jablonka P., Sarajedini A., Bridges T., Djorgovski G., Meylan G., 2008, A&A, 483, 769
Geehan J. J., Fardal M. A., Babul A., Guhathakurta P., 2006, MNRAS, 366, 996
Goerdt T., Moore B., Kazantzidis S., Kaufmann T., Macciò A. V., Stadel J., 2008, MNRAS, 385, 2136
Graham A. W., Spitler L. R., 2009, MNRAS, 397, 2148
Gregg M. D. et al., 2009, AJ, 137, 498
Guo Q. et al., 2011, MNRAS, 413, 101
Guo Q., White S., Angulo R. E., Henriques B., Lemson G., Boylan-Kolchin M., Thomas P., Short C., 2013, MNRAS, 428, 1351
Han S.-I., Lee Y.-W., Joo S.-J., Sohn S. T., Yoon S.-J., Kim H.-S., Lee J.-W., 2009, ApJ, 707, L190
Harris W. E., 1996, AJ, 112, 1487
Haşegan M. et al., 2005, ApJ, 627, 203
Hau G. K. T., Spitler L. R., Forbes D. A., Proctor R. N., Strader J., Mendel J. T., Brodie J. P., Harris W. E., 2009, MNRAS, 394, L97
Hilker M., 2009, Rev. Modern Astron., Vol. 21, Formation and Evolution of Cosmic Structures. Wiley-VCH, Weinheim, p. 199
Hilker M., Richtler T., 2000, A&A, 362, 895
Hilker M., Infante L., Richtler T., 1999, A&AS, 138, 55

Hilker M., Baumgardt H., Infante L., Drinkwater M., Evstigneeva E., Gregg M., 2007, A&A, 463, 119

Hopkins P. F. et al., 2010, ApJ, 724, 915

Humphrey P. J., Buote D. A., Gastaldello F., Zappacosta L., Bullock J. S., Brighenti F., Mathews W. G., 2006, ApJ, 646, 899

Ibata R. A., Wyse R. F. G., Gilmore G., Irwin M. J., Suntzeff N. B., 1997, AJ, 113, 634

Jalali B., Baumgardt H., Kissler-Patig M., Gebhardt K., Noyola E., Lützgendorf N., de Zeeuw P. T., 2012, A&A, 538, A19

Jones J. B. et al., 2006, AJ, 131, 312

Jordán A. et al., 2007, ApJS, 171, 101

King I., 1962, AJ, 67, 471

Klypin A. A., Trujillo-Gomez S., Primack J., 2011, ApJ, 740, 102

Komatsu E. et al., 2011, ApJS, 192, 18

Kroupa P., 1998, MNRAS, 300, 200

Lanzoni B. et al., 2010, ApJ, 717, 653

Lee Y.-W., Joo J.-M., Sohn Y.-J., Rey S.-C., Lee H.-C., Walker A. R., 1999, Nature, 402, 55

Lisker T., Grebel E. K., Binggeli B., Glatt K., 2007, ApJ, 660, 1186

McLaughlin D. E., 1999, ApJ, 512, L9

McLaughlin D. E., van der Marel R. P., 2005, ApJS, 161, 304

McMillan P. J., 2011, MNRAS, 414, 2446

Madrid J. P., 2011, ApJ, 737, L13

Maraston C., 2005, MNRAS, 362, 799

Marino A. F., Milone A. P., Piotto G., Villanova S., Bedin L. R., Bellini A., Renzini A., 2009, A&A, 505, 1099

Meylan G., Sarajedini A., Jablonka P., Djorgovski S. G., Bridges T., Rich R. M., 2001, AJ, 122, 830

Mieske S., Hilker M., Infante L., 2002, A&A, 383, 823

Mieske S. et al., 2004, AJ, 128, 1529

Mieske S., Hilker M., Infante L., Jordán A., 2006, AJ, 131, 2442

Mieske S., Hilker M., Jordán A., Infante L., Kissler-Patig M., 2007, A&A, 472, 111

Mieske S. et al., 2008, A&A, 487, 921

Mieske S., Hilker M., Misgeld I., 2012, A&A, 537, A3

Mieske S., Frank M. J., Baumgardt H., Lützgendorf N., Neumayer N., Hilker M., 2013, A&A, 558, A14

Misgeld I., Hilker M., 2011, MNRAS, 414, 3699

Misgeld I., Mieske S., Hilker M., 2008, A&A, 486, 697

Misgeld I., Mieske S., Hilker M., Richtler T., Georgiev I. Y., Schuberth Y., 2011, A&A, 531, A4

Murray N., 2009, ApJ, 691, 946

Naab T., Johansson P. H., Ostriker J. P., 2009, ApJ, 699, L178

Navarro J. F., Frenk C. S., White S. D. M., 1996, ApJ, 462, 563

Norris M. A., Kannappan S. J., 2011, MNRAS, 414, 739

Oh S.-H., de Blok W. J. G., Brinks E., Walter F., Kennicutt R. C., Jr, 2011, AJ, 141, 193

Paudel S., Lisker T., Kuntschner H., 2011, MNRAS, 413, 1764

Penny S. J., Forbes D. A., Conselice C. J., 2012, MNRAS, 422, 885

Pfeffer J., Baumgardt H., 2013, MNRAS, 433, 1997

Planck Collaboration XVI, 2013, preprint (arXiv:1303.5076)

Richtler T., Dirsch B., Larsen S., Hilker M., Infante L., 2005, A&A, 439, 533

Saviane I., da Costa G. S., Held E. V., Sommariva V., Gullieuszik M., Barbuy B., Ortolani S., 2012, A&A, 540, A27

Schuberth Y., Richtler T., Hilker M., Dirsch B., Bassino L. P., Romanowsky A. J., Infante L., 2010, A&A, 513, A52

Sérsic J. L., 1963, Bol. Asociacion Argentina Astron., 6, 41

Seth A. C., Dalcanton J. J., Hodge P. W., Debattista V. P., 2006, AJ, 132, 2539

Simmerer J., Ivans I. I., Filler D., Francois P., Charbonnel C., Monier R., James G., 2013, ApJ, 764, L7

Spergel D. N. et al., 2003, ApJS, 148, 175

Springel V. et al., 2005, Nature, 435, 629

Strader J., Caldwell N., Seth A. C., 2011, AJ, 142, 8

Strader J. et al., 2013, ApJ, 775, L6

Thomas P. A., Drinkwater M. J., Evstigneeva E., 2008, MNRAS, 389, 102

Turner M. L., Côté P., Ferrarese L., Jordan A., Blakeslee J. P., Mei S., Peng E. W., West M. J., 2012, ApJS, 203, 5

Weinmann S. M., Lisker T., Guo Q., Meyer H. T., Janz J., 2011, MNRAS, 416, 1197

Zentner A. R., Bullock J. S., 2003, ApJ, 598, 49

This paper has been typeset from a TeX/LaTeX file prepared by the author.

5

Constraining ultra-compact dwarf galaxy formation with galaxy clusters in the local Universe

In Chapter 4 we presented our semi-analytic model for UCD formation by tidal stripping of nucleated dwarf galaxies. Some preliminary analysis comparing the predicted numbers of stripped nuclear clusters with the number of observed UCDs was presented, however a complete comparison between the model and observations was deferred for future work. In this chapter we compare the predictions of our model in Chapter 4 with UCDs from the local Universe.

5.1   Introduction

It has been shown that tidal stripping of nucleated galaxies can produce objects with similar properties to observed UCDs (Chapter 2; Bekki et al. 2003). A number of studies presented estimates for the number of UCDs expected to be formed via this channel (Bekki et al. 2003; Goerdt et al. 2008; Thomas, Drinkwater & Evstigneeva 2008). However as these estimates were based on UCD formation in clusters with static potentials they suffer from a number of problems. Static models do not take into account UCD formation that may have occurred within subclusters that later fell into the main cluster. Since galaxy clusters are expected to undergo many mergers during their formation, galaxies in clusters may be on chaotic orbits providing a few close pericentre passages necessary for UCD formation but far from the cluster centre at other times (Chapter 2). Galaxies orbiting in clusters may also have interactions with other satellite galaxies thereby making tidal disruption more likely.

In Chapter 4 we presented the first model for UCD formation based on cosmological simulations of galaxy formation. Our model uses a semi-analytic galaxy formation model to select possible UCD progenitor galaxies and to determine when they become disrupted by tidal forces. Assuming at all times galaxies have the distribution in nucleus-to-galaxy mass and nucleation fraction of galaxies in the present day Universe we determined the numbers and masses of UCDs formed by tidal stripping. Some preliminary analysis was presented comparing the number of UCDs predicted with the observed number in the Fornax cluster, finding at most ~ 10 per cent of UCDs have formed by tidal stripping.

In this chapter we compare in detail the predictions of our model in Chapter 4 with the properties of UCDs from the local Universe. In particular we compare the predicted mass functions, radial and velocity distributions, metallicities and central black hole masses with the observed distributions.

Throughout the chapter we refer to objects formed in the simulation by tidal stripping of nucleated galaxies as stripped nuclei since such objects may resemble both GCs and UCDs and because the observed UCD populations may be the result of more than one formation channel.

5.2   Semi-analytic modelling

Here we summarize the stripped nucleus formation model of Chapter 4 and detail our selection criteria for comparing against observed galaxy clusters.

The model makes use of the semi-analytic model (SAM) of Guo et al. (2011, hereafter G11) which was applied to the subhalo merger trees of the Millennium-II simulation (Boylan-Kolchin et al. 2009, hereafter MS-II). The MS-II is a cosmological dark-matter only simulation which has a box size of 137 Mpc and a particle mass of $9.42 \times 10^6 \, \mathrm{M}_\odot$. The G11 SAM is constrained by low-redshift abundance and clustering in the Sloan Digital Sky Survey and is tuned to reproduce the $z = 0$ mass distribution of galaxies down to stellar masses of $10^{7.5} \, \mathrm{M}_\odot$. For all data associated with MS-II and the G11 SAM we assume a cosmology consistent with the *Wilkinson Microwave Anisotropy Probe* 1-year data (WMAP1) results (Spergel et al. 2003) and assume $h = 0.73$ for all masses and distances[1]. The data associated with the MS-II and G11 SAM are publicly provided by the Virgo-Millennium Database (Lemson & Virgo Consortium 2006)[2].

In Chapter 4 a sample of galaxy clusters is chosen such that $M_{\mathrm{vir}} > 10^{13} \, \mathrm{M}_\odot/h$. Here we limit the cluster sample according to the mass of the cluster we are comparing with. For the Fornax cluster we choose all clusters within the range $M_{\mathrm{vir}} = 7 \pm 2 \times 10^{13} \, \mathrm{M}_\odot$ (Drinkwater et al. 2001), giving 37 clusters for comparison. For the Virgo cluster we choose all clusters within the range $M_{\mathrm{vir}} = (1.4 - 4.2) \times 10^{14} \, \mathrm{M}_\odot$ (McLaughlin 1999; Urban et al. 2011), giving 11 clusters for comparison.

After the SAM clusters are chosen, stripped nuclei are identified in the simulations in the following way:

(i)   The galaxy merger trees of all galaxies in the SAM clusters at $z = 0$ are searched for possible stripped nucleus progenitors (hereafter referred to as candidate galaxies and the dark matter halo of the galaxies as candidate haloes). A galaxy is defined as a possible progenitor when the stellar mass first exceeds $10^{7.5} \, \mathrm{M}_\odot$ (i.e. all progenitors of

---

[1]In Chapter 4 we tested semi-analytic models for both a WMAP1 (Guo et al. 2011) and WMAP7 cosmology (Guo et al. 2013), finding no significant difference between the predictions. Therefore modelling with an updated cosmology would not change our results.

[2]http://www.mpa-garching.mpg.de/millennium

the candidate galaxy have a stellar mass less than this limit). This lower mass cut is chosen based on the lower mass limit observed for nucleated galaxies (see Figure 1 of Chapter 4).

(ii) To form a stripped nucleus the galaxy must undergo a merger and be completely disrupted according to the galaxy disruption criteria in the SAM (equation 30 of G11).

(iii) The galaxy merger must be a minor merger, where a minor merger is defined as those with 'dynamical' mass ratios smaller than 1:3. The dynamical mass M_{dyn} is defined as $M_{\mathrm{dyn}} = M_* + M_{\mathrm{gas}} + M_{\mathrm{DM}}(< r_{\mathrm{s}})$ where M_* is the stellar mass of the galaxy, M_{gas} is the cold gas mass and $M_{\mathrm{DM}}(< r_{\mathrm{s}})$ is the mass of the dark matter halo within the NFW scale radius.

(iv) The merger happened at least 2 Gyr ago so there is enough time to form a UCD (Chapter 2).

(v) The dynamical friction time of the stripped nucleus, calculated using equation 7-26 from Binney & Tremaine (1987), must be shorter than the time the stripped nucleus has been orbiting within the halo it's associated with at $z = 0$.

Since the particle mass of the MS-II is similar to the mass of UCDs, the most bound particle of the candidate halo in the snapshot before merging is defined as the stripped nucleus that formed after the galaxy merges. The stripped nuclei therefore take the position and velocity of the most bound particle. The stripped nucleus is assigned a mass randomly chosen from a log-normal mass function for the nucleus-to-galaxy mass ratio with a mean of 0.3 per cent and a log-normal standard deviation of 0.5 dex, based on figure 14 from Côté et al. (2006). Note that tidal stripping of the stripped nuclei is not taken into account (i.e. once a stripped nucleus has formed it does not lose mass). The fraction of galaxies that are nucleated is taken from observations of galaxies in the Virgo and Fornax clusters (see Figure 1 of Chapter 4). We take an average nucleation fraction of 80 per cent for galaxies more massive than $M = 4.7 \times 10^8 \, \mathrm{M_\odot}$. For galaxies less massive than this, we choose a fraction that varies linearly (in log-space) between 80 per cent at $M = 4.7 \times 10^8 \, \mathrm{M_\odot}$ and 0 per cent at $M = 3.0 \times 10^7 \, \mathrm{M_\odot}$. For galaxies with masses larger than $10^{11} \, \mathrm{M_\odot}$ we assume nuclei no longer

exist due to destruction by supermassive black holes (e.g. Graham & Spitler 2009). Where possible we work with fractions of stripped nuclei instead of randomly choosing galaxies to satisfy the nucleated fraction (e.g. instead of letting only 80 per cent of disrupted galaxies form a stripped nuclei we let every galaxy create 0.8 stripped nuclei). This improves our statistics.

5.3 Observational data

For all data associated with the Fornax cluster we use the distance modulus $m - M = 31.39$ mag (Freedman et al. 2001) corresponding to a distance of 19 Mpc and a spatial scale of 92 pc arcsec^{-1}. For all data associated with the Virgo cluster we use the distance modulus $m - M = 31.09$ mag (Mei et al. 2007) corresponding to a distance of 16.5 Mpc and a spatial scale of 80 pc arcsec^{-1}.

5.3.1 Fornax cluster

GCs and UCDs

The Fornax cluster has the best studied UCD population of any galaxy cluster (e.g. Mieske et al. 2004a; Gregg et al. 2009) and therefore offers the best possibility to compare our predictions with observations. The observed number of GCs and UCDs in Fornax and their luminosities and for some cases dynamical masses are taken from a compilation of confirmed objects from work by Hilker et al. (1999b), Drinkwater et al. (2000), Mieske et al. (2002, 2004a), Bergond et al. (2007), Hilker et al. (2007), Firth et al. (2007), Mieske et al. (2008), Gregg et al. (2009), Schuberth et al. (2010) and Chilingarian et al. (2011).The masses were calculated from the V-band luminosity and $(V - I)$ colour of the UCDs, assuming a M/L_V-$(V - I)$ relation according to Maraston (2005) SSP models (Kroupa IMF, blue horizontal branch) for ages above 11 Gyr (see Misgeld & Hilker 2011).

Within a clustercentric radius of 0.9 degree, which corresponds to ~300 kpc at the Fornax distance, the number of UCDs with masses above 10^7 M$_\odot$ are more than 95 per cent complete thanks to the all-targets approach by the 2dF Fornax surveys of Drinkwater et al. (2000)

and Gregg et al. (2009). For UCDs with masses above $2 \times 10^6 \, \mathrm{M_\odot}$ the completeness is not easy to access. Most spectroscopic surveys concentrated on the inner 15 arcmin from the cluster centre, i.e. a projected radius of <83 kpc at Fornax distance. Within 50 kpc the UCD number counts above $2 \times 10^6 \, \mathrm{M_\odot}$ are nearly complete (see discussion in Mieske et al. 2012). Beyond this radius the spectroscopic coverage becomes patchy (see Schuberth et al. 2010) and the completeness drops to below 70 per cent within 100 kpc and probably is even lower beyond that. In terms of the total number the effect is not that dramatic, since the radial number density profile of UCDs decreases rapidly with clustercentric distance. In Fig. 5.1 we compare the number of Fornax GCs and UCDs with the GC luminosity function. Based on this figure, the number of GCs/UCDs is probably incomplete below masses of $\sim 10^{6.5} \, \mathrm{M_\odot}$.

Dwarf galaxies

We take the sample of Fornax dwarf galaxies from the Fornax Cluster Catalogue (FCC, Ferguson 1989) with updated radial velocities from Thomas et al. (2008). The catalogue is complete to $B_\mathrm{T} \sim -18$ mag, or $M_B \sim -13.4$ mag, and therefore we take this as the lower luminosity limit for the sample. Assuming a mass-to-light ratio $M/L_B = 3 \, (\mathrm{M/L})_\odot$ this corresponds to a mass $M = 10^8 \, \mathrm{M_\odot}$. We exclude one galaxy (FCC2) as a background galaxy due to its high radial velocity ($cz = 4540$ km s^{-1}) compared to that of the cluster ($cz \sim 1500$ km s^{-1}, Gregg et al. 2009). A galaxy is considered to be a dwarf galaxy if it has a luminosity $M_B > -19.6$, corresponding to $M = 10^{10.5} \, \mathrm{M_\odot}$ assuming a mass-to-light ratio $M/L_B = 3 \, (\mathrm{M/L})_\odot$. Therefore when comparing against dwarf galaxies in the FCC, we choose dwarf galaxies in the simulations as having masses $10^8 < M/\mathrm{M_\odot} < 10^{10.5}$.

5.3.2 GC and UCD metallicities

We compile a list of GC and UCD metallicities for galaxies and clusters in the local Universe from Mieske et al. (2008), Chilingarian et al. (2011) and Francis et al. (2012). For common objects between the Mieske et al. (2008) and Chilingarian et al. (2011) samples we take data from Chilingarian et al.. For common objects between the Mieske et al. (2008) and Francis et al. (2012) samples we take data from Francis et al.. For the Chilingarian et al. sample we
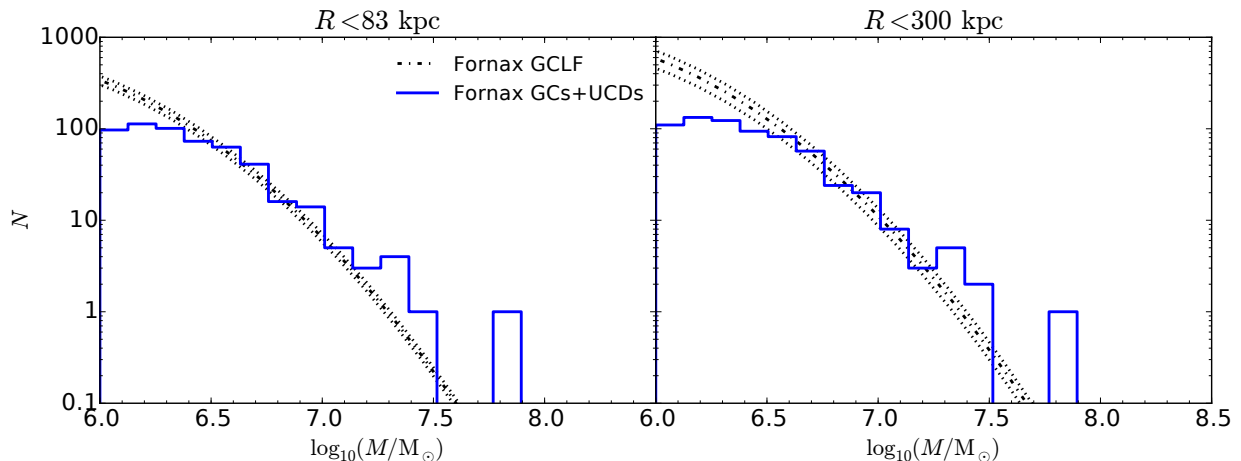
FIGURE 5.1: Number of confirmed Fornax GCs and UCDs (solid line, from Section 5.3.1) compared with the Fornax GC luminosity function (GCLF, dash-dotted line with the error shown by dotted lines) within 83 kpc $(6,450 \pm 700$ GCs, Dirsch et al. 2003) and 300 kpc $(11,100 \pm 2,400$ GCs, Gregg et al. 2009, derived from the data of Bassino et al. 2006). The luminosity functions were converted to mass functions assuming a mass-to-light ratio of $M/L_V = 2.86 \, (\mathrm{M/L})_\odot$.

use the dynamical mass-to-light ratios to calculate the UCD masses where possible. For the Francis et al. sample we take dynamical masses from Mieske et al. (2013) for objects UCD1, UCD5, VUCD3 and VUCD5. For the other objects masses were calculated using the g and r colours and the stellar mass-to-light relations of Bell et al. (2003). For NGC1407-GC1 the g and r colours were taken from Romanowsky et al. (2009). For NGC1407 we assume a distance modulus of 31.99 mag (Jerjen, Tully, & Trentham 2004).

5.4 Analysis and discussion

5.4.1 Mass function

In Figure 5.1 we compare the number of confirmed Fornax GCs and UCDs compiled in Section 5.3.1 with the GC luminosity function within 83 kpc (Dirsch et al. 2003) and 300 kpc (Gregg et al. 2009, derived from the data of Bassino et al. 2006). The luminosity functions were converted to mass functions assuming a mass-to-light ratio of $M/L_V = 2.86 \, (\mathrm{M/L})_\odot$, the median for the Fornax GC/UCD sample described in Section 5.3.1. The luminosity function is approximated as a Gaussian with a width $\sigma = 1.3$ mag and peak magnitude of $M_V = -7.6$ mag (Dirsch et al. 2003) with a total of $6,450 \pm 700$ GCs within 83 kpc (Dirsch et
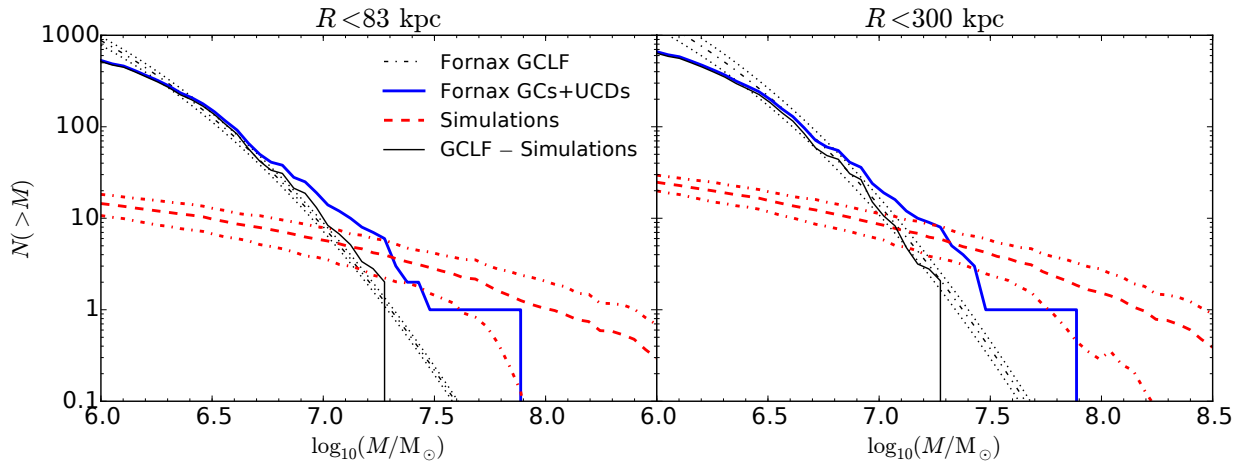
FIGURE 5.2: Cumulative mass function of GCs/UCDs in the Fornax cluster and simulated stripped nuclei in Fornax-like clusters. The red dashed and dash-dotted lines show the mean and standard deviation between clusters for simulated stripped nuclei. The thin dash-dotted shows the integrated Fornax GC luminosity function (GCLF) with the standard deviation given by dotted lines. The thin solid line shows the mean for the simulations subtracted from the Fornax GCLF.

al. 2003) and $11,100 \pm 2,400$ GCs within 300 kpc (Gregg et al. 2009). The figure suggests an excess of ~ 10 objects with masses $\gtrsim 10^7 \, \mathrm{M_\odot}$ compared to the GC mass function. As noted by Gregg et al. (2009), given the low number of objects at the high mass/luminosity end the number of UCDs is consistent with being the high-mass tail of the GC mass function. The most massive Fornax UCD (UCD3) is also very extended ($R_{\mathrm{eff}} = 90$ pc, Hilker et al. 2007) while all other Fornax UCDs have sizes less than 30 pc (e.g. Misgeld & Hilker 2011). This may indicate it is not part of the GC luminosity function even if the total number is consistent (although GCs/UCDs formed by hierarchical merging of star clusters in cluster complexes may also reach such sizes, Brüns & Kroupa 2012).

In Figure 5.2 we show the integrated Fornax GC luminosity function, the cumulative mass function for Fornax GCs/UCDs and the simulated stripped nuclei in Fornax-like clusters. The number of stripped nuclei predicted at the high-mass end are reasonably consistent, although slightly over-predicted, compared to the number of UCDs observed. The simulations predict ~ 1 stripped nucleus with a mass greater than $10^8 \, \mathrm{M_\odot}$, close to the observed number of UCDs. Taking into account tidal stripping of stripped nuclei might bring the predictions in better agreement with the observations. As already noted in Chapter 4, for UCDs more massive than $10^6 \, \mathrm{M_\odot}$ the simulations underpredict the number of objects by a factor > 10.

For masses between 10^6 and $10^7 \, \mathrm{M_\odot}$ and within a radius of 300 pc we predict stripped nuclei account for only ~ 2.5 per cent of GCs/UCDs. For masses larger than $10^7 \, \mathrm{M_\odot}$ and within a radius of 300 pc we predict stripped nuclei account for ~ 45 per cent of GCs/UCDs and become the dominant formation mechanism for masses larger than $10^{7.1} \, \mathrm{M_\odot}$. As the number of dwarf galaxies is over-predicted in galaxy clusters by 50 per cent (Weinmann et al. 2011, see also Figure 5.5), the number of predicted stripped nuclei might increase by a factor of two if more efficient tidal processes were implemented in the simulations[3]. However this is still too low to account for all observed UCDs. The difference between the observed number of GCs/UCDs and the number of simulated stripped nuclei shows remarkably good agreement with the integrated GC luminosity function and suggests the most massive genuine GC has a mass of $\sim 3 \times 10^7 \, \mathrm{M_\odot}$. This is in good agreement with the most massive GC suggested from the GC luminosity function (Hilker 2009). Given the low numbers involved, distinguishing between a scenario where all UCDs are genuine GCs or one where UCDs are a combination of stripped nuclei and genuine GCs is nearly impossible by numbers alone. However, a combination of the Fornax GC luminosity function and the predicted mass function for stripped nuclei shows good agreement with the observed mass function of GCs/UCDs in the Fornax cluster.

5.4.2 Kinematics

In Figure 5.3 we show the velocity dispersions of the Fornax GC, UCD and dwarf galaxy populations compared with the predictions for stripped nuclei and dwarf galaxies from the simulations. We chose a mass limit between GCs and UCDs of $M_{\mathrm{UCD}} > 5 \times 10^6 \, \mathrm{M_\odot}$ in order to have reliable dispersion measurements for the UCDs. For the simulations the Fornax-like clusters were observed from three sight-lines (the x-, y- and z-axes of the simulation) and the dwarf galaxies and stripped nuclei from all clusters were combined for the velocity dispersion measurements to improve statistics. The typical deviation in average stripped nuclei velocity dispersion between individual clusters is $\sim 90 \, \mathrm{km \, s^{-1}}$. For the dwarf galaxies we take all

---

[3]Although the over-abundance of dwarf galaxies might also be related to the too efficient star formation in low-mass galaxies at early times or the over-clustering of galaxies at scales below 1 Mpc (Guo et al. 2011). See Section 5.2 in Chapter 4 for a discussion about how this affects our predictions.
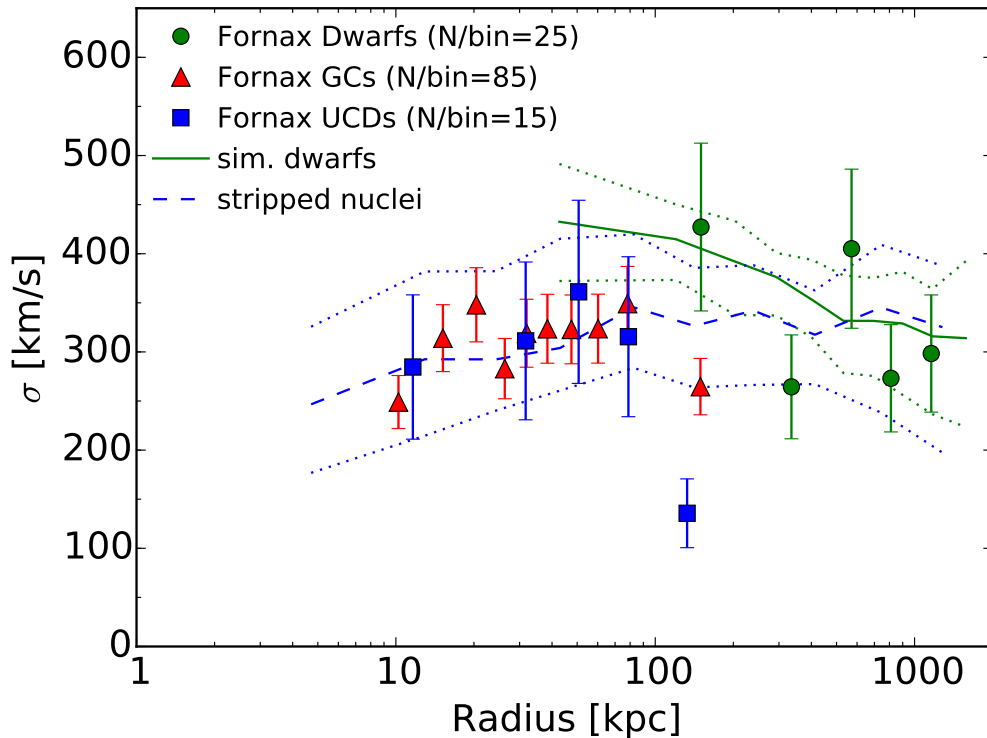
FIGURE 5.3: Comparison of the velocity dispersions of GC (triangles), UCD (squares) and dwarf galaxy (circles) populations in the Fornax cluster with simulated stripped nuclei (dashed line) and dwarf galaxies (solid line). All data is split into bins of equal numbers, where the point for radius is given by the mean of all objects within a bin. The mass limit between GCs and UCDs is chosen to be $M_{\rm UCD} > 5 \times 10^6 \, {\rm M}_\odot$. For the observed populations the 1σ errors are determined by $\sqrt{N}$ statistics[4]. The lines for the simulation data are averages of all clusters over three sight-lines (along the x-, y- and z-axes of the simulation) with the 1σ deviation between individual clusters given by the dotted lines.

observed galaxies with $-19.6 < M_B/{\rm mag} < -13.4$ corresponding to $10^8 < M/\,{\rm M}_\odot < 10^{10.5}$ in the simulations assuming a mass-to-light ratio $M/L_B = 3\,({\rm M/L})_\odot$. There is good agreement between the simulations and observations. Almost all data points from the simulations fall within the errorbars of the observations for both UCDs/stripped nuclei and dwarf galaxies. However the most distant point (in radius) for the observed UCDs has a velocity dispersion significantly lower than the other points. The cause of this is unclear. We caution here that since the velocities of the stripped nuclei are determined by a single particle in the simulations the velocities could be incorrect compared to that expected for a system of particles. However, since we are calculating velocity dispersions and not comparing the velocities of individual nuclei we expect this will not affect our results significantly.
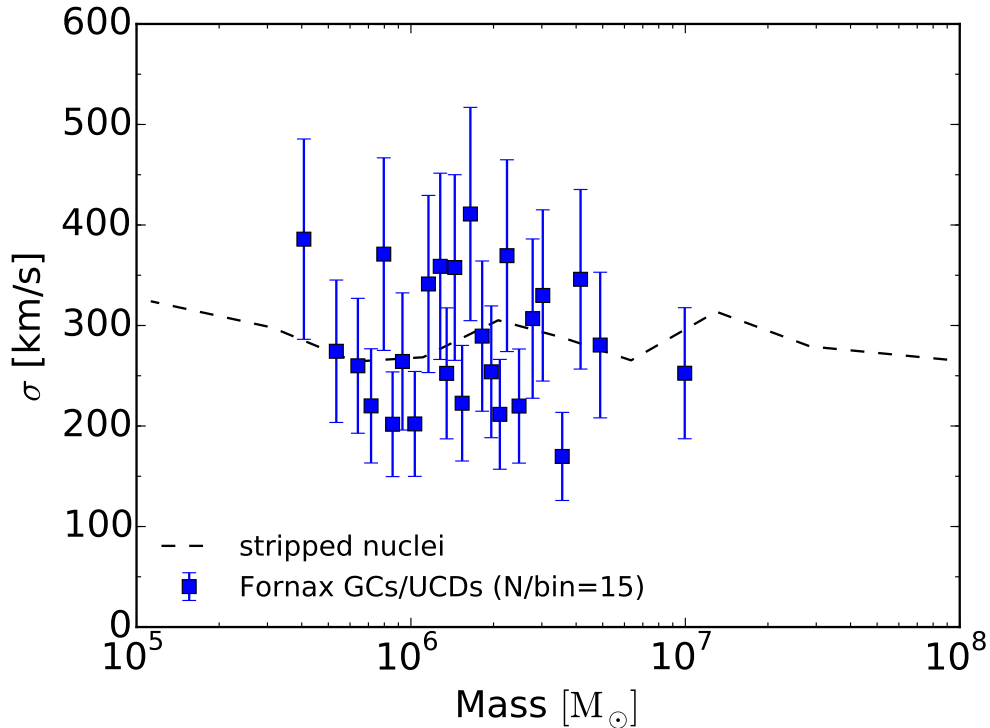
FIGURE 5.4: Velocity dispersions of Fornax GCs and UCDs within 30 kpc of the cluster centre as a function of mass. The 1σ errors are determined by $\sqrt{N}$ statistics. The average velocity dispersion for the whole sample is ~ 300 km s^{-1}.

The velocity dispersions found for the UCD population are very similar to the velocity dispersions of the genuine GCs. This is in contrast to the findings of Gregg et al. (2009) who found UCDs within ~ 30 kpc have a velocity dispersion half that of GCs. Assuming $M/L_B = 2\,(\text{M/L})_\odot$ for UCDs, their luminosity cut between GCs and UCDs of $M_B = -10$ mag corresponds to a mass of $\sim 3 \times 10^6\,\text{M}_\odot$, slightly lower than our mass cut of $5 \times 10^6\,\text{M}_\odot$. In Figure 5.4 we show the velocity dispersion of Fornax GCs and UCDs within 30 kpc of the cluster centre as a function of mass. The UCDs with masses $\sim 2.5 \times 10^6$ and $\sim 3.5 \times 10^6\,\text{M}_\odot$ have particularly low velocity dispersions on the order of that found by Gregg et al. (2009). However the UCDs with masses $\sim 3 \times 10^6\,\text{M}_\odot$ have velocity dispersions around the mean for all GCs/UCDs. The difference in the velocity dispersions of UCDs between our sample and that of Gregg et al. (2009) is likely due to our increased sample size of UCDs.

---

[4]Note that $\sqrt{N}$ statistics leads to underestimated errors of the velocity dispersion if the distribution even slightly deviates from normality (Beers et al. 1990) and therefore the errors for the Fornax UCDs and dwarfs are probably underestimated.

Interestingly the predicted velocity dispersions for stripped nuclei agree very well with the observed GCs and UCDs. This may be a consequence of many GCs being accreted from dwarf galaxies by the central cluster galaxy, and thus having a similar origin and velocities to stripped nuclei (e.g. Côté, Marzke & West 1998). As found by Gregg et al. (2009), UCDs and stripped nuclei have lower velocity dispersions than dwarf galaxies in the central regions of the Fornax cluster. The difference between dwarfs and stripped nuclei implies there is a bias towards galaxies with low relative velocities (compared to the host galaxy) being disrupted in galaxy clusters. Given the finding of similar velocity dispersions for GCs and stripped nuclei, velocity dispersions are therefore unable to distinguish between the formation mechanisms of UCDs in the Fornax cluster.

In contrast to the Fornax cluster, studies of other clusters show differences between GCs and UCDs. Misgeld et al. (2011) found in the Hydra I cluster that bright objects have lower velocity dispersions than faint objects (with the largest difference occurring with a dividing magnitude $M_V = -10.75$ mag). Zhang et al. (2015) found in the Virgo cluster that UCDs (defined as having $R_e > 10$ pc) have velocity dispersions more similar to blue GCs than red GCs and red GCs have an overall lower velocity dispersion than both blue GCs and UCDs. All three populations have dispersions lower than dE galaxies. As the studies for each galaxy cluster have used different criteria to differentiate between GCs and UCDs interpreting these results is difficult as different methods may obtain different results within the same cluster. Future work should investigate each galaxy cluster using consistent methods to enable comparison between clusters.

5.4.3   Radial distributions

The radial distributions of UCDs/stripped nuclei and dwarf galaxies in the Fornax cluster and the predictions from simulations are shown in Fig. 5.5. Here we include galaxies without radial velocity measurements in the observed dwarf galaxy sample. In the normalized distributions, there is good agreement between the observed UCDs and simulated stripped nuclei for masses larger than $10^7\,\mathrm{M_\odot}$ despite the predicted number of stripped nuclei being a factor of two lower than the number of observed UCDs. According to a KS test, 92 per
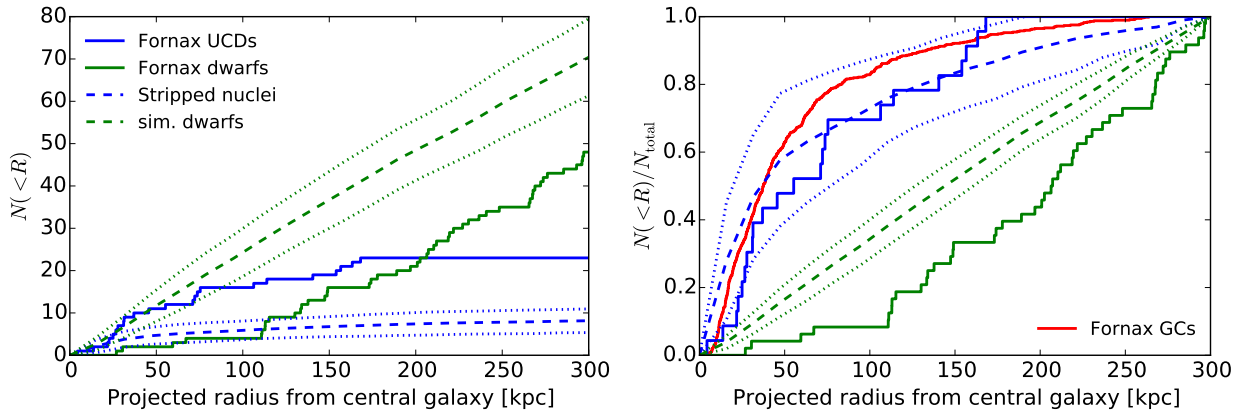
FIGURE 5.5: Absolute (left) and normalized (right) projected radial distributions of UCDs with masses larger than $10^7 \, \mathrm{M_\odot}$ in the Fornax cluster compared with the predictions of stripped nuclei from simulations. The distributions for dwarf galaxies (observed sample $-19.6 < M_B/\mathrm{mag} < -13.4$ corresponding to $10^8 < M/\mathrm{M_\odot} < 10^{10.5}$ in the simulations assuming a mass-to-light ratio $M/L_B = 3 \, (\mathrm{M/L})_\odot$) is also shown.

cent of simulated clusters have a > 5 per cent probability of the stripped nuclei being drawn from the same distribution as the observed UCDs and 60 per cent of clusters have a > 10 per cent probability of being drawn from the same sample. There is some evidence the simulations predict too many stripped nuclei within the central 20 kpc of the galaxy cluster. This might be alleviated by taking into account tidal stripping in the modelling of stripped nuclei. The radial distributions of both the stripped nuclei and observed UCDs in Fornax are slightly more extended than the GC population in Fornax, although this is possibly due to incompleteness of the GC population beyond 83 kpc.

Both the numbers and shape of the distribution for dwarf galaxies disagrees strongly between the observations and simulations. The simulations predict a factor of two more dwarf galaxies than observed and also show a more concentrated distribution than the observations. The over-production of dwarf galaxies in clusters in the G11 SAM is already well known (G11; Weinmann et al. 2011) and might be due to too efficient star formation in dwarf galaxies, too strong clustering on small scales or inaccurate modelling of tidal effects. As discussed in Section 5.2 of Chapter 4, the too strong clustering of galaxies at small scales does not affect our predictions since the fraction of mass in a halo that was accreted in subhaloes of a given mass is relatively insensitive to the shape of the power spectrum (Zentner & Bullock 2003; Dooley et al. 2014). Whether a change in the efficiency of star formation will affect our
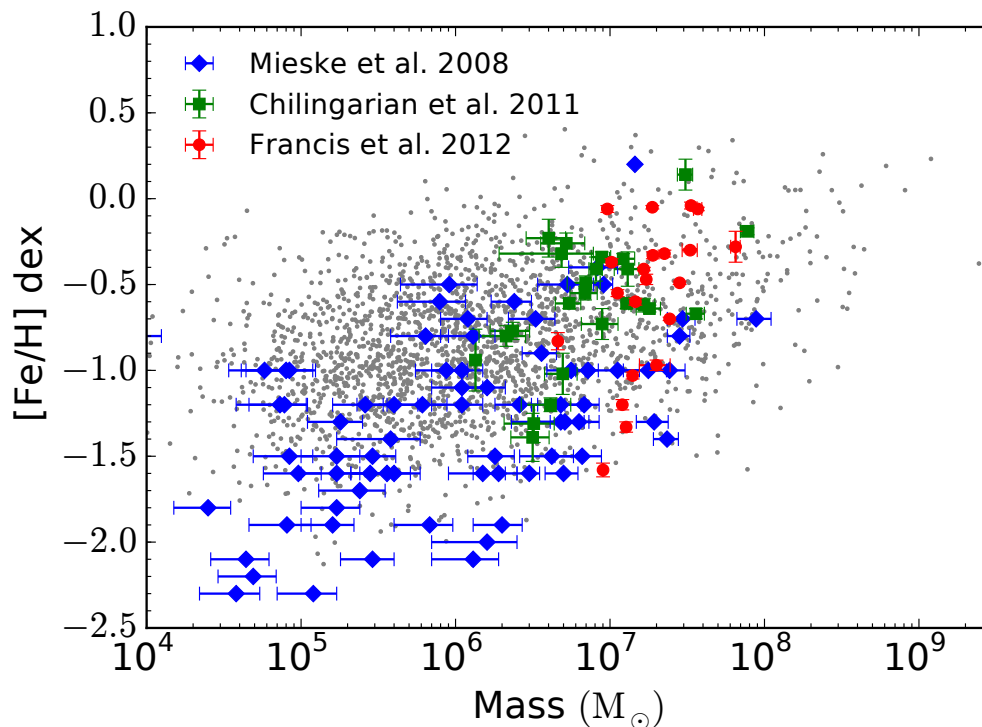
FIGURE 5.6: Metallicities of GCs/UCDs from nearby galaxies and galaxy clusters from Mieske et al. (2008), Chilingarian et al. (2011) and Francis et al. (2012) compared to the predicted metallicities of stripped nuclei in Fornax- and Virgo-sized clusters (grey points).

predictions is unclear as changes to a parameter in the SAM may be offset by other factors. In Section 6.4 we find inaccurate modelling of tidal effects is not likely to significantly affect our predictions.

5.4.4 Metallicities

In order to compare the predicted metallicities for stripped nuclei with the observed metallicities of UCDs we must assign metallicities to the stripped nuclei. We first assign metallicities to the progenitor galaxies using equation 4 of Kirby et al. (2013) for galaxies with stellar masses $M_* <= 10^{9.4}\,M_\odot$ and the SDSS relation from (Gallazzi et al. 2005) for galaxies with $M_* > 10^{9.4}\,M_\odot$. For each galaxy we add a random value chosen from a Gaussian function with a dispersion of 0.17 dex. We then assign the nucleus of each galaxy the metallicity of their host galaxy with an offset of 0.067 dex given nuclei are typically slightly more metal rich that their host galaxies (Paudel et al. 2011) and add a Gaussian dispersion of 0.3 dex
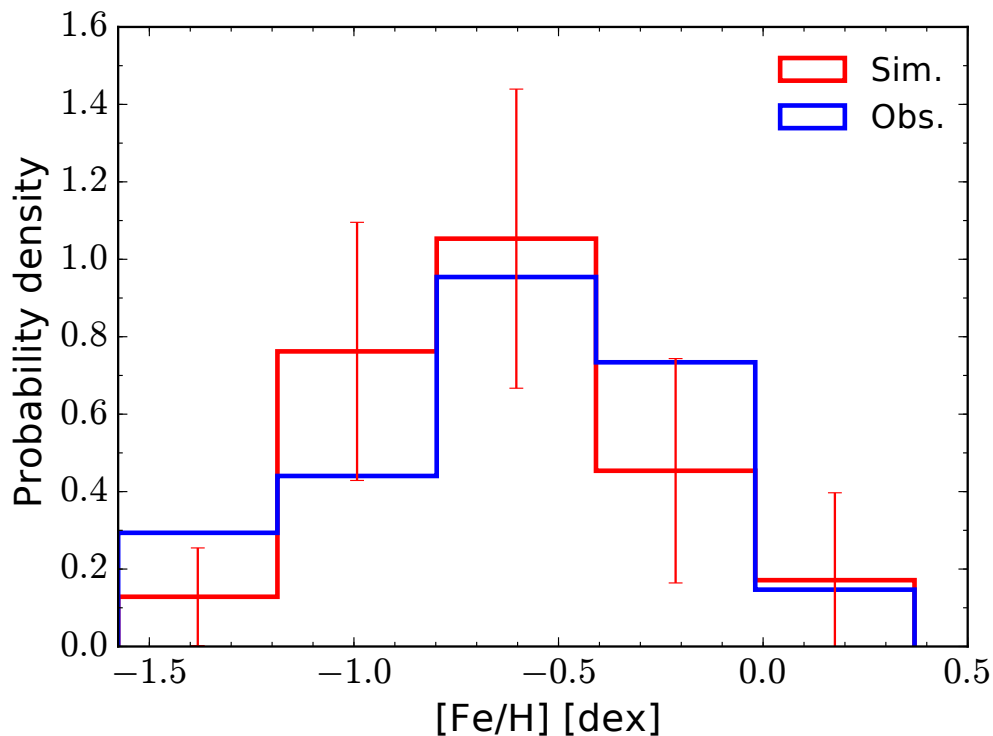
FIGURE 5.7: Normalized histogram (such that the integral under the histogram is 1) of the metallicities of UCDs (Obs.) and stripped nuclei (Sim.) from Fig. 5.6 with masses between $10^7 < M/\mathrm{M_\odot} < 10^8$. Error bars for the stripped nuclei show the 1σ uncertainties for individual clusters.

for the typical scatter between nuclei and their host galaxies.

We show the predicted metallicities for stripped nuclei compared to the metallicities of GCs and UCDs from the local Universe in Figure 5.6. For masses $\gtrsim 10^6 \, \mathrm{M_\odot}$ there is good agreement between the metallicities predicted for stripped nuclei and those of the observed GCs/UCDs. Below masses of $10^6 \, \mathrm{M_\odot}$ the stripped nuclei are predicted to be 0.5 dex more metal rich on average than the observed GCs.

To compare in more detail the predictions for metallicities of stripped nuclei with those observed for UCDs, in Figure 5.7 we show the normalized histogram of UCDs and stripped nuclei with masses between $10^7 < M/\mathrm{M_\odot} < 10^8$. Given the scatter for individual clusters, we find good agreement between the predictions and the observations. This shows that many of the most massive UCDs could have formed from the tidal stripping of nucleated galaxies.
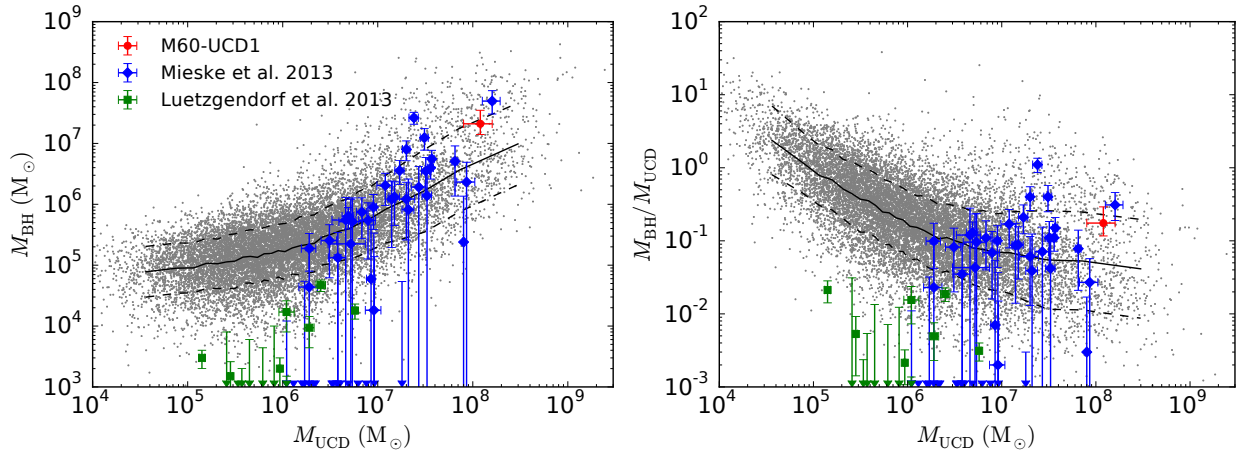
FIGURE 5.8: Predicted masses of central black holes in stripped nuclei. The mean and 1σ confidence interval for the simulated stripped nuclei are given by the solid and dashed lines, respectively, using bin sizes of 500 objects. The typical 1σ confidence interval in both M_{BH} and M_{BH}/M_{UCD} is approximately 0.5 dex. For comparison we also show the black hole mass of M60-UCD1 (Seth et al. 2014), the inferred black hole masses of UCDs assuming elevated mass-to-light ratios are due to central black holes (Mieske et al. 2013) and the limits for central black holes in GCs (Lützgendorf et al. 2013). For the observed UCDs and GCs, objects with implied black hole masses of zero are given by triangles at the bottom of the figure.

5.4.5   Central black holes

UCDs are known to have dynamical mass-to-light ratios above what is expected from their stellar populations (see Chapter 3). One suggestion is that these elevated mass-to-light ratios are caused by UCDs harbouring central intermediate mass (IMBH) or supermassive (SMBH) black holes (Mieske et al. 2013). The finding of the first UCD to contain a SMBH (Seth et al. 2014) has given plausibility to the possibility that many UCDs may host black holes.

In Fig. 5.8 we show the predicted masses of central black holes in stripped nuclei, where the black hole masses are taken from the progenitor galaxies of the stripped nuclei in the G11 SAM. Here we show the predictions for all galaxy clusters in Chapter 4 and not just in Fornax- and Virgo-sized clusters. In the model, black holes form during gas-rich mergers and thereafter grow either by the merger of black holes or the accretion of cold or hot gas ('quasar' and 'radio' mode, respectively). According to the model, the fraction of stripped nuclei with a central black hole is 97 per cent.

In Fig. 5.8 we also show M60-UCD1, the first UCD to have a confirmed central black hole (Seth et al. 2014), the implied black hole masses of UCDs assuming their elevated dynamical

mass-to-light ratios are due to central black holes (Mieske et al. 2013) and the limits for central black holes in Milky Way GCs (Lützgendorf et al. 2013). The black hole mass of M60-UCD1 agrees well with the predictions from our model and falls within the 1σ error bars. There is also remarkable agreement between the simulations and the inferred black hole masses of UCDs from Mieske et al. (2013). For UCDs with an implied black hole mass above zero, 74 per cent (23/31) of the data points fall within the 1σ confidence interval of the simulation predictions. For UCDs with a lower black hole mass limit above zero, 79 per cent (15/19) of the data points fall within the 1σ confidence interval of the simulation predictions.

However, assuming these GCs are stripped nuclei, the central black hole mass limits determined for Milky Way GCs show strong disagreement with the model: the BH masses from simulated nuclei with masses of 10^4–$10^6\,\mathrm{M_\odot}$ are a factor of 10–100 larger than the masses implied by observations. Taken together, the implied black hole masses of observed UCDs and GCs suggests a much steeper slope to the M_{BH}-M_{NC} relation than is predicted from the simulations.

There are a number of possible reasons for the disagreement between the predictions from the simulations and implied black hole masses of observed GCs and UCDs. The most likely reason is that the modelling is inadequate for galaxies with masses $\sim 10^8\,\mathrm{M_\odot}$ (corresponding to a nucleus masses of $\sim 10^{5.5}\,\mathrm{M_\odot}$). The best fitting M_{BH}-M_* relation for spheroidal galaxies from Scott, Graham, & Schombert (2013) predicts black holes with masses of $\sim 10^2$–$10^3\,\mathrm{M_\odot}$ for galaxies with stellar masses $\sim 10^8\,\mathrm{M_\odot}$, although there is significant scatter about the relation and the relation is unconstrained below stellar masses of $10^9\,\mathrm{M_\odot}$. This mass is much lower than the predictions of the modelling and would bring the modelling in line with the black hole masses implied by the observations. Alternatively, if none of the Milky Way GCs formed as stripped nuclei then the GCs cannot be used to constrain the low-mass end of the relation.

5.5 Summary

In this chapter we compared in detail the findings of our semi-analytic model for stripped nucleus formation with the observed properties of UCDs in the local universe. Our main findings are as follows.

(i) The number of stripped nuclei predicted at the high-mass end of the UCD mass function in the Fornax cluster is consistent with the most massive UCDs observed. The difference of the observed number of GCs/UCDs and the predicted number of stripped nuclei agrees well with the GC luminosity function and therefore the GC/UCD mass function is consistent with being a combination of genuine GCs and stripped nuclei. This suggests the most massive genuine GC in the Fornax cluster has a mass of $\sim 3 \times 10^7 \, \mathrm{M_\odot}$.

(ii) The velocity distributions of UCDs in the Fornax cluster agree well with both the observed GC population and the predictions for stripped nuclei in Fornax-sized clusters.

(iii) For UCDs with masses $> 10^7 \, \mathrm{M_\odot}$ the normalized radial distributions predicted for stripped nuclei in Fornax-sized clusters agree well with the observed radial distribution of UCDs.

(iv) For masses between 10^7 to $10^8 \, \mathrm{M_\odot}$, the predicted metallicities of stripped nuclei agree well with the observed metallicities of UCDs. Below masses of $10^6 \, \mathrm{M_\odot}$, stripped nuclei are predicted to be $\sim$0.5 dex more metal-rich on average than the observed GCs in the Milky Way.

(v) The predicted central black hole masses for stripped nuclei agree well with the observed black hole mass of M60-UCD1 and the black hole masses implied for UCDs assuming their elevated mass-to-light ratios are due to central black holes. However, assuming Milky Way GCs with possible central black holes formed as stripped nuclei, the predictions from the modelling are 10-100 time higher than the observed values.

These finding together suggest that, although not the dominant mechanism of UCD formation, a significant fraction of the highest mass UCDs ($M > 10^7 \, \mathrm{M_\odot}$) are likely to have formed by tidal stripping on nucleated galaxies. However since the predictions for both

the giant GC and tidal stripping channels of UCD formation are very similar, distinguishing between the formation mechanisms of individual UCDs may only be possible through the presence of central black holes (Seth et al. 2014) or recent star formation (Norris & Kannappan 2011).

6

Tidal stripping in semi-analytic models of galaxy formation

In Chapter 4 we developed a model for stripped nucleus formation using a semi-analytic model of galaxy formation. The criteria for stripped nucleus formation was based on a simple criterion for galaxy disruption in the semi-analytic model that is likely too simple compared to the actual process in galaxy clusters. In this chapter we develop a method for including tidal stripping in semi-analytic models of galaxy formation in order to assess the consequences for our model of stripped nucleus formation, finding the results from either method are generally in good agreement.

6.1 Introduction

Semi-analytic models (SAMs) of galaxy formation allow one to predict the properties of galaxies and how they evolve over cosmic time by applying analytic recipes to the dark matter merger trees of cosmological simulations. SAMs enable predictions of galaxy properties over large volumes without the computational cost of including hydrodynamics (although large-scale hydrodynamical simulations such as the Illustris (Vogelsberger et al. 2014) and EAGLE (Schaye et al. 2015) projects are becoming more common-place). An effect that is not typically included in SAMs is tidal stripping. When studying the properties and evolution of dwarf galaxies in galaxy clusters, tidal effects become very important (through harassment or extreme mass loss).

The Millennium-II simulation (Boylan-Kolchin et al. 2009, hereafter MS-II) is one of the highest resolution cosmological simulations to date, allowing SAMs to include the formation of dwarf galaxies. The first SAM built upon MS-II was made by G11. The G11 SAM is currently the only SAM with sufficient resolution to include the formation of dwarf galaxies and has the added benefit of being well studied in comparison to observed dwarf galaxy populations (e.g. Weinmann et al. 2011; Lisker et al. 2013). The G11 SAM is constrained by low-redshift abundance and clustering in the Sloan Digital Sky Survey and is tuned to reproduce the $z = 0$ mass distribution of galaxies down to stellar masses of $10^{7.5}\,\mathrm{M_\odot}$.

Weinmann et al. (2011) showed that the ratio of dwarf galaxies to giant galaxies in the G11 SAM is too high, suggesting the prescription for tidal disruption in the model is not efficient enough. In this chapter we postprocess the SAM of G11 to include tidal stripping in galaxy clusters with the aim of testing whether incorporating tidal stripping in SAMs can alleviate these problems. This work also has consequences for UCD numbers predicted from tidal stripping (Chapter 4) since the criterion for galaxy disruption in the G11 SAM is likely not realistic.

Throughout this chapter we assume a cosmology consistent with the *Wilkinson Microwave Anisotropy Probe* 1-year data (WMAP1) results (Spergel et al. 2003) and assume $h = 0.73$ for all masses and distances.

6.2 Semi-analytic modelling of tidal stripping

We make use of the G11 SAM which was applied to the subhalo merger trees of the MS-II. The MS-II is a cosmological dark-matter only simulation which has a box size of 137 Mpc, particle mass of $9.42 \times 10^6 \, \mathrm{M_\odot}$ (resolving subhaloes to $1.88 \times 10^8 \, \mathrm{M_\odot}$ at the 20 particle mass limit) and Plummer-equivalent gravitational force softening of $1h^{-1}$ kpc in co-moving units (which may be taken as the spatial resolution limit of the simulation). The data associated with the MS-II and G11 SAM are publicly provided by the Virgo-Millennium Database (Lemson & Virgo Consortium 2006)[1].

6.2.1 Galaxy selection

We select all galaxy clusters in the G11 SAM at $z = 0$ with virial masses larger than $10^{13} \, \mathrm{M_\odot}/h$, rejecting any which are at a distance less than twice the cluster virial radius from the edge of the simulation box. This gives a sample of 289 clusters. To find galaxies which may undergo tidal stripping we select all galaxies within twice the cluster virial radius with stellar masses greater than $10^{7.5} \, \mathrm{M_\odot}$, limiting the sample to masses for which the SAM is constrained. We then search the merger history of these galaxies to find all galaxies which are disrupted or have lost their dark matter halo (i.e. have become a Type 2 galaxy in the SAM). We exclude all galaxies which have undergone major mergers since these galaxies won't undergo tidal stripping, where major mergers are those between galaxies with baryonic masses (stellar mass plus cold gas) differing by less than a factor of 3 (as in the SAM).

For galaxies which were disrupted according to the SAM their branch in the galaxy merger tree must be extended since they may survive for a longer time when taking into account tidal stripping. We follow the method for Type 2 galaxies in the SAM, where once the dark matter halo of the galaxy becomes unresolved the position and velocity of the galaxy traces the most-bound particle of halo when it was last resolved. The position of the satellite galaxy is modified to take into account the expected decay of its orbit through dynamical friction. The offset of the most-bound particle from the host halo is multiplied by a factor $(1 - \Delta t / t_{\mathrm{friction}})$, where Δt is the time since the merger clock was set (i.e. when the

---

[1]`http://www.mpa-garching.mpg.de/millennium`

halo mass dropped below the stellar mass of the galaxy). After a time t_{friction} the satellite galaxy is assumed to merge with the central galaxy of the host halo. As in G11 we determine the merging time for a satellite due to dynamical friction from equation 7-26 of Binney & Tremaine (1987):

$$t_{\text{friction}} = \alpha \frac{V_{\text{vir}} r_{\text{sat}}^2}{G m_{\text{sat}} \ln\Lambda},$$

(6.1)

where $\alpha = 2.34$, $\ln\Lambda = \ln(1 + M_{\text{vir}}/m_{\text{sat}})$, r_{sat} is the distance between the satellite and the host halo and M_{vir} and V_{vir} are the virial mass and velocity of the host halo. Here m_{sat} is the sum of the baryonic mass of the satellite and dark matter mass of its subhalo just before the dynamical friction time is calculated (when the merger clock was set).

6.2.2   Tidal stripping method

While orbiting within a larger system, the tidal forces on a satellite are strongest at pericentre. Therefore a simple way to determine the mass loss due to tidal stripping of a satellite is by calculating the bound mass within the Jacobi radius at pericentre and assuming all mass beyond the Jacobi radius is lost, although in practice one also has to take into account the eccentricity of the orbit.

It is assumed tidal stripping in the SAM is not important until the dark matter halo of the satellite galaxy becomes unresolved. Note that the stellar matter will likely be affected before this point and thus tidal effects are likely underestimated in our method (especially for galaxies where the halo is only just resolved). It is also assumed the galaxy has lost all of its gas once it has lost its dark matter halo. As in the SAM, for each galaxy we assume an exponential profile for the stellar disk

$$\Sigma(R) = \Sigma_0 \exp\left(\frac{-R}{R_d}\right),$$

(6.2)

where R_d is the disk scale length and Σ_0 is the central surface density, and a Jaffe profile for the bulge

$$\rho(r) = \frac{\rho_0}{4\pi} \left(\frac{r}{r_0}\right)^{-2} \left(1 + \frac{r}{r_0}\right)^{-2},$$

(6.3)

where r_0 is the scale length and ρ_0 is the central density. For simplicity, it is assumed the

satellite orbits within a singular isothermal potential

$$\Phi(r) = V_{\mathrm{vir}}{}^2 \ln R. \tag{6.4}$$

For consistency we also check for disk instabilities using the same criterion as G11 to determine instability:

$$V_{\mathrm{max}} < \sqrt{\frac{GM_d}{3R_d}} \tag{6.5}$$

where M_d and R_d are the mass and scale radius of the disk, respectively, and V_{max} is the maximum circular velocity of the subhalo at its last resolved time. When equation 6.5 is satisfied, mass δM is transferred from the disk to the bulge to keep the disk marginally stable. The size of the new bulge, R_b, formed by this process is determined by equation 35 of G11:

$$\delta M = 2\pi \Sigma_0 R_d \left[R_d - (R_b + R_d) \exp\left(\frac{-R_b}{R_d}\right) \right]. \tag{6.6}$$

However, as M_d decreases at a faster rate than R_d during stripping, by this criterion disks become more stable.

A key assumption in this method is that the central density/surface density for the spheroidal and disk components, respectively, remain constant during the stripping process while the scale length decreases. This is approximately true for both disk (Villalobos et al. 2012) and spheroidal systems (Peñarrubia et al. 2010) and the assumption likely remains valid with the exception of extreme mass loss. For the Jaffe profile we set the density constant at 10^{-9} kpc.

The tidal stripping of a satellite galaxy between snapshots is calculated by the following process. First the peri- and apocentre distances are calculated for the satellite using equation 3-13 of Binney & Tremaine (1987)

$$u^2 + \frac{2\left[\Phi(1/u) - E\right]}{L^2} = 0, \tag{6.7}$$

where the equation normally has two roots $r_1 = u_1{}^{-1}$ and $r_2 = u_2{}^{-1}$, the peri- and apocentre distances. Then the number of pericentre passages the satellite can have between snapshots

(or otherwise its closest approach to the central halo) are determined based on whether the satellite is approaching pericentre or apocentre and calculating the radial period T_r and time to pericentre T_{peri} from equation 3-16 of Binney & Tremaine (1987)

$$T_r = 2 \int_{r_1}^{r_2} \frac{dr}{\sqrt{2 \left[E - \Phi(1/u) \right] - L^2/r^2}}, \tag{6.8}$$

where the factor of two is removed when integrating from pericentre to current position to obtain T_{peri}. If an apocentre distance cannot be found (due to the assumption of an isothermal potential being too simplistic) we consider the orbit unbound and the satellite can have at most one pericentre passage. Finally the number of pericentres is looped over (updating the satellite's parameters each time) to determine the stripping between snapshots. If the mass of the galaxy falls below $10^3 \, \mathrm{M_\odot}$ we consider the galaxy disrupted to save computation time, although in practice this is rarely required.

To determine the mass stripped from the satellite the Jacobi radius is calculated at pericentre from the formula of King (1962)

$$r_J = \left(\frac{GM_s(< r_J) r_G^2}{2 V_{\mathrm{vir}}^2} \right)^{(1/3)}, \tag{6.9}$$

where r_G is the galactocentric radius (here the pericentre distance) and $M_s(< r_J) = M_d(< r_J) + M_b(< r_J)$ is the mass of the satellite galaxy within the Jacobi radius. In practice we iterate over the equation until convergence. We then modify the Jacobi radius as

$$r_J' = f_{r_J} r_J, \tag{6.10}$$

where f_{r_J} is a factor required to take into account that for elliptic orbits as a galaxy returns to apocentre material that is considered unbound at pericentre may become bound again. The mass to be stripped from the galaxy is then $M_d - M_d(< r_J')$ and $M_b - M_b(< r_J')$ for the disk and bulge component, respectively.

Additionally after each calculation of the tidal radius we check the ratio of the half mass radius to the Jacobi radius separately for the disk and bulge of the galaxy. If $r_J' \leq r_h/3$ then the component (disk or bulge) is considered to be disrupted. This point is required
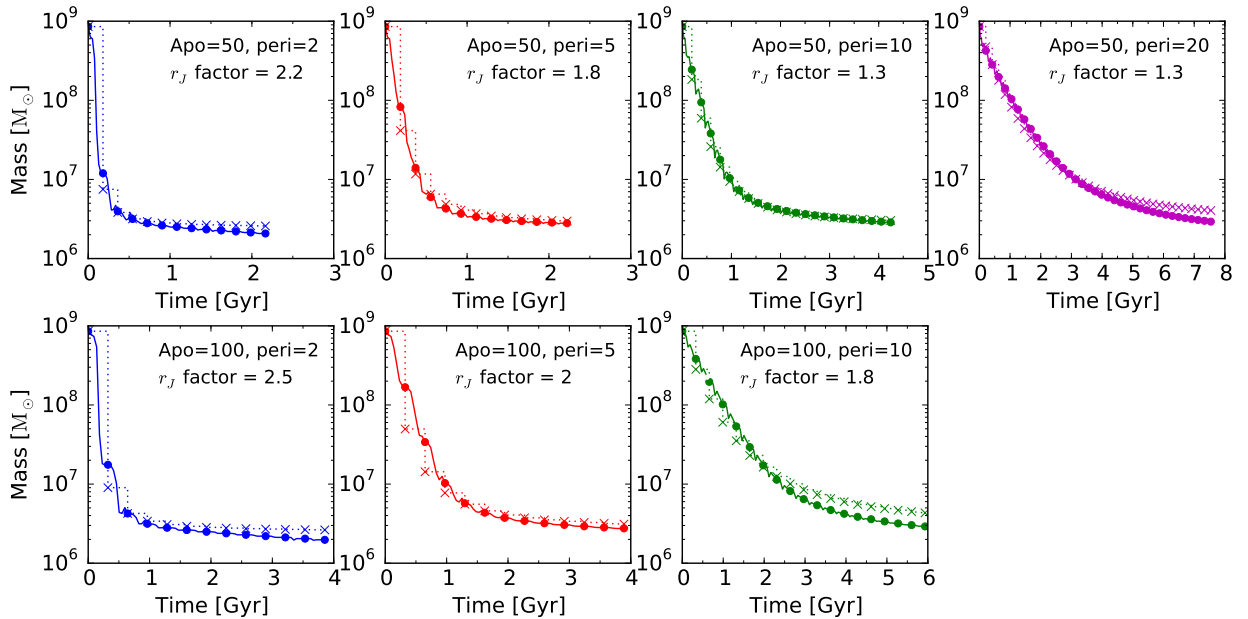
FIGURE 6.1: Comparison of galaxy mass loss using the analytic tidal stripping method method (dotted line, crosses mark apocentre) with the N-body simulations from Chapter 2 (solid line, dots mark apocentre). The apocentre and pericentre distances (in kpc) for the simulations are indicated in each panel.

since many stars will have orbits that go beyond several r_h, causing further decrease of r_J, and the galaxy would become rapidly unbound. We check each component of the galaxy separately since a compact component of the galaxy would remain bound despite an extended component being disrupted.

To determine the form of f_{r_J} this method is tested against the N-body simulations from Chapter 2 of nucleated dwarf galaxies being tidally stripped in the potential of a Virgo-like galaxy cluster. In the analytic method, a Sérsic (1963) profile is used for the main body of each galaxy (where the mass profile is of the form given by Terzić & Graham 2005) and a Plummer (1911) profile is used for the nucleus (instead of a King profile used in the simulations) in order to have an analytic form for the mass profile. The half-mass radius for the Plummer profile was set identical to that of the King profile. For the Sérsic profile the central density and Sérsic index were kept constant throughout the stripping, while for the Plummer profile the scale radius was modified as $a_{\rm new} = (M_{\rm old}/M_{\rm new})^{-1/3}a_{\rm old}$. In Fig. 6.1 the comparison against the Model 3 elliptical orbit simulations is shown (comparisons with Models 1 and 2 give similar results). For each simulation f_{r_J} is chosen to give a reasonable

approximation to the N-body simulations. The agreement between the analytical method and the N-body simulations is very good, with most analytic points located within a factor of two of the simulations. The analytic method generally differs most from the N-body simulations in the first pericentre passage since mass loss in the N-body simulations is not instantaneous and unbound material may take longer than an orbital time to escape.

In Fig. 6.2 we compare f_{r_J} with the ratio of pericentre-to-apocentre distance for each simulation. Although not simulated, we impose the condition of $f_{r_J} = 1$ for circular orbits. There is a slight dependence on apocentre distance for the simulations: simulations with a larger apocentre require a larger f_{r_J} for a given pericentre-to-apocentre distance ratio. This is a consequence of the smaller potential at larger cluster-centric distance meaning more particles can become re-bound. Since there are only two different apocentres used in the simulations we did not take this effect into account when fitting for the form of f_{r_J}. There may also be a dependence on cluster mass although we did not investigate this since the simulations were performed in one cluster potential only. A larger suite of simulations would be required to determine the exact dependence of f_{r_J} on all of these factors which is beyond the scope of this work. Assuming f_{r_J} only depends on $r_{\mathrm{peri}}/r_{\mathrm{apo}}$, we fit the points in Fig. 6.2 using the least-squares method with the equation

$$f_{r_J}(r_{\mathrm{peri}}/r_{\mathrm{apo}}) = 1.63 \frac{e^{-7.36\left(r_{\mathrm{peri}}/r_{\mathrm{apo}}\right)} - e^{-7.36}}{1 - e^{-7.36}} + 1. \qquad (6.11)$$

6.2.3   Comparison with other methods

A simple analytic model for tidal stripping was implemented by Peñarrubia et al. (2010) for subhaloes orbiting in a Milky Way-type system, showing reasonable agreement with full N-body simulations of the process. Their method modified the parameters of the subhalo mass profiles according to scaling relations fit to the N-body simulations. Contini et al. (2014) implemented a tidal stripping method in a SAM to study the formation of intracluster light. They determined the tidal radius of the satellite galaxy at the distance from the main halo centre for each snapshot. Mass beyond the tidal radius was considered stripped and disk's scale length was set to one tenth of the tidal radius. If the tidal radius was less than the
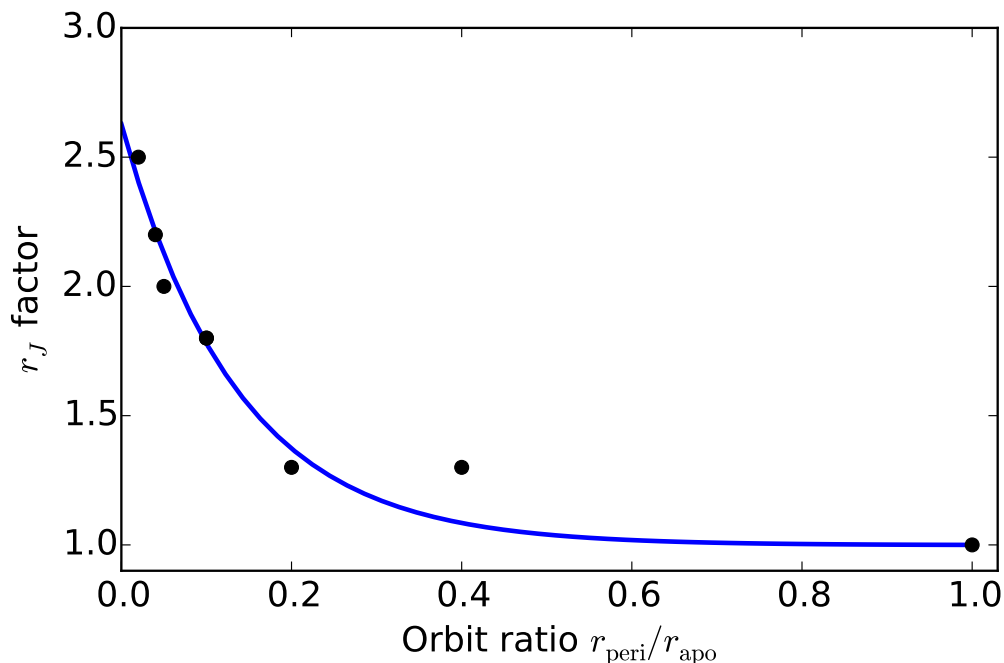
FIGURE 6.2: f_{r_J} factors from Fig. 6.1 compared with the pericentre-to-apocentre distance ratio for each simulation. The point $f_{r_J} = 1$ at $r_{\text{peri}}/r_{\text{apo}} = 1$ is the limiting case defined for a circular orbit. The fitted line is given by Equation 6.11.

bulge scale radius the galaxy was considered completely disrupted.

Although there are broad similarities between methods, such as stripping all mass beyond the tidal radius and calculating mass loss at pericentre similar to Peñarrubia et al., our method differs from the previous two in the following ways: We assume a constant central density/surface brightness throughout the stripping process and modify the scale radii accordingly. The bound mass of the galaxy is determined by the Jacobi radius at pericentre multiplied by a factor to account for the ellipticity of the orbit. Compared to Contini et al. we allow the satellite galaxies to have more than one pericentre passage between snapshots.

6.3 Analysis and discussion

6.3.1 Galaxy mass function

The mass function for the G11 SAM gives a good match to the observed mass function of galaxies (see figure 7 in G11). Therefore applying our tidal stripping method to the SAM
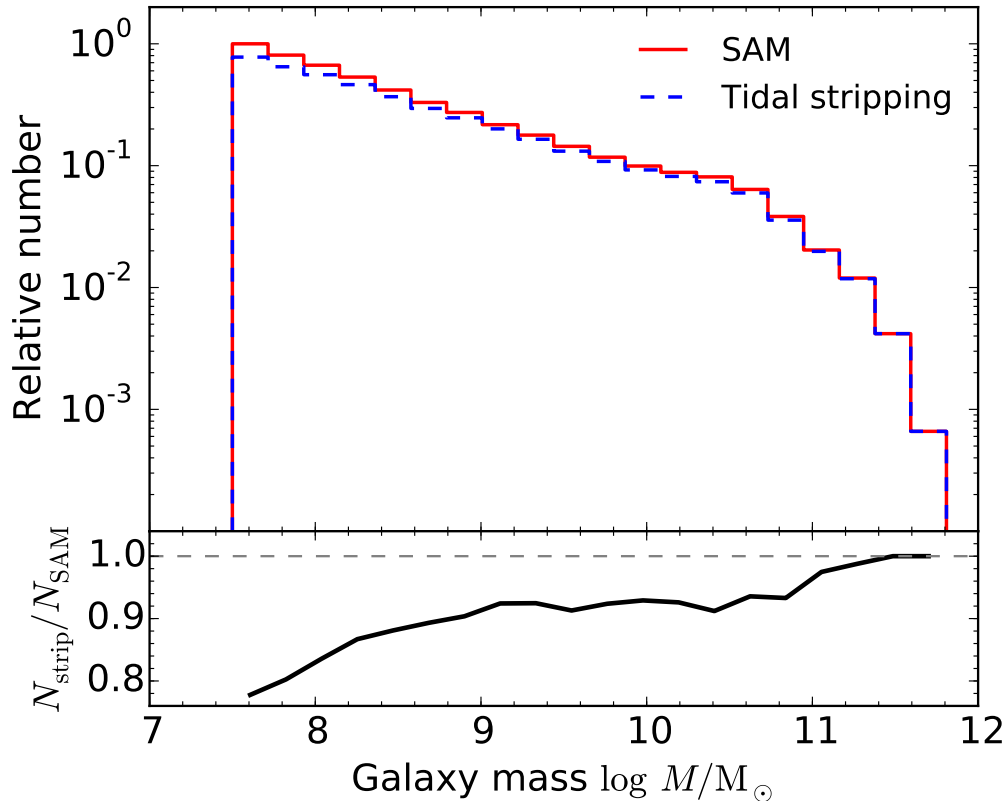
FIGURE 6.3: Mass function for galaxies more massive than $10^{7.5}\,\mathrm{M_\odot}$ at $z = 0$ in the G11 SAM compared to the mass function when tidal stripping is incorporated. The lower panel shows the ratio of the number of galaxies in the tidal stripping method to that in the G11 SAM. The dashed line indicates a ratio of unity.

must not significantly change the galaxy mass function. The resulting galaxy mass function at $z = 0$ for galaxies with masses $> 10^{7.5}\,\mathrm{M_\odot}$ after applying our tidal stripping method is shown in Figure 6.3. Compared to the mass function of the G11 SAM there is a slight reduction in the number of galaxies with masses $< 10^{11}\,\mathrm{M_\odot}$, while the number of galaxies more massive than this is unaffected. For galaxies with masses $\sim 10^{7.5}\,\mathrm{M_\odot}$ tidal stripping reduces the number of galaxies by $\sim$22 per cent. As expected, the effect of stripping decreases with galaxy mass as massive galaxies are more resilient to tidal forces. The difference between the methods is sufficiently small that applying our tidal stripping method to the SAM will still give good agreement with the observed mass function.

The criterion for galaxy disruption in the G11 SAM is that the density of the satellite within its half-mass radius is less than the host halo density at pericentre. This effectively
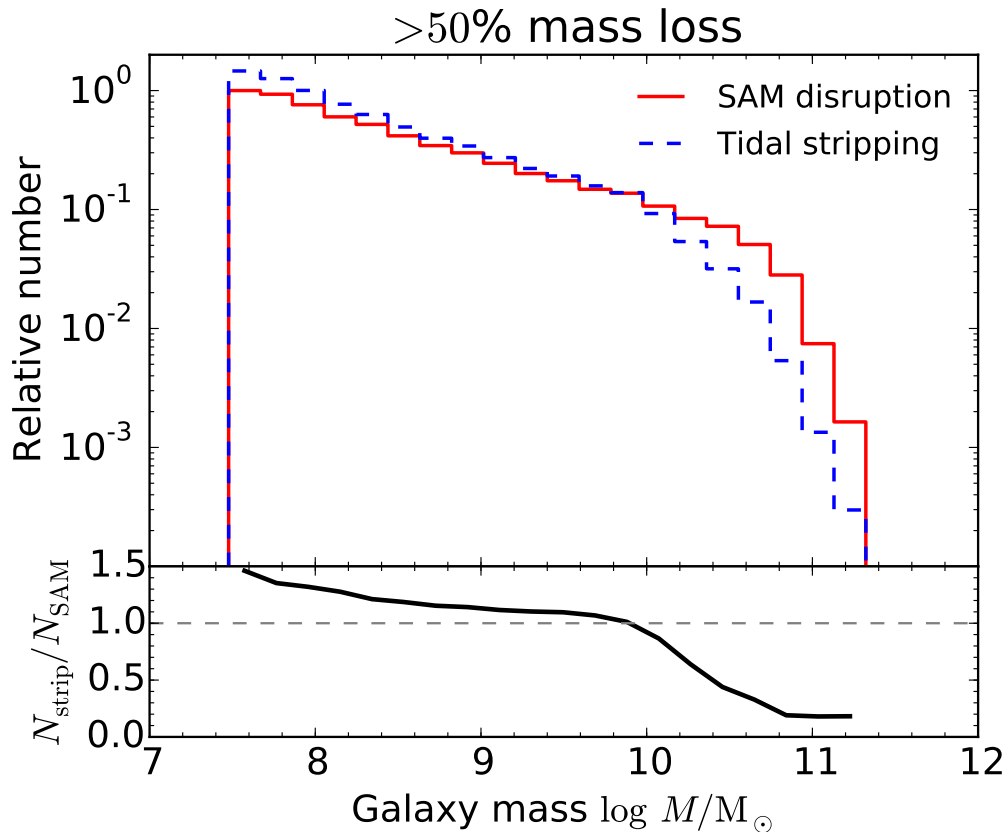
FIGURE 6.4: Mass function for galaxies with masses $> 10^{7.5}\,\mathrm{M_\odot}$ in the SAM disrupted by minor mergers compared to galaxies in the tidal stripping model which lose more than 50 per cent of their mass. The lower panel shows the ratio of the number of galaxies in the tidal stripping method to that in the G11 SAM. The dashed line indicates a ratio of unity.

states that any galaxy that will lose more than 50 per cent of its mass is disrupted. In Figure 6.4 we compare the mass function of galaxies with masses larger than $10^{7.5}\,\mathrm{M_\odot}$ which are disrupted by minor mergers in the SAM with the galaxies that lose more than 50 per cent of their stellar mass according to our tidal stripping model. Here we compare the masses of the galaxies before they undergo any mass loss. This comparison also includes galaxies that merged via dynamical friction. The agreement between the two methods is reasonable, except for masses larger than $10^{10}\,\mathrm{M_\odot}$. Above this mass the SAM predicts more galaxies are disrupted than our tidal stripping method. This does not result in an overabundance of $\sim 10^{11}\,\mathrm{M_\odot}$ galaxies in the $z = 0$ mass function for the tidal stripping method (Figure 6.3) since the number of such galaxies that may undergo tidal stripping is small compared to the total number of galaxies. The difference between the two methods can be attributed
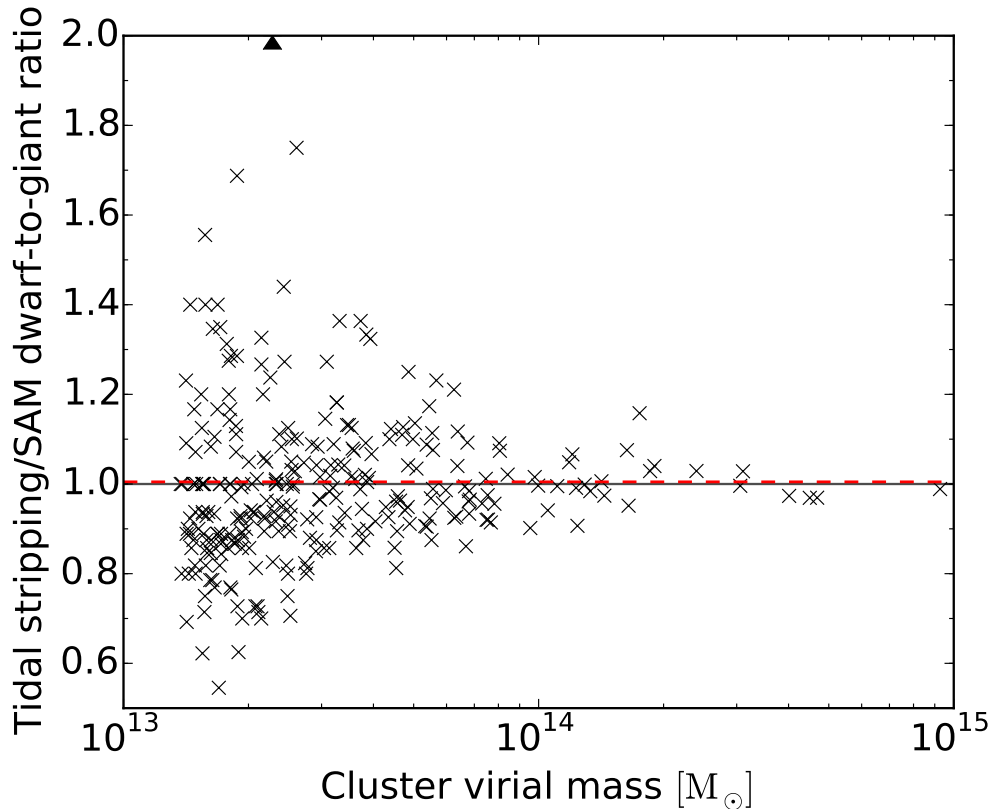
FIGURE 6.5: Ratio of the dwarf-to-giant galaxy ratios when taking into account tidal stripping to the dwarf-to-giant galaxy ratios of the initial SAM. One cluster (indicated by the triangle) has a ratio 4.27. The dashed line shows the mean (1.005) for all clusters.

to our modification of the Jacobi radius to account for elliptical orbits (Equation 6.10) and repeated interactions where a galaxy loses less than half its mass each time.

6.3.2   Dwarf-to-giant ratio

One of the motivations for this study was to test whether incorporating tidal stripping in a SAM can decrease the dwarf-to-giant galaxy ratios in clusters and thereby give better agreement with the observed values (Weinmann et al. 2011). In their study, Weinmann et al. (2011) defined a dwarf galaxy as having luminosities of $-19 < M_r < -16.7$ and giant galaxies as having $M_r < -19$. Assuming a mass-to-light ratio of $M/L_r = 3\,(M/L)_\odot$, this corresponds to masses of $10^9 < M/\mathrm{M_\odot} < 10^{10}$ for dwarf galaxies and $M > 10^{10}\,\mathrm{M_\odot}$ for giant galaxies. We therefore take these mass cuts when calculating the dwarf-to-giant ratios.

In Figure 6.5 we compare the dwarf-to-giant ratios for the tidal stripping method to
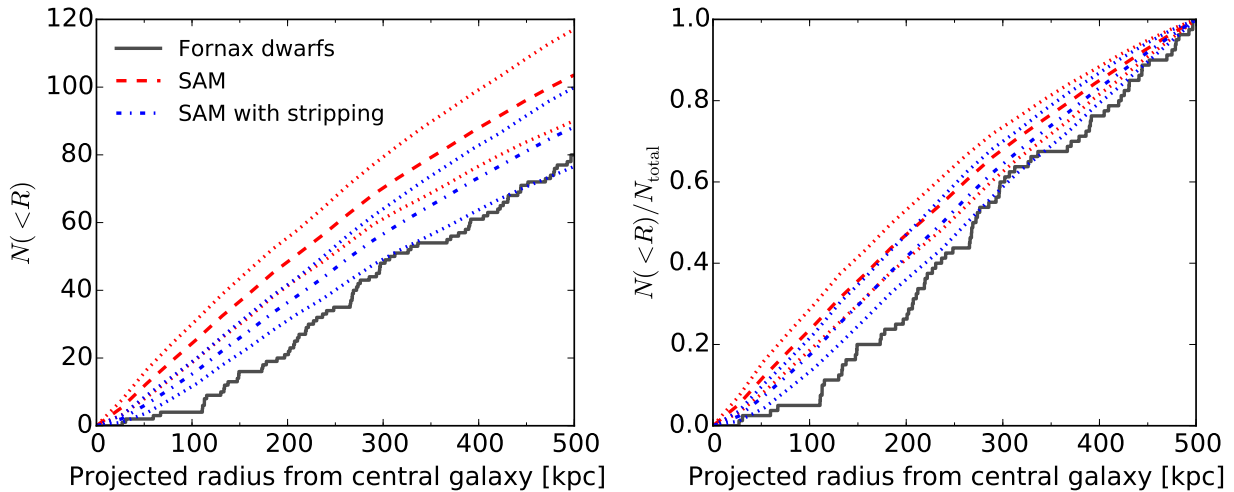
FIGURE 6.6: Projected radial distribution of dwarf galaxies in Fornax-like clusters for the SAM (dashed line) and the tidal stripping method (dash-dotted line) compared to the radial distribution of observed dwarf galaxies in the Fornax cluster (solid line). The dotted lines show the standard deviation for the simulated clusters.

those of the initial SAM for all galaxy clusters in our sample. Contrary to our expectation on average there is almost no change (0.5 per cent increase) in the dwarf-to-giant ratios when including tidal stripping. This is due to tidal stripping acting almost equally on dwarf and giant galaxies: in Figure 6.3 the number of galaxies with masses $10^9 < M/\mathrm{M}_\odot < 10^{10}$ and galaxies with mass $M > 10^{10}\,\mathrm{M}_\odot$ are both decreased by about 7 per cent. A number of clusters (especially the cluster with the largest ratio of 4.27) have significantly increased dwarf-to-giant ratios after including tidal stripping due to disproportional tidal stripping of 'giant' galaxies compared to dwarf galaxies.

One possible reason the dwarf-to-giant ratios of the SAM are not improved when including tidal stripping is because we only allow galaxies in the SAM to be stripped once they have lost their dark matter halo. Since the less massive haloes of dwarf galaxies will be less resilient to tidal forces in clusters, and therefore less effective at shielding the baryonic matter from tidal forces, tidal stripping should be more effective when acting on dwarf galaxies. There may also be many dwarf galaxies with just resolved dark matter haloes which we ignore that will be strongly affected by tidal forces.

6.3.3 Radial distributions

In Figure 6.6 we show the radial distributions of dwarf galaxies predicted for the Fornax cluster by the SAM and our tidal stripping method. Here we choose Fornax-like clusters as having virial masses $5 \times 10^{13} < M_{\mathrm{vir}}/\mathrm{M}_\odot < 9 \times 10^{13}$ (Drinkwater et al. 2001) and dwarf galaxies as having stellar masses $10^8 < M/\mathrm{M}_\odot < 10^{10.5}$. For each cluster we take the mean over three lines of sight (the x-, y- and z-axis of the simulation) to determine the radial distribution. We also show the radial distribution for dwarf galaxies in the Fornax cluster (Ferguson 1989), where we choose dwarf galaxies as having luminosities $-19.6 < M_B/\mathrm{mag} < -13.4$. For a mass-to-light ratio of $M/L_B = 3\,(\mathrm{M/L})_\odot$ the mass cuts for the simulations and observations are approximately equal. We caution here that our method for choosing cluster galaxies in the simulations is not identical to that for observed galaxies. However, within 500 kpc we find almost all simulated dwarf galaxies have radial velocities less than 1000 km s^{-1} relative to the central galaxy, similar to the velocity cut made by (Weinmann et al. 2011) for their Fornax cluster sample.

We find that dwarf galaxies in the SAM are both too numerous and too concentrated compared to the observed population. This is contrary to the findings of Weinmann et al. (2011), however we have included fainter galaxies. When taking into account tidal stripping the dwarf galaxy numbers are improved but still too numerous and concentrated compared to the observed galaxies. This is mostly caused by an overabundance of galaxies within the central 250 kpc of the galaxy cluster. Dwarf galaxy numbers might be further improved by allowing tidal stripping to affect dwarf galaxies before their dark matter haloes are lost, including the stellar mass of the central galaxy when determining the Jacobi radius of a satellite, or including galaxy harassment (Moore et al. 1996) which will have the largest effect near the cluster centre.

6.3.4 Galaxy sizes

In Figure 6.7 we show the sizes and masses of galaxies determined using our tidal stripping method which may have undergone tidal stripping. For comparison we also show the sizes of galaxies which have resolved dark matter haloes and therefore suffer no stripping in our
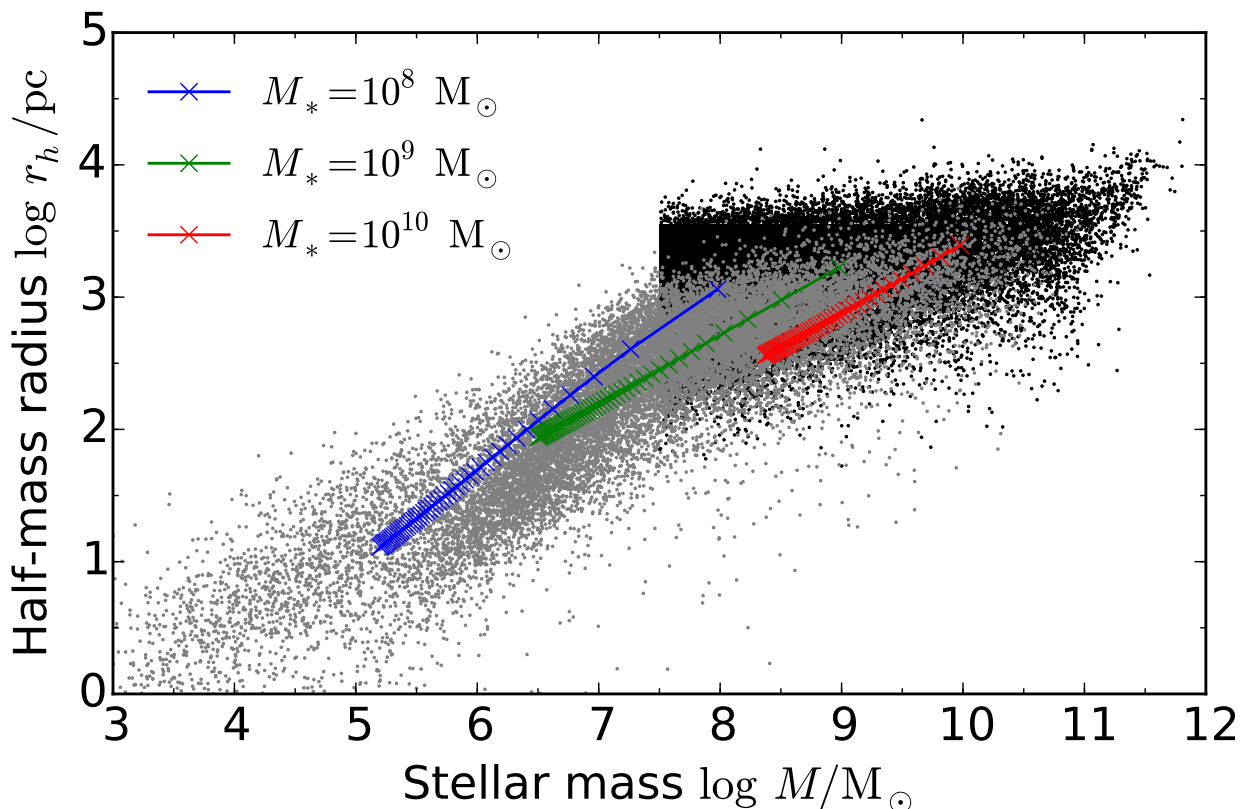
FIGURE 6.7: Sizes and masses of all galaxies at $z = 0$. Black dots show all galaxies in the SAM which have a resolved dark matter halo (non-stripped galaxies) and grey dots show galaxies which have lost their dark matter halo (possibly undergo stripping). Tidal stripping tracks for typical galaxies with stellar masses of 10^8, 10^9 and $10^{10}\,\mathrm{M}_\odot$ orbiting in a halo of $10^{14}\,\mathrm{M}_\odot$ with a pericentre of 10 kpc and an apocentre of 100 kpc are shown by the solid lines. The properties of the galaxies are summarized in Table 6.1. The crosses indicate the location of the galaxies after each pericentre passages.

method. Due to the tidal effects, galaxies which have undergone some amount of stripping are generally more compact than galaxies which have had no stripping. Additionally, extended low-mass galaxies are preferentially removed due to the condition $r'_J <= r_h/3$.

Below masses of $10^{7.5}\,\mathrm{M}_\odot$ the sizes of the galaxies from our tidal stripping method are generally too compact compared to observed galaxies (e.g. Misgeld & Hilker 2011). Elliptical galaxies with stellar masses $\sim 10^6\,\mathrm{M}_\odot$ have typical sizes of 400-500 pc. This indicates that the assumption of a constant central density (for the bulge) and central surface density (for the disk) does not hold during extreme mass loss. Further simulations are needed to determine how the density profile of a galaxy is modified during extreme tidal stripping and at what point the assumption of a constant central density no longer holds.

TABLE 6.1: Median properties of satellite galaxies in the G11 SAM with stellar masses within 0.1 dex of M_*. Column 2 shows the maximum circular velocity of the subhalo at its last resolved time. Columns 3 and 4 show the mass of the disk and disk scale length. Columns 5 and 6 show the bulge mass and bulge scale length.

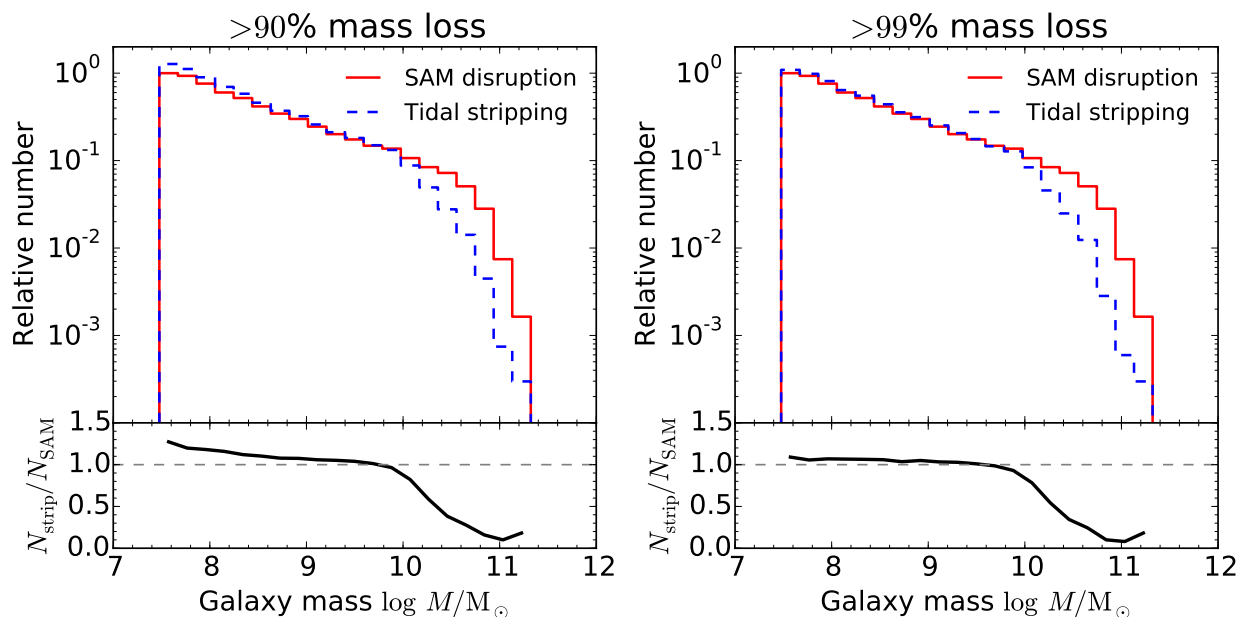| M_* (log $M_\odot$)	Infall V_{max} (km s^{-1})	M_d (log $M_\odot$)	R_d (kpc)	M_b (log $M_\odot$)	r_b (kpc)
8	62	7.9	0.7	7.3	0.67
9	87	9.0	1.0	7.4	0.75
10	124	10.0	1.5	8.7	0.83

FIGURE 6.8: Mass function for galaxies with masses $> 10^{7.5}\,M_\odot$ in the SAM disrupted by minor mergers compared to galaxies in the tidal stripping model which lose more than 90 (left) and 99 per cent (right) of their mass. The lower panels show the ratio of the number of galaxies in the tidal stripping method to that in the G11 SAM. The dashed line indicates a ratio of unity.

6.4 Consequences for stripped nucleus formation

The exact amount of mass loss necessary for a nucleated galaxy to become a UCD depends strongly on the mass profile of the galaxy, however it is probably in the range of 90–99 per cent (Chapter 2). In Figure 6.8 we show the mass function for galaxies which lose more than 90 and 99 per cent of their mass according to our tidal stripping model compared to the mass function of disrupted galaxies for the G11 SAM. The mass function for 90 and 99 per cent mass loss generally agree well with the mass function for disrupted galaxies in the SAM. The largest difference is for galaxies with stellar masses $\gtrsim 10^{10.2}\,M_\odot$ or, assuming a

nucleus-to-galaxy mass ratio of 0.3 per cent, for nuclei with masses $\gtrsim 10^{7.7} \, \mathrm{M}_\odot$. Therefore for nucleus masses $> 10^{7.7} \, \mathrm{M}_\odot$, the number of stripped nuclei predicted will decrease by about an order of magnitude compared to the prediction in Chapter 4. We expect all other predictions from Chapter 4 will remain largely unchanged as the number of such objects is low.

6.5   Summary

In this chapter we presented a method for including tidal stripping in semi-analytic models of galaxy formation. We post-processed the SAM of Guo et al. (2011), the first SAM with sufficient resolution to follow the formation of dwarf galaxies. We assume tidal stripping is only important for galaxies which have lost their dark matter halo and that all such galaxies have lost their gas and undergo no star formation. We tested our method against N-body simulations of tidal stripping and find good agreement. Our main findings are as follows.

(i) Tidal stripping removes $\sim$20 per cent of galaxies with masses $\sim 10^{7.5} \, \mathrm{M}_\odot$ in clusters compared to the G11 SAM, but does not significantly alter the galaxy mass function.

(ii) Tidal stripping acts equally on both dwarf and giant galaxies that have lost their dark matter halo (for galaxies with stellar masses larger than $10^9 \, \mathrm{M}_\odot$) and therefore the dwarf-to-giant galaxy ratios in clusters is largely unaffected. Allowing tidal stripping to act on galaxies with resolved dark matter haloes may solve this problem.

(iii) The radial distribution of dwarf galaxies in Fornax-like clusters is improved when taking into account tidal stripping compared to the SAM without stripping. However even with stripping included dwarf galaxies are still too numerous and the distribution too concentrated compared to observed dwarfs in the Fornax cluster.

(iv) When taking into account tidal stripping, the number of possible stripped nucleus progenitor galaxies is decreased for galaxies with stellar masses $> 10^{10} \, \mathrm{M}_\odot$. Therefore the number of nuclei with masses $> 10^{7.7} \, \mathrm{M}_\odot$ is likely to decrease by up to a factor of 10 compared to the prediction in Chapter 4. We expect all other predictions will not be significantly affected as the number of such objects is low.

Although our method offers an improvement compared to a SAM without tidal stripping, further refinements of the method are still needed. The stellar mass of the central galaxy should be included when determining the Jacobi radius of a satellite galaxy. The assumption of a constant central density does not hold after extreme mass and produces objects too compact for a given mass compared to observed galaxies. Galaxy harassment (high-speed encounters between galaxies causing collisional shocks, Moore et al. 1996) should be included, although this is computationally expensive. We have also neglected spheroidal formation through disk thickening (e.g. Moore et al. 1999) as the G11 SAM does not include a disk thickness parameter. To thoroughly test the method it should be included natively into semi-analytic models so that stripping may act on galaxies with resolved dark matter haloes, the gas mass in galaxies can be included and continued star formation can be taken into account.

7

Conclusion

In this thesis we have tested the formation of UCDs by tidal stripping using numerical simulations. The overall aim of the thesis was to address the following scientific questions:

  (i) Can tidal stripping account for the sizes and masses of all observed UCDs?

 (ii) What is the number of UCDs predicted by tidal stripping?

(iii) How do ultra-compact dwarf galaxies form?

In the following sections we discuss how this work addresses those questions.

7.1   Properties of UCDs formed by tidal stripping

In Chapter 2 we used numerical simulations of nucleated dwarf galaxies undergoing tidal stripping in a galaxy cluster to investigate the possible sizes and masses of UCDs formed by

tidal stripping and the origin of the difference in sizes between UCDs and nuclear clusters. We found nuclear clusters undergo very little expansion during tidal stripping and therefore cannot explain the size difference between nuclear clusters and UCDs. However depending on their orbit in the galaxy cluster UCDs may retain part of the progenitor galaxy as a stellar envelope. This can increase the size of the UCD significantly compared to that of the nuclear cluster while only marginally increasing its mass and can thus account for the size difference between nuclear clusters and UCDs. Depending on the orbital distribution of galaxies in clusters tidal stripping can therefore account for the complete range of sizes and masses of observed UCDs.

In Chapter 3 we addressed the recent claim that UCDs formed by tidal stripping have elevated dynamical-to-stellar mass ratios. We reanalysed the tidal stripping simulations from Chapter 2 and determined the velocity dispersions and dynamical-to-stellar mass ratio as would be seen by an observer. However a key limitation of these simulations is that we did not include a dark matter halo for the UCD progenitor galaxies and thus may be underestimating the dynamical masses of UCDs formed by tidal stripping. We found that the dynamical-to-stellar mass ratios of UCDs formed by tidal stripping are generally close to unity. However for recent mergers ($\lesssim 2$ Gyr) and compact UCDs where the UCD size is much smaller than the aperture slit width the line-of-sight becomes important and UCDs may have ratios of ~ 10. As the UCDs are approximately in virial equilibrium within the tidal radius, this is cause by extra-tidal material being projected onto the UCD. For these cases evidence of a recent merger (such as tidal tails and low surface brightness shells) might be visible in deep imaging. For UCDs formed by tidal stripping the elevated mass-to-light ratios of UCDs must therefore be accounted for by some other mechanism (i.e. IMF variations, central black holes or dark matter).

In Chapter 4 we presented the first work to predict the properties of UCDs using a cosmologically motivated galaxy formation model. We find that for masses $> 2 \times 10^6 \, \mathrm{M_\odot}$ tidal stripping can only account for ~ 10 per cent of observed UCDs. For masses larger than $10^7 \, \mathrm{M_\odot}$ tidal stripping can only account for ~ 50 per cent of observed UCDs. The most massive UCD predicted to form in galaxy clusters by tidal stripping also agrees well with the most massive UCDs observed. Additionally we find the predicted ages of UCDs

formed by tidal stripping agree well with those observed in the Fornax and Virgo clusters. Young objects such as W3 (300-500 Myr, Maraston et al. 2004) are difficult to reconcile with this scenario unless the disruption of a gas rich dwarf galaxy ignites star formation in the nucleus.

In Chapter 5 we compared the predictions of our model in Chapter 4 with the observed properties of UCDs in the local universe. We find the number of UCDs predicted to form by tidal stripping in the Fornax cluster agrees reasonably well with the number of UCDs observed at the very high-mass end of the UCD mass function. The GC/UCD mass function is therefore consistent with being a combination of genuine GCs and stripped nuclei. This implies the most massive genuine GC in the Fornax cluster has a mass $\sim 3 \times 10^7\,\mathrm{M_\odot}$. We find the predicted radial velocity dispersions, radial distributions and metallicities of UCDs formed by tidal stripping agrees well with the observed properties of UCDs in the Fornax cluster. For masses above $\sim 2 \times 10^6\,\mathrm{M_\odot}$, the predicted masses of central black holes in UCDs formed by tidal stripping agree well with the first UCD with a confirmed central black hole (Seth et al. 2014) and the inferred black hole masses of UCDs (Mieske et al. 2013).

In Chapter 6 we presented a new method to include tidal stripping in semi-analytic models of galaxy formation. When compared with dwarf galaxies in the Fornax cluster, we find this method gives much improved numbers and radial distributions compared to semi-analytic modelling without tidal stripping. For the predictions of UCDs formed by tidal stripping, we find including tidal stripping in the semi-analytic model will decrease the number of UCDs with masses larger than $10^8\,\mathrm{M_\odot}$ by a factor of ten, but the predictions will remain largely unchanged for other masses.

7.2 The origin of ultra-compact dwarf galaxies

Although the properties of UCDs formed by tidal stripping generally agree well with that of observed UCDs (Chapters 2 & 5), we find UCD formation by tidal stripping cannot be the dominant formation mechanism of UCDs (Chapter 4). Instead we suggest most UCDs are simply the high-mass end of the GC mass function with the contribution of UCDs formed by tidal stripping increasing towards higher masses. Above masses of $\sim 3 \times 10^7\,\mathrm{M_\odot}$ UCDs

in the Fornax cluster are consistent with being entirely formed by tidal stripping. The most extended UCDs ($R_{\text{eff}} > 10$ pc) are also consistent (by numbers) with being UCDs formed by tidal stripping as these objects are extremely rare compared to compact GCs/UCDs (for masses less than $10^7\,\text{M}_\odot$), although what fraction of UCDs formed by tidal stripping will be extended objects remains unclear. Very extended and massive UCDs ($R_{\text{eff}} \sim 100$ pc, $M \sim 10^8\,\text{M}_\odot$) have a nucleus plus stellar envelope structure (e.g. UCD3 and VUCD 7, Evstigneeva et al. 2008) which is predicted for very extended UCDs by our simulations in Chapter 2. Mergers of star cluster complexes may also form extended UCDs (Brüns et al. 2011; Brüns & Kroupa 2012) however a prediction for the number of these objects expected to form in clusters has not yet been made.

These findings are consistent with the findings of other recent studies. Mieske et al. (2012) calculated the fraction of GCs that contribute to the UCD population based on the specific frequencies of GCs around galaxies and found less than 50 per cent of UCDs can have formed by tidal stripping. Mieske et al. (2013) investigated the dynamical-to-stellar mass ratios Ψ of UCDs and found evidence for a bimodal distribution, with one population having $\Psi < 1$ similar to GCs and the other having $\Psi > 1$ (see Figure 1.4). In the Fornax cluster less than 10 per cent ($17/\sim200$) of GCs/UCDs with masses $> 2 \times 10^6\,\text{M}_\odot$ have measured dynamical mass-to-light ratios. Of these 17, 9 have $\Psi < 1$ and are thus consistent with being genuine GCs, while 5 have $\Psi > 1$ at the 1σ level and require some additional dark mass. The remaining 3 might be either genuine GCs or UCDs formed by tidal stripping that do not host central black holes (the occupation fraction of supermassive black holes in UCD progenitor galaxies is likely not 100 per cent). As we find about 20 UCDs more massive than $2 \times 10^6\,\text{M}_\odot$ will have formed by tidal stripping in the Fornax cluster within 300 kpc (Figure 5.2), we expect most of the GC/UCD population without measured dynamical mass-to-light ratios would not have an elevated Ψ if this scenario is correct. Therefore a combination of genuine GCs (where some fraction of GCs/UCDs are formed in starbursts similar as YMCs, e.g. Renaud et al. 2015) and stripped nuclear clusters is sufficient to explain the properties of all observed UCDs.

7.3 Future work

Our predictions are subject to a number of caveats which may be improved upon:

- Future tidal stripping simulations (Chapter 2) should include dark matter haloes, extend the simulations to galaxies of different morphologies and perform stripping simulations in different sized galaxy clusters. This will enable more accurate predictions of the properties of UCDs formed by tidal stripping (e.g. mass-to-light ratios).

- Our predictions for the number of UCDs formed by tidal stripping (Chapter 4) depend crucially on the fraction of galaxies with nuclei in the early universe since most UCD formation happens at early times (see Figure 8 in Chapter 4). As observing nuclei in galaxies during this period ($z > 1$) is impossible and likely to remain so for the foreseeable future, other means such like simulations are necessary to address this problem.

- Cosmological scale hydrodynamical simulations of galaxy formation have recently been performed (i.e. the Illustris and Eagle projects: Vogelsberger et al. 2014; Schaye et al. 2015, respectively). These simulations naturally include galaxy disruption and dynamical friction and therefore UCD formation models based on these simulations will improve upon our estimates using semi-analytic modelling (for which the disruption criteria is likely unrealistic as we show in Chapter 6).

- Comparisons between our UCD models and observations (Chapter 5) should be extended beyond the central galaxy of a galaxy cluster. Programs like the Next Generation Virgo Cluster Survey (Ferrarese et al. 2012) combined with further spectroscopic surveys will enable a systematic comparison over the main subclusters of a galaxy cluster.

- Observational constraints on the SMBH occupation fraction in nucleated dwarf galaxies could be used to determine what fraction of UCDs should have elevated dynamical mass-to-light ratios due to the presence of central black holes and, together with more

observations of UCD dynamical mass-to-light ratios, determine if central black holes alone are sufficient to explain UCDs with elevated mass-to-light ratios.

- Future models of UCD formation by tidal stripping should include a prediction of UCD sizes to determine what fraction of extended GCs/UCDs ($10 < R_{\mathrm{eff}}/\mathrm{pc} < 100$) can be explained by tidal stripping. Our tidal stripping simulations of Chapter 2 also suggest transition objects between UCDs and dwarf galaxies should exist ($R_{\mathrm{eff}} \sim 100$ pc, $10^6 \lesssim M_*/\mathrm{M}_\odot \lesssim 10^7$). Currently no confirmed objects are observed (see Figure 1.1). Further observation work is required to determine if such objects are indeed very rare or if observational selection criteria rejects such objects (e.g. as background galaxies). The existence or non-existence of such objects puts constraints on the orbits of galaxies in clusters and therefore on the number of UCDs that can form by tidal stripping.

- Our model for including tidal stripping in semi-analytic modelling (Chapter 6) should be incorporated into semi-analytic models rather than by post-processing the outcome of these simulations. Additionally a larger suite of tidal stripping simulations needs to be performed to determine more accurately how the density profile of a galaxy is modified by extreme mass loss and the dependence of the Jacobi radius on orbital ellipticity, apocentre distance and host cluster mass.

References

Annibali F., Tosi M., Aloisi A., van der Marel R. P., Martinez-Delgado D., 2012, ApJ, 745, LL1

Ashman K. M., Zepf S. E., 1998, Globular cluster systems. Cambridge Astrophysics Series, vol. 30. Cambridge Univ. Press. Cambridge

Bassino L. P., Muzzio J. C., Rabolli M., 1994, ApJ, 431, 634

Bassino L. P., Faifer F. R., Forte J. C., Dirsch B., Richtler T., Geisler D., Schuberth Y., 2006, A&A, 451, 789

Bastian N., Saglia R. P., Goudfrooij P., Kissler-Patig M., Maraston C., Schweizer F., Zoccali M., 2006, A&A, 448, 881

Baumgardt H., Makino J., 2003, MNRAS, 340, 227

Baumgardt H., Makino J., Hut P., McMillan S., Portegies Zwart S., 2003, ApJ, 589, L25

Baumgardt H., Mieske S., 2008, MNRAS, 391, 942

Beers T. C., Flynn K., Gebhardt K., 1990, AJ, 100, 32

Bekki K., Couch W. J., Drinkwater M. J., 2001, ApJ, 552, L105

Bekki K., Couch W. J., Drinkwater M. J., Shioya Y., 2003, MNRAS, 344, 399

Bell E. F., McIntosh D. H., Katz N., Weinberg M. D., 2003, ApJS, 149, 289

Bender R., Burstein D., Faber S. M., 1992, ApJ, 399, 462

Bergond G., et al., 2007, A&A, 464, L21

Bertin G., Ciotti L., Del Principe M., 2002, A&A, 386, 149

Binggeli B., Sandage A., Tammann G. A., 1985, AJ, 90, 1681

Binney J., Tremaine S., 1987, Galactic Dynamics. Princeton Univ. Press, Princeton

Böker T., Laine S., van der Marel R. P., Sarzi M., Rix H.-W., Ho L. C., Shields J. C., 2002, AJ, 123, 1389

Boylan-Kolchin M., Springel V., White S. D. M., Jenkins A., Lemson G., 2009, MNRAS, 398, 1150

Boylan-Kolchin M., Bullock J. S., Sohn S. T., Besla G., van der Marel R. P., 2013, ApJ, 768, 140

Brodie J. P., Larsen S. S., 2002, AJ, 124, 1410

Brodie J. P., Strader J., 2006, ARA&A, 44, 193

Brodie J. P., Romanowsky A. J., Strader J., Forbes D. A., 2011, AJ, 142, 199

Brüns R. C., Kroupa P., Fellhauer M., Metz M., Assmann P., 2011, A&A, 529, A138

Brüns R. C., Kroupa P., 2012, A&A, 547, A65

Burkert A., 1995, ApJ, 447, L25

Carollo C. M., Stiavelli M., de Zeeuw P. T., Mack J., 1997, AJ, 114, 2366

Chiboucas K., Tully R. B., Marzke R. O., Trentham N., Ferguson H. C., Hammer D., Carter D., Khosroshahi H., 2010, ApJ, 723, 251

Chiboucas K. et al., 2011, ApJ, 737, 86

Chilingarian I. V., 2009, MNRAS, 394, 1229

Chilingarian I. V., Mamon G. A., 2008, MNRAS, 385, L83

Chilingarian I. V., Mieske S., Hilker M., Infante L., 2011, MNRAS, 412, 1627

Cohen J. G., Kirby E. N., Simon J. D., Geha M., 2010, ApJ, 725, 288

Contini E., De Lucia G., Villalobos Á., Borgani S., 2014, MNRAS, 437, 3787

Côté P., Marzke R. O., West M. J., 1998, ApJ, 501, 554

Côté P. et al., 2006, ApJS, 165, 57

Dabringhausen J., Kroupa P., Baumgardt H., 2009, MNRAS, 394, 1529

Dabringhausen J., Fellhauer M., Kroupa P., 2010, MNRAS, 403, 1054

Dabringhausen J., Kroupa P., Pflamm-Altenburg J., Mieske S., 2012, ApJ, 747, 72

Da Costa G. S., Held E. V., Saviane I., 2014, MNRAS, 438, 3507

Da Rocha C., Mieske S., Georgiev I. Y., Hilker M., Ziegler B. L., Mendes de Oliveira C., 2011, A&A, 525, A86

Dirsch B., Richtler T., Geisler D., Forte J. C., Bassino L. P., Gieren W. P., 2003, AJ, 125, 1908

Dooley G. A., Griffen B. F., Zukin P., Ji A. P., Vogelsberger M., Hernquist L. E., Frebel A., 2014, ApJ, 786, 50

Drinkwater M. J., Jones J. B., Gregg M. D., Phillipps S., 2000, PASA, 17, 227

Drinkwater M. J., Gregg M. D., Colless M., 2001, ApJ, 548, L139

Drinkwater M. J., Gregg M. D., Hilker M., Bekki K., Couch W. J., Ferguson H. C., Jones J. B., Phillipps S., 2003, Nature, 423, 519

Evstigneeva E. A., Gregg M. D., Drinkwater M. J., Hilker M., 2007a, AJ, 133, 1722

Evstigneeva E. A., Drinkwater M. J., Jurek R., Firth P., Jones J. B., Gregg M. D., Phillipps S., 2007b, MNRAS, 378, 1036

Evstigneeva E. A. et al., 2008, AJ, 136, 461

Fardal M. A., et al., 2013, MNRAS, 434, 2779

Fellhauer M., Kroupa P., Baumgardt H., Bien R., Boily C. M., Spurzem R., Wassmer N., 2000, New A, 5, 305

Fellhauer M., Kroupa P., 2002, MNRAS, 330, 642

Fellhauer M., Kroupa P., 2005, MNRAS, 359, 223

Ferguson H. C., 1989, AJ, 98, 367

Ferrarese L., et al., 2000, ApJ, 529, 745

Ferrarese L., et al., 2012, ApJS, 200, 4

Ferraro F. R., et al., 2009, Nature, 462, 483

Firth P., Drinkwater M. J., Evstigneeva E. A., Gregg M. D., Karick A. M., Jones J. B., Phillipps S., 2007, MNRAS, 382, 1342

Firth P., Drinkwater M. J., Karick A. M., 2008, MNRAS, 389, 1539

Firth P., Evstigneeva E. A., Drinkwater M. J., 2009, MNRAS, 394, 1801

Forbes D. A., Pota V., Usher C., Strader J., Romanowsky A. J., Brodie J. P., Arnold J. A., Spitler L. R., 2013, MNRAS, 435, L6

Forbes D. A., Norris M. A., Strader J., Romanowsky A. J., Pota V., Kannappan S. J., Brodie J. P., Huxor A., 2014, MNRAS, 444, 2993

Francis K. J., Drinkwater M. J., Chilingarian I. V., Bolt A. M., Firth P., 2012, MNRAS, 425, 325

Frank M. J., Hilker M., Mieske S., Baumgardt H., Grebel E. K., Infante L., 2011, MNRAS, 414, L70

Freedman W. L., et al., 2001, ApJ, 553, 47

Fuentes-Carrera I., Jablonka P., Sarajedini A., Bridges T., Djorgovski G., Meylan G., 2008, A&A, 483, 769

Gallazzi A., Charlot S., Brinchmann J., White S. D. M., Tremonti C. A., 2005, MNRAS, 362, 41

Geehan J. J., Fardal M. A., Babul A., Guhathakurta P., 2006, MNRAS, 366, 996

Geha M., Guhathakurta P., van der Marel R. P., 2002, AJ, 124, 3073

Geha M., Guhathakurta P., van der Marel R. P., 2003, AJ, 126, 1794

Ghigna S., Moore B., Governato F., Lake G., Quinn T., Stadel J., 1998, MNRAS, 300, 146

Gieles M., Baumgardt H., Heggie D. C., Lamers H. J. G. L. M., 2010, MNRAS, 408, L16

Gilmore G., Wilkinson M. I., Wyse R. F. G., Kleyna J. T., Koch A., Evans N. W., Grebel E. K., 2007, ApJ, 663, 948

Goerdt T., Moore B., Kazantzidis S., Kaufmann T., Macciò A. V., Stadel J., 2008, MNRAS, 385, 2136

Graham A. W., 2012, ApJ, 746, 113

Graham A. W., Spitler L. R., 2009, MNRAS, 397, 2148

Grant N. I., Kuipers J. A., Phillipps S., 2005, MNRAS, 363, 1019

Gregg M. D., et al., 2009, AJ, 137, 498

Guo Q. et al., 2011, MNRAS, 413, 101

Guo Q., White S., Angulo R. E., Henriques B., Lemson G., Boylan-Kolchin M., Thomas P., Short C., 2013, MNRAS, 428, 1351

Han S.-I., Lee Y.-W., Joo S.-J., Sohn S. T., Yoon S.-J., Kim H.-S., Lee J.-W., 2009, ApJ, 707, L190

Harris W. E., 1996, AJ, 112, 1487

Harris W. E., 2001, Star Clusters: Saas-Fee Advanced Course 28. Springer-Verlag, New York, p. 223

Hau G. K. T., Spitler L. R., Forbes D. A., Proctor R. N., Strader J., Mendel J. T., Brodie J. P., Harris W. E., 2009, MNRAS, 394, L97

Haşegan M. et al., 2005, ApJ, 627, 203

Henriques B. M., Bertone S., Thomas P. A., 2008, MNRAS, 383, 1649

Hilker M., 2009, Rev. Modern Astron., Vol. 21, Formation and Evolution of Cosmic Structures. Wiley-VCH, Weinheim, p. 199

Hilker M., Richtler T., 2000, A&A, 362, 895

Hilker M., Infante L., Vieira G., Kissler-Patig M., Richtler T., 1999a, A&AS, 134, 75

Hilker M., Infante L., Richtler T., 1999b, A&AS, 138, 55

Hilker M., Baumgardt H., Infante L., Drinkwater M., Evstigneeva E., Gregg M., 2007, A&A, 463, 119

Hilker M., 2011, EAS Publ. Ser., 48, 219

Hopkins P. F., Murray N., Quataert E., Thompson T. A., 2010a, MNRAS, 401, L19

Hopkins P. F., et al., 2010b, ApJ, 724, 915

Humphrey P. J., Buote D. A., Gastaldello F., Zappacosta L., Bullock J. S., Brighenti F., Mathews W. G., 2006, ApJ, 646, 899

Huxor A. P., Tanvir N. R., Irwin M. J., Ibata R., Collett J. L., Ferguson A. M. N., Bridges T., Lewis G. F., 2005, MNRAS, 360, 1007

Ibata R. A., Wyse R. F. G., Gilmore G., Irwin M. J., Suntzeff N. B., 1997, AJ, 113, 634

Jalali B., Baumgardt H., Kissler-Patig M., Gebhardt K., Noyola E., Lützgendorf N., de Zeeuw P. T., 2012, A&A, 538, A19

Janz J., Forbes D. A., Norris M. A., Strader J., Penny S. J., Fagioli M., Romanowsky A. J., 2015, preprint (arXiv:1502.06598)

Jerjen H., Tully B., Trentham N., 2004, PASA, 21, 356

Jones J. B. et al., 2006, AJ, 131, 312

Jordán A., et al., 2007, ApJS, 171, 101

King I., 1962, AJ, 67, 471

Kirby E. N., Cohen J. G., Guhathakurta P., Cheng L., Bullock J. S., Gallazzi A., 2013, ApJ, 779, 102

Kissler-Patig M., Jordán A., Bastian N., 2006, A&A, 448, 1031

Klypin A. A., Trujillo-Gomez S., Primack J., 2011, ApJ, 740, 102

Komatsu E., et al., 2011, ApJS, 192, 18

Kormendy J., Fisher D. B., Cornell M. E., Bender R., 2009, ApJS, 182, 216

Kroupa P., 1998, MNRAS, 300, 200

Kruijssen J. M. D., Mieske S., 2009, A&A, 500, 785

Lanzoni B., et al., 2010, ApJ, 717, 653

Lee Y.-W., Joo J.-M., Sohn Y.-J., Rey S.-C., Lee H.-C., Walker A. R., 1999, Nature, 402, 55

Lemson G., Virgo Consortium t., 2006, preprint (arXiv:0608019)

Lisker T., Grebel E. K., Binggeli B., Glatt K., 2007, ApJ, 660, 1186

Lisker T., Weinmann S. M., Janz J., Meyer H. T., 2013, MNRAS, 432, 1162

Lützgendorf N., et al., 2013, A&A, 555, A26

Madrid J. P., ApJ, 2011, 737, L13

Maraston C., Kissler-Patig M., Brodie J. P., Barmby P., Huchra J. P., 2001, A&A, 370, 176

Maraston C., Bastian N., Saglia R. P., Kissler-Patig M., Schweizer F., Goudfrooij P., 2004, A&A, 416, 467

Maraston C., 2005, MNRAS, 362, 799

Marino A. F., Milone A. P., Piotto G., Villanova S., Bedin L. R., Bellini A., Renzini A., 2009, A&A, 505, 1099

McLaughlin D. E., 1999, ApJ, 512, L9

McLaughlin D. E., van der Marel R. P., 2005, ApJS, 161, 304

McMillan P. J., 2011, MNRAS, 414, 2446

Mei S., et al., 2007, ApJ, 655, 144

Merritt D., Schnittman J. D., Komossa S., 2009, ApJ, 699, 1690

Meylan G., Sarajedini A., Jablonka P., Djorgovski S. G., Bridges T., Rich R. M., 2001, AJ, 122, 830

Mieske S., Kroupa P., 2008, ApJ, 677, 276

Mieske S., Hilker M., Infante L., 2002, A&A, 383, 823

Mieske S., Hilker M., Infante L., 2004a, A&A, 418, 445

Mieske S. et al., 2004b, AJ, 128, 1529

Mieske S., Hilker M., Infante L., Jordán A., 2006, AJ, 131, 2442

Mieske S., Hilker M., Jordán A., Infante L., Kissler-Patig M., 2007, A&A, 472, 111

Mieske S. et al., 2008, A&A, 487, 921

Mieske S., Hilker M., Misgeld I., 2012, A&A, 537, A3

Mieske S., Frank M. J., Baumgardt H., Lützgendorf N., Neumayer N., Hilker M., 2013, A&A, 558, A14

Misgeld I., Hilker M., 2011, MNRAS, 414, 3699

Misgeld I., Mieske S., Hilker M., 2008, A&A, 486, 697

Misgeld I., Mieske S., Hilker M., Richtler T., Georgiev I. Y., Schuberth Y., A&A, 2011, 531, A4

Moore B., Katz N., Lake G., Dressler A., Oemler A., 1996, Nature, 379, 613

Moore B., Lake G., Quinn T., Stadel J., 1999, MNRAS, 304, 465

Murphy J. D., Gebhardt K., Adams J. J., 2011, ApJ, 729, 129

Murray N., 2009, ApJ, 691, 946

Naab T., Johansson P. H., Ostriker J. P., 2009, ApJ, 699, L178

Navarro J. F., Frenk C. S., White S. D. M., 1996, ApJ, 462, 563

Norris M. A., Kannappan S. J., 2011, MNRAS, 414, 739

Norris M. A., et al., 2014, MNRAS, 443, 1151

Oh S.-H., de Blok W. J. G., Brinks E., Walter F., Kennicutt R. C., Jr., 2011, AJ, 141, 193

Paudel S., Lisker T., Janz J., 2010, ApJ, 724, L64

Paudel S., Lisker T., Kuntschner H., 2011, MNRAS, 413, 1764

Peñarrubia J., Benson A. J., Walker M. G., Gilmore G., McConnachie A. W., Mayer L., 2010, MNRAS, 406, 1290

Peng E. W. et al., 2006, ApJ, 639, 838

Peng E. W. et al., 2008, ApJ, 681, 197

Penny S. J., Forbes D. A., Conselice C. J., MNRAS, 2012, 422, 885

Pfeffer J., Baumgardt H., 2013, MNRAS, 433, 1997

Phillipps S., Drinkwater M. J., Gregg M. D., Jones J. B., 2001, ApJ, 560, 201

Phillipps S., Young A. J., Drinkwater M. J., Gregg M. D., Karick A., 2013, MNRAS, 433, 1444

Planck Collaboration, et al., 2014, A&A, 571, A16

Plummer H. C., 1911, MNRAS, 71, 460

Price J., et al., 2009, MNRAS, 397, 1816

Prugniel P., Simien F., A&A, 321, 111

Rejkuba M., Dubath P., Minniti D., Meylan G., 2007, A&A, 469, 147

Renaud F., Bournaud F., Duc P.-A., 2015, MNRAS, 446, 2038

Richtler T., Dirsch B., Larsen S., Hilker M., Infante L., 2005, A&A, 439, 533

Richtler T., 2012, preprint (astro-ph/1210.0045)

Romanowsky A. J., Strader J., Spitler L. R., Johnson R., Brodie J. P., Forbes D. A., Ponman T., 2009, AJ, 137, 4956

Saviane I., da Costa G. S., Held E. V., Sommariva V., Gullieuszik M., Barbuy B., Ortolani S., 2012, A&A, 540, A27

Schaye J., et al., 2015, MNRAS, 446, 521

Schuberth Y., Richtler T., Hilker M., Dirsch B., Bassino L. P., Romanowsky A. J., Infante L., 2010, A&A, 513, A52

Schweizer F., Seitzer P., 1998, AJ, 116, 2206

Scott N., Graham A. W., Schombert J., 2013, ApJ, 768, 76

Sérsic J. L., 1963, Boletin de la Asociacion Argentina de Astronomia, 6, 41

Sérsic J. L., 1968, Atlas de Galaxias Australes. Observatorio Astronomico, Cordoba

Seth A. C., Dalcanton J. J., Hodge P. W., Debattista V. P., 2006, AJ, 132, 2539

Seth A., Agüeros M., Lee D., Basu-Zych A., 2008, ApJ, 678, 116

Seth A. C., et al., 2010, ApJ, 714, 713

Seth A. C., et al., 2014, Nature, 513, 398

Simmerer J., Ivans I. I., Filler D., Francois P., Charbonnel C., Monier R., James G., 2013, ApJ, 764, L7

Spergel D. N. et al., 2003, ApJS, 148, 175

Springel V. et al., 2005, Nature, 435, 629

Strader J., Caldwell N., Seth A. C., 2011, AJ, 142, 8

Strader J., et al., 2013, ApJ, 775, L6

Taylor M. A., Puzia T. H., Harris G. L., Harris W. E., Kissler-Patig M., Hilker M., 2010, ApJ, 712, 1191

Terzić B., Graham A. W., 2005, MNRAS, 362, 197

Thomas P. A., Drinkwater M. J., Evstigneeva E., 2008, MNRAS, 389, 102

Trager S. C., King I. R., Djorgovski S., 1995, AJ, 109, 218

Turner M. L., Cote P., Ferrarese L., Jordan A., Blakeslee J. P., Mei S., Peng E. W., West M. J., 2012, ApJS, 203, 5

Urban O., Werner N., Simionescu A., Allen S. W., Böhringer H., 2011, MNRAS, 414, 2101

Villalobos Á., De Lucia G., Borgani S., Murante G., 2012, MNRAS, 424, 2401

Vogelsberger M., et al., 2014, MNRAS, 444, 1518

Weinmann S. M., Lisker T., Guo Q., Meyer H. T., Janz J., 2011, MNRAS, 416, 1197

Whitmore B. C., Zhang Q., Leitherer C., Fall S. M., Schweizer F., Miller B. W., 1999, AJ, 118, 1551

Willman B., et al., 2005, ApJ, 626, L85

Zentner A. R., Bullock J. S., 2003, ApJ, 598, 49

Zhang H.-X., et al., 2015, ApJ, 802, 30

Zucker D. B., et al., 2006, ApJ, 643, L103